NASA CONTRACTOR
REPORT

NASA CR-18

C. 1

LAMINAR OR TURBULENT BOUNDARY-LAYER
FLOWS OF PERFECT GASES OR REACTING
GAS MIXTURES IN CHEMICAL EQUILIBRIUM

by E. C. Anderson and C. H. Lewis

Prepared by
VIRGINIA POLYTECHNIC INSTITUTE AND STATE UNIVERSITY
Blacksburg, Va. 24061
for Langley Research Center

1. Report No. NASA CR-1893	2. Government Accession No.	3. Recipient's Catalog No.
4. Title and Subtitle Laminar or Turbulent Boundary-Layer Flows of Perfect Gases or Reacting Gas Mixtures in Chemical Equilibrium		5. Report Date October 1971
		6. Performing Organization Code
7. Author(s) E. C. Anderson and C. H. Lewis		8. Performing Organization Report No.
		10. Work Unit No.
9. Performing Organization Name and Address Virginia Polytechnic Institute and State University Blacksburg, Virginia 24060		11. Contract or Grant No. NAS1-9337
		13. Type of Report and Period Covered Contractor Report
12. Sponsoring Agency Name and Address National Aeronautics and Space Administration Washington, D.C. 20546		14. Sponsoring Agency Code

15. Supplementary Notes
Computer Program Documentation: Miner, E. W., Anderson, E. C., and Lewis, C. H., "Two-Dimensional and Axisymmetric Nonreacting Perfect Gas and Equilibrium Chemically Reacting Laminar, Transitional and/or Turbulent Boundary Layer Flows," VPI-E-71-8, 1971.

16. Abstract

Turbulent boundary-layer flows of non-reacting gases are predicted for both internal (nozzle) and external flows. Effects of favorable pressure gradients on two eddy viscosity models were studied in rocket and hypervelocity wind tunnel flows. Nozzle flows of equilibrium air with stagnation temperatures up to 10,000°K were computed. Predictions of equilibrium nitrogen flows through hypervelocity nozzles were compared with experimental data. A slender spherically blunted cone was studied at 70,000 ft. altitude and 19,000 ft./sec. in the earth's atmosphere. Comparisons with available experimental data showed good agreement. A computer program was developed and fully documented during this investigation for use by interested individuals.

17. Key Words (Suggested by Author(s)) Laminar or turbulent boundary layer, perfect gas, equilibrium gas, nozzle, blunt body	18. Distribution Statement Unlimited		
19. Security Classif. (of this report) Unclassified	20. Security Classif. (of this page) Unclassified	21. No. of Pages 174	22. Price* $3.00

I. ABSTRACT

An implicit finite-difference scheme is used to solve the laminar
and turbulent boundary-layer equations for perfect gases and reacting
gas mixtures in chemical equilibrium. The formulation of the boundary-
layer equations neglects transverse curvature effects, and the equili-
brium chemistry model assumes that the element composition across the
boundary-layer is constant. Thus, injection of a foreign gas at the
wall boundary cannot be considered.

The numerical procedure is applied to both internal and external
flow problems and the results are compared with experimental data and
other numerical solutions where these data were available. The solu-
tions for laminar and turbulent flows of perfect gases and laminar
flow of an equilibrium gas without mass transfer are in good agreement
with experimental data and/or other numerical solutions. For the case
of mass transfer at the wall, the numerical solution is in good agree-
ment with experimental heat-transfer data, but the velocity profiles
and skin-friction predictions are not in good agreement with the
available data. Additional experimental data are needed to assess the
accuracy of the numerical solutions with mass transfer effects.

The experimental data which were available for turbulent flows of
an equilibrium gas were in a range of pressure and/or temperature where
the effects of equilibrium chemistry are not large. With the exception
of an integral method of solution for turbulent flow of an equilibrium
gas in nozzles - which failed to converge for the problem considered -
other numerical methods were not available for comparison. However,
the solutions obtained are in good agreement with the limited data
available.

II. TABLE OF CONTENTS

III. LIST OF FIGURES AND TABLES

IV. LIST OF SYMBOLS

A_o, A_1, A_2, A_3, A_4, A_i coefficients of parabolic differential equation (88, 89, and 90).

A_n coefficient matrix of difference equation (101)

A^* damping factor (52), dimensional

A^+ damping constant (53)

A_{1_n}, A_{2_n}, A_{3_n}, A_{4_n} matrix arrays of A_1, A_2, A_3, A_4

A/A_t ratio of local cross-sectional area to minimum cross-sectional area

a^* unit reference length

B_n coefficient matrix of difference equation (101)

C density-viscosity product ratio, $\rho\mu/(\rho_e\mu_e)$

C_1 $1 - \frac{1}{Pr}$, constant for perfect gas

C_n coefficient matrix of difference equation (101)

C_{f_∞} skin-friction coefficient based on free-stream conditions

$\hat{C}_{f_\infty}$ skin-friction coefficient, $C_{f_\infty}/\varepsilon_{VD}$

C_{f_e} skin-friction coefficient based on local edge conditions

C_{h_∞} heat-transfer coefficient based on free-stream conditions

C_{h_e} heat-transfer coefficient based on local edge conditions

xii

c^*	constant in Sutherland's viscosity law (21), 198.6°R for air
$\bar{c}$	c^*/T^*_{ref}
c_i	mass fraction of species i
c^j	mass fraction of chemical element j
c_p^*	specific heat of perfect gas or mixture, $ft^2/(sec^2 - °R)$
$\bar{c}_p^*$	frozen specific heat of mixture, $ft^2/(sec^2 - °R)$
c_p	$c_p^*/RGAS$, °R or °K
D_i^{T*}	thermal diffusion coefficient, lb sec/ft
D_{ij}	multi-component diffusion coefficient, ft^2/sec
D_n	coefficient matrix of difference equation (101)
E_n	coefficient matrix of difference equation (102)
F	normalized tangential velocity component, u/u_e or f'
f	streamfunction (25)
F_n	coefficient matrix of difference equation (102)
G	dummy variable (92)
g	stagnation enthalpy ratio, H/H_e
H^*	total enthalpy, ft^2/sec^2

H'^*	fluctuating component of total enthalpy, ft^2/sec^2
H	nondimensionalized total enthalpy, H^*/u_{ref}^{*2}
H'	nondimensionalized fluctuating component of total enthalpy, H'^*/u_{ref}^{*2}
h^*	static enthalpy, ft^2/sec^2
h_i^*	static enthalpy of species i, ft^2/sec^2
h	nondimensionalized static enthalpy, h^*/u_{ref}^{*2}
$\tilde{h}$	$log_{10}(h^*/RGAS)$
h_{g_1}	film coefficient, $BTU/in^2 - sec - °R$
h_{g_2}	film coefficient, $lb_m/in^2 - sec$
ISS	number of species in mixture
J_i^*	mass flux relative to mass-average velocity, $slugs/(ft^2 - sec)$
K^*	thermal conductivity of mixture, $lb/(ft^2 - sec)$, (10)
k	ratio of adjacent intervals of step sizes in normal coordinate direction (106)
k_f^*	frozen value of thermal conductivity, $lb/(ft^2 - sec)$
k_1	constant in Van Driest expression for mixing-length, 0.4, (52)
k_2	constant in outer eddy-viscosity expression, 0.168, (79)
L^*	reference length, ft

$L_i^{T^*}$	thermal Lewis-Seminar number, $\overline{c}_p^* D_i^{T^*}/k_f^*$
L_{ij}	multi-component Lewis-Seminar number, $\overline{c}_p^* \rho^* D_{ij}/k_f^*$
M	Mach number
$\overline{M}$	molecular weight of mixture, lb/(lb-mole)
M_i	molecular weight of species i, lb/(lb-mole)
M^j	atomic weight of element j, lb/(lb-mole)
N	number of strips in boundary-layer
P^*	pressure, lb/ft^2
P_{ref}^*	reference pressure, $\rho_{ref}^* u_{ref}^{*2}$, lb/ft^2
P	nondimensionalized pressure, P^*/P_{ref}^*
P_a	pressure, atmospheres
$\mathcal{P}$	$\log_{10}(P_a)$
P_o'	stagnation pressure behind a normal shock
P^+	pressure gradient paramater (59)
Pr	Prandtl number of mixture, $c_p^* \mu^*/K^*$
Pr_f	frozen Prandtl number, $\overline{c}_p^* \mu^*/k_f^*$
Pr_t	turbulent Prandtl number, $c_p^* \varepsilon^{+^*}/\varepsilon_k^*$, assumed constant - 0.9
$RGAS$	gas constant, ft^2/(sec^2 - °K) or ft^2/(sec^2 - °R)
R_o	universal gas constant (1.98647 $\frac{gm\text{-}cal}{gm\text{-}mole\text{-}°K}$)
R_e	Reynolds number
r^*	body radius, dimensional
r	body radius, r^*/a^*, nondimensional

S_{t_∞} Stanton number based on freestream conditions

S_{t_e} Stanton number based on edge conditions

T^* temperature, °R or °K

T_{ref}^* reference temperature, u_{ref}^{*2}/c_P^*, °R

$T_{ref_1}^*$ reference temperature used in computing freestream Reynolds number

T nondimensional temperature, T^*/T_{ref}^*

u^* tangential velocity, ft/sec

u'^* fluctuating component of tangential velocity, ft/sec

u_f^* friction velocity, $(\tau_w^*/\rho^*)^{1/2}$, ft/sec

u_{ref}^* reference velocity, u_∞^*, ft/sec

u nondimensional tangential velocity, u^*/u_{ref}^*

u' nondimensional fluctuating component of tangential velocity, u'^*/u_{ref}^*

V transformed normal velocity (34, 35, 85, and 86)

v^* normal velocity, ft/sec

v'^* fluctuating component of normal velocity, ft/sec

v nondimensional normal velocity, $v^*/(u_{ref}^* \, \varepsilon_{VD})$

v' nondimensional fluctuating component of normal velocity, $v'^*/(u_{ref}^* \, \varepsilon_{VD})$

v_w^+ v_w^*/u_f^*

W	dummy variable (88)
W_{1_n}	array of W at $x = x_1$
W_{2_n}	array of W at $x = x_1 + \Delta x$
X_i	mole fraction of species i, $\overline{M} c_i/M_i$
x^*	distance along surface, dimensional
x	nondimensional surface distance, x^*/a^*
y^*	normal coordinate, dimensional
y	nondimensional normal coordinate, $y^*/(a^* \varepsilon_{VD})$
y^+	$y^* u_f^*/\nu^*$
z^*	distance along body axis, dimensional
z	nondimensional distance along body axis, z^*/a^*
α_i^j	number of atoms of element j per molecule of species i
β	pressure gradient paramater (41,42)
γ	ratio of specific heats, or intermittancy factor (81)
δ	boundary-layer thickness, dimensional
δ^*	compressible displacement thickness, dimensional
δ_k^*	incompressible displacement thickness, dimensional
ε^{+*}	eddy-viscosity, lb-sec/ft^2

xvii

ε_i^{+*} inner eddy-viscosity, lb-sec/ft^2

ε^{+*} outer eddy-viscosity, lb-sec/ft^2

ε_k^* eddy thermal conductivity, lb/sec - °R)

ε^+ nondimensional eddy-viscosity, ε^{+*}/μ^*

ε_i^+ nondimensional inner eddy viscosity

$$\varepsilon_i^{+*}/\mu_{ref}^*$$

ε_o^+ nondimensional outer eddy viscosity,

$$\varepsilon_o^{+*}/\mu^*$$

ε_{VD} coordinate stretching paramater

$$\left(\frac{\mu_{ref}^*}{\rho_{ref}^* \, u_{ref}^* \, a^*} \right)^{1/2}$$

η transformed normal coordinate (27, 29)

θ^* momentum thickness, dimensional

θ static temperature ratio, T/T_e

λ implicit - explicit indicator in finite difference equation (98)

μ^* viscosity, lb-sec/ft^2

μ_{ref}^* viscosity corresponding to T_{ref}^*, lb-sec/ft^2

$\mu_{ref_1}^*$ viscosity corresponding to $T_{ref_1}^*$, lb-sec/ft^2

μ nondimensional viscosity, μ^*/μ_{ref}^*

ν^*	kinematic viscosity, μ^*/ρ^*, ft^2/sec
ν	nondimensional kinematic viscosity, $\nu^* \rho_{ref}^*/\mu_{ref}^*$
ξ	transformed surface coordinate (26, 28)
ρ^*	density, $slugs/ft^3$
ρ_{ref}^*	reference density, ρ_∞^*, $slugs/ft^3$
ρ	nondimensional density, ρ^*/ρ_{ref}^*
σ	shock angle
τ^*	shear stress, $\mu^* \dfrac{\partial u^*}{\partial y^*}$, lb/ft^2
τ	nondimensional shear stress $\dfrac{\tau^* \varepsilon_{VD} a^*}{\mu_{ref}^* u_{ref}^*}$
ψ	streamfunction (25)
ω	exponent for power law viscosity expression

Subscripts and Superscripts

e	condition at outer edge of boundary layer
m	designates node point in ξ-direction
n	designates node point in η-direction
ref	reference condition
w	condition at wall boundary
x	differentiation with respect to x
o	stagnation condition
η	differentiation with respect to η
ξ	differentiation with respect to ξ

xix

∞	freestream condition
$(\ )'$	differentiation with respect to η
$(\ )^*$	dimensional quantity

V. INTRODUCTION

The existing literature on the numerical solution of the laminar boundary-layer equations for two-dimensional and axisymmetric flows is extensive. A recent review of the most commonly used techniques for solving the laminar boundary-layer equations for non-equilibrium, equilibrium, and non-reacting chemistry is given by Blottner [ref. 1]. Kline et al. [ref. 2] present a similar review of the prediction methods used for the solution of the incompressible turbulent boundary-layer equations. Examples of the more recent solutions of the turbulent boundary-layer equations are the reports by Harris [ref. 3] and Pletcher [ref. 4].

The implicit finite-difference scheme of the Crank-Nicolson [ref. 5] type has been developed extensively by Blottner [refs. 1, 6, 7] and by Davis [refs. 8, 9, 10] for a wide range of laminar boundary-layer flows. This method of solution has been demonstrated to be accurate and stable and does not require an excessive amount of computing time. This type of finite-difference scheme has been used by Harris [ref. 3] to solve the turbulent boundary-layer equations for non-reacting gases. Harris considered mass transfer at the wall and the laminar-turbulent transitional regieme. Cebeci et al. [refs. 11, 12, 13] used an implicit finite-difference scheme to obtain the solution of the turbulent boundary-layer equations. However, the numerical procedure used by Cebeci differed considerably from the Crank-Nicolson type scheme. The solution of Pletcher used an explicit finite-difference calculation procedure based on the DuFort-Frankel [ref. 14] scheme. The turbulent solutions of Cebeci and Pletcher also

1

considered only non-reacting chemistry.

In the references cited above, the authors have considered only external flows. Elliott, Bartz, and Silver [ref. 15] have developed an integral method of solution for predicting turbulent boundary-layer flows in rocket nozzles. Boldman et al. [ref. 16] have applied the method to predict turbulent flows in supersonic nozzles. Edenfield [ref. 17] has extended the method to predict turbulent flows in hypervelocity nozzles in which the gas was considered to be in chemical equilibrium.

For the lower Mach number perfect gas cases considered by Elliott, Bartz, and Silver and by Boldman, relatively good agreement between the predictions and the experimental data for the heat-transfer distribution was obtained. Edenfield found that the method did not predict the boundary-layer displacement thickness accurately downstream of the nozzle throat and failed to converge for local Mach numbers of about 16. Thus, for hypersonic nozzle flows, a limit exists for the use of the integral method. Other disadvantages of the integral method are the amount of empirical data needed and the number of adjustable para-maters which strongly influence the results of the predictions.

As a result of the excellent agreement between experiment and theory which has been obtained by Blottner and Davis for both reacting and non-reacting chemistry for laminar boundary-layer flows and by Harris for non-reacting turbulent flows using the Crank-Nicolson type implicit finite-difference scheme, this method of solution was se-lected for the present investigation. Both laminar and turbulent flows of perfect gases and mixtures of perfect gases in chemical equilibrium

2

are considered for flat plates, wedges, two-dimensional or axisymmetric blunt bodies and nozzles. Mass transfer is considered for the case where the injected gas is the same as that of the external flow. The primary emphasis has been to obtain solutions for high Mach number flows having strongly favorable pressure gradients and highly cooled walls.

VI. ANALYSIS

The equations of motion for laminar or turbulent flow of perfect gases and equilibrium gas mixtures are developed in Levy-Lees variables and expressed in the general parabolic form necessary for the implicit finite-difference solution procedure employed by Blottner [ref. 6] and by Davis [ref. 8].

Semi-empirical expressions for the turbulent eddy viscosity are presented for the cases of a solid wall and a porous wall. The finite-difference scheme is developed and the procedures employed for determining the initial profile data, and the specification of edge conditions are discussed. Definitions of the boundary-layer parameters which have been employed are also given.

6.1 Governing Equations

The governing equations for laminar or turbulent boundary-layer flow of an arbitrary gas in thermodynamic equilibrium or of a perfect gas are presented in dimensional variables and transformed to Levy-Lees variables. The rate of mass transfer at the wall boundary for porous-walls is assumed small in comparison to the boundary-layer mass flow and normal gradients are negligible. The boundary-layer thickness is assumed to be small in comparison to the body radius of curvature and centrifugal forces are neglected. The coordinate system is shown in Figure 1.

6.1.1 Laminar Boundary-Layer Conservation Equations

The conservation equations for laminar boundary-layer flows of a perfect gas or of a chemically reacting gas mixture in equilibrium are

developed in this section. For a multicomponent gas mixture, the laminar boundary-layer equations are expressed in dimensional variables as; (see Hirschfelder et al. [ref. 18]):

Continuity

$$\frac{\partial \rho^* u^* r^{*j}}{\partial x^*} + \frac{\partial \rho^* v^* r^{*j}}{\partial y^*} \tag{1}$$

where

$$j = 0 \text{ for two dimensional flow}$$

$$j = 1 \text{ for axisymmetric flow}$$

Momentum

$$\rho^* u^* \frac{\partial u^*}{\partial x^*} + \rho^* v^* \frac{\partial u^*}{\partial y^*} = -\frac{d P_e^*}{d x^*} + \frac{\partial}{\partial y^*}\left(\mu^* \frac{\partial u^*}{\partial y^*}\right) \tag{2}$$

Energy

$$\rho^* u^* \frac{\partial h^*}{\partial x^*} + \rho^* v^* \frac{\partial h^*}{\partial y^*} = u^* \frac{d P_e^*}{d x^*} - \frac{\partial q^*}{\partial y^*} + \mu^*\left(\frac{\partial u^*}{\partial y^*}\right)^2 \tag{3}$$

where

$$q^* = - k_f^* \frac{\partial T^*}{\partial y^*} + \sum_{i=1}^{ISS} h_i^* J_i^* \tag{4}$$

and

$$J_i^* = \frac{\mu^*}{Pr}\left\{\sum_{j=1}^{ISS} \frac{M_i M_j}{\overline{M}^2} L_{ij} \frac{\partial X_i}{\partial y^*} - \frac{L_i^{T^*}}{T^*} \frac{\partial T^*}{\partial y^*}\right\} \tag{5}$$

5

Species

$$\rho^* u^* \frac{\partial c_i}{\partial x^*} + \rho^* v^* \frac{\partial c_i}{\partial y^*} = - \frac{\partial}{\partial y^*} (J_i^*) \tag{6}$$

Assuming the gas mixture to be in local chemical equilibrium, the species composition is a function of the pressure, temperature, and concentrations of the chemical elements. The diffusion equation for the jth chemical element is obtained from equation (6) after multiplication by $\left(\alpha_i^j \frac{M^j}{M_i} \right)$ and summing over all species, ISS, as

$$\rho^* u^* \frac{\partial c^j}{\partial x^*} + \rho^* v^* \frac{\partial c^j}{\partial y^*} = - \frac{\partial}{\partial y^*} \left[\sum_{i=1}^{ISS} \alpha_i^j \frac{M^j}{M_i} J_i^* \right] \tag{7}$$

where

$$c^j = \sum_{i=1}^{ISS} \alpha_i^j \frac{M^j}{M_i} c_i \tag{8}$$

Assuming that the element composition, c^j, remains constant across the boundary-layer, the conservation of energy, equation (3), can be expressed in terms of total enthalpy in the same general form as that for a perfect gas. If c^j is constant, the heat transfer can be expressed as

$$q^* = - K^* \frac{\partial T^*}{\partial y^*} \tag{9}$$

where

$$K^* = k_f^* - \frac{\mu^*}{Pr_f} \sum_{i=1}^{ISS} h_i^* \left[\sum_{j=1}^{ISS} \frac{M_i M_i}{\overline{M}^2} L_{ij} \frac{\partial X_i}{\partial T^*} - \frac{L_i^{T^*}}{T^*} \right] \tag{10}$$

6

Using the definitions,

$$H^* = h^* + \frac{u^{*2}}{2} \tag{11}$$

$$h^* = h^*(P^*, T^*) \tag{12}$$

and the normal momentum equation

$$\frac{\partial P^*}{\partial y^*} = 0 \tag{13}$$

the heat transfer, equation (9), can be expressed as

$$q^* = -\frac{\mu^*}{Pr}\left[\frac{\partial H^*}{\partial y^*} - u^* \frac{\partial u^*}{\partial y^*}\right] \tag{14}$$

where

$$Pr = \frac{c_p^* \mu^*}{K^*} \tag{15}$$

Multiplying equation (2) by u^* and adding to equation (3) with the use of equation (14) gives

$$\rho^* u^* \frac{\partial H^*}{\partial x^*} + \rho^* v^* \frac{\partial H^*}{\partial y^*} = \frac{\partial}{\partial y^*}\left[\frac{\mu^*}{Pr}\frac{\partial H^*}{\partial y^*} + \mu^*\left(1 - \frac{1}{Pr}\right) u^* \frac{\partial u^*}{\partial y^*}\right] \tag{16}$$

The conservation of energy as expressed by equation (16) has the same form as that for a perfect gas, but for an equilibrium gas the thermodynamic and transport properties are determined for the specified gas mixture. This approach is limited since the element composition is not strictly constant across the boundary layer. This approach cannot be used for injection of a foreign gas, since the element composition

7

is not a constant across the boundary layer. Therefore, the case of mass transfer into the boundary layer is restricted to injection of the same equilibrium gas mixture or perfect gas as that at the outer edge of the boundary layer.

For high Reynolds number flow, the conservation equations are non-dimensionalized by variables, given by Van Dyke [ref. 19], which are of order one in the boundary layer. The nondimensional variables are defined in the list of symbols. The conservation equations in non-dimensional variables have the same form as the dimensional equations and are:

Continuity

$$\frac{\partial \ \rho u r^j}{\partial x} + \frac{\partial \ \rho v r^j}{\partial y} = 0 \tag{17}$$

Momentum

$$\rho u \ \frac{\partial u}{\partial x} + \rho v \ \frac{\partial u}{\partial y} = - \ \frac{dP_e}{dx} + \frac{\partial}{\partial y} \left(\mu \ \frac{\partial u}{\partial y} \right) \tag{18}$$

Energy

$$\rho u \ \frac{\partial H}{\partial x} + \rho v \ \frac{\partial H}{\partial y} = \frac{\partial}{\partial y} \left[\frac{\mu}{Pr} \ \frac{\partial H}{\partial y} + \mu \left(1 - \frac{1}{Pr} \right) u \ \frac{\partial u}{\partial y} \right] \tag{19}$$

For a perfect gas,

$$Pr = constant$$

$$c_p^* = constant$$

$$h = T \tag{20}$$

and the viscosity may be expressed by Sutherland's law

8

$$\mu = \frac{1+\overline{c}}{T+\overline{c}} T^{3/2} \tag{21}$$

where

$$\overline{c} = \frac{c^*}{T^*_{ref}} = \frac{c^*}{(\gamma-1) M^2_\infty T^*_\infty}$$

$$c^* = 198.6°R \text{ for air}$$

or by a simple power law

$$\mu = T^\omega \tag{22}$$

The equations of state are:

$$P = \frac{\gamma-1}{\gamma} \rho T \text{ for a perfect gas} \tag{23}$$

and

$$P = \rho \frac{R_o}{\overline{M} c^*_p} T \text{ for an equilibrium gas} \tag{24}$$

The thermodynamic and transport properties of an equilibrium gas are functions of the chemical composition and internal energies of the species in the gas mixture, and have been determined using a modification of the computer program developed by Lordi, Mates, and Moselle [ref. 20]. A description of the modified program is given in Appendix A.

6.1.2 Laminar Boundary-Layer
Equations Expressed in Levy-Lees Variables

A more convenient form of the conservation equations for numerical

9

solution is obtained by the introduction of a stream function defined as

$$\psi(x,y) = (2\xi)^{1/2} f(\xi,\eta) \tag{25}$$

where ξ and η are the Levy-Lees transformed coordinates:

$$\xi(x) = \int_0^x \rho_e u_e \mu_e r^{2j} dx \tag{26}$$

$$\eta(x,y) = \frac{\rho_e u_e r^j}{(2\xi)^{1/2}} \int_0^y \rho/\rho_e \, dy \tag{27}$$

At the stagnation point of a blunt body the boundary-layer equations have a removable singularity. As $\xi \to 0$, the limiting process gives

$$\xi(x) = \rho_e \frac{du_e}{dx} \mu_e \frac{x^{2(j+1)}}{2(j+1)} \tag{28}$$

$$\eta(x,y) = \frac{\rho_e x^{(j+1)}}{(2\xi)^{1/2}} \frac{du_e}{dx} \int_0^y \frac{\rho}{\rho_e} \, dy \tag{29}$$

or

$$\eta(0,y) = \left[\frac{\rho_e \frac{du_e}{dx} (j+1)}{\mu_e} \right]^{1/2} \int_0^y \frac{\rho}{\rho_e} \, dy \tag{30}$$

The differential operators expressed in the ξ,η coordinate system

are:

$$\frac{\partial}{\partial x} = \rho_e u_e \mu_e r^{2j} \frac{\partial}{\partial \xi} + \eta_x \frac{\partial}{\partial \eta} \tag{31}$$

and

$$\frac{\partial}{\partial y} = \frac{\rho u_e r^j}{(2\xi)^{1/2}} \frac{\partial}{\partial \eta} \tag{32}$$

Using equations (25), (31), and (32) gives

$$-r^j \cdot \rho v = \rho_e u_e \mu_e r^{2j} \left[\frac{f}{(2\xi)^{1/2}} + (2\xi)^{1/2} f_\xi \right] + (2\xi)^{1/2} \eta_x F$$

or

$$2\xi f_\xi + V + f = 0 \tag{33}$$

where

$$V = \frac{2\xi}{\rho_e u_e \mu_e r^{2j}} \left[\eta_x F + \frac{r^j \rho v}{(2\xi)^{1/2}} \right] \tag{34}$$

At the stagnation point,

$$V = \frac{\rho v}{\left[\rho_e \mu_e \frac{du_e}{dx} (j+1) \right]^{1/2}} \tag{35}$$

Differentiation of equation (25) with respect to y using equation (32)
gives:

$$f' = u/u_e \tag{36}$$

11

Evaluation of equation (18) at the outer edge of the boundary-layer gives the pressure gradient as:

$$\frac{dP_e}{dx} = - \rho_e \, u_e \, \frac{du_e}{dx} \tag{37}$$

With the use of equations (31) - (37), the conservation equations for laminar boundary layers are; (Blottner [ref. 7]):

Continuity

$$2\xi \, F_\xi + V' + F = 0 \tag{38}$$

Momentum

$$2\xi F \, F_\xi + VF' = \beta \left(\frac{\rho_e}{\rho} - F^2 \right) + (CF')' \tag{39}$$

Energy

$$2\xi F \, g_\xi + V \, g' = \frac{C}{Pr} \, g'' + \frac{C}{Pr} \, g' +$$

$$\frac{u_e^2}{H_e} \left\{ \left(1 - \frac{1}{Pr} \right) [C'F'F + CF'^2 + CF''] + CFF' \left(1 - \frac{1}{Pr} \right)' \right\} \tag{40}$$

where

$$F = f' = \frac{u}{u_e} \; ; \; g = \frac{H}{H_e} \; ; \; C = \frac{\rho\mu}{\rho_e \, \mu_e}$$

and

$$\beta = \frac{2\xi}{u_e} \, \frac{du_e}{d\xi} \tag{41}$$

12

or at the stagnation point

$$\beta = \frac{1}{j+1} \qquad (42)$$

6.1.3 Turbulent Boundary-Layer Conservation Equations

In this section, the conservation equations for turbulent flow and the semi-empirical formulations of the eddy viscosity model and the eddy thermal conductivity are presented. Following the usual practice, the symbols H, P, ρ, u, and v are to be interpreted as time averaged properties. The nondimensionalized form of the conservation equations are:

Continuity

$$\frac{\partial \; \rho u r^j}{\partial x} + \frac{\partial [(\rho v + \overline{\rho' v'}) \; r^j]}{\partial y} = 0 \qquad (43)$$

Momentum

$$\rho u \frac{\partial u}{\partial x} + (\rho v + \overline{\rho' v'}) \frac{\partial u}{\partial y} = \rho_e \; u_e \frac{du_e}{dx} + \frac{\partial}{\partial y} \left[\mu \frac{\partial u}{\partial y} - \rho \overline{u' v'} \right] \qquad (44)$$

Energy

$$\rho u \frac{\partial H}{\partial x} + (\rho v + \overline{\rho' v'}) \frac{\partial H}{\partial y} = \frac{\partial}{\partial y} \left[\frac{\mu}{Pr} \frac{\partial H}{\partial y} - \rho \overline{v' H'} + \mu \left(1 - \frac{1}{Pr} \right) \right] \qquad (45)$$

The solution of equations (42)-(44) requires expressions relating the Reynolds shear stress term $\overline{-u' v'}$ and $\overline{v' H'}$ to the mean variables u, v and H. These expressions are obtained by introducing an eddy viscosity, ϵ^{+*}, and an eddy thermal conductivity, ϵ_k^{*}, where it is assumed that

$$\overline{-u'^{*}v'^{*}} = \varepsilon^{+^{*}} \frac{\partial u^{*}}{\partial y^{*}} \tag{46}$$

and

$$\overline{-v'^{*}H'^{*}} = \varepsilon_{k}^{*} \frac{\partial H^{*}}{\partial y^{*}} \tag{47}$$

or

$$\overline{-v'^{*}H'^{*}} = \frac{c_{p}^{*} \varepsilon^{+^{*}}}{Pr_{t}} \frac{\partial H^{*}}{\partial y^{*}} \tag{48}$$

where

$$Pr_{t} = \frac{c_{p}^{*} \varepsilon^{+^{*}}}{\varepsilon_{k}^{*}} \tag{49}$$

The value of the turbulent Prandtl number is taken to be 0.9 for both perfect gases and equilibrium gas mixtures.

The eddy viscosity, $\varepsilon^{+^{*}}$, is evaluated using the concept of a two-layer eddy viscosity model consisting of an inner law, $\varepsilon_{i}^{+^{*}}$, valid near the wall and an outer law, $\varepsilon_{o}^{+^{*}}$, for the remainder of the boundary layer. This procedure has been employed successfully by a number of authors; for example, Cebeci, Smith, and Mosinskis [ref. 12], and Harris [ref. 3]. These authors used expressions for the inner eddy viscosity law which were based on Prandtl's mixing-length concept stated as

$$\varepsilon_{i}^{+^{*}} = \ell^{*2} \left| \frac{\partial u^{*}}{\partial y^{*}} \right| \tag{50}$$

where ℓ^{*} is the mixing-length. In the present solution of the turbulent boundary-layer equations, a number of expressions based on equation

14

(50) have been used, and in addition to these models, an eddy viscosity based on the Boussinesq [ref. 21] relation

$$\tau^* = \mu^* \left[1 + \frac{\varepsilon_i^{+*}}{\mu^*} \right] \frac{\partial u^*}{\partial y^*} \tag{51}$$

has been used for the non-porous wall cases. For the porous wall case the eddy viscosity expression considered was based on equation (50). These expressions are given below.

A. Expressions for the Inner Eddy Viscosity Law
for no Mass Transfer at the Wall

The eddy viscosity laws based on equation (50) have been derived by analogy with Van Driest's proposal for the mixing-length. Van Driest [ref. 22] considered Stokes' flow for an infinite flat plate with periodic oscillations in the plane parallel to the plate to arrive at an expression for the mixing length. The expression given by Van Driest is

$$\ell^* = k_1 y^* [1 - \exp(y^*/A^*)] \tag{52}$$

or using law of the wall coordinates

$$\ell^* = k_1 y^* [1 - \exp(-y^+/A^+)] \tag{53}$$

where

$$y^+ = \frac{y^* u_f^*}{\nu^*}$$

15

$$u_f^* = (\tau_w^*/\rho^*)^{1/2}$$

By correlation of experimentally determined velocity profiles for incompressible turbulent flows in tubes the constants were found to be

$$k_1 = 0.4$$

and

$$A^+ = 26$$

or

$$A^* = 26\nu^* \left(\frac{\tau_w^*}{\rho^*}\right)^{-1/2} \tag{54}$$

Patankar and Spalding [ref. 23] proposed the shear stress at the wall, τ_w^*, in equation (54) be replaced by the local value τ^*. The expression for A^* using this proposal is

$$A^* = 26\nu^* (\tau^*/\rho^*)^{-1/2} \tag{55}$$

The conservation of momentum, equation (44), for an incompressible two-dimensional flow can be expressed as

$$\frac{\partial \tau^*}{\partial y^*} = \frac{dP_e^*}{dx^*} \tag{56}$$

for the region near the wall. Integration of equation (56) and substituting into equation (55) gives A^* as

16

$$A^* = 26\nu^* \left[\frac{\tau_w^*}{\rho^*} + \frac{y^*}{\rho^*} \frac{dP_e^*}{dx^*} \right]^{-1/2} \tag{57}$$

or

$$A^+ = 26[1 - P^+ y^+]^{-1/2} \tag{58}$$

where

$$P^+ = - \frac{dP_e^*}{dx^*} \nu^* / \rho^* (u_f^*)^3 \tag{59}$$

Cebeci and Smith [ref. 11] note that the term in brackets of equations (57) and (58) may become negative for accelerating flows leading to the square root of a negative number. To avoid the numerical difficulty Cebeci and Smith replaced equations (57) and (58) by

$$A^* = 26\nu^* \left[\left| \frac{\tau_w^*}{\rho^*} + \frac{y^*}{\rho^*} \frac{dP_e^*}{dx^*} \right| \right]^{-1/2} \tag{60}$$

and

$$A^+ = 26[|1 - P^+ y^+|]^{-1/2} \tag{61}$$

As a result of the difficulties encountered using equations (57), (60) and (61), equation (57) was arbitrarily modified by replacing the pressure gradient with the absolute value giving

17

$$A^* = 26\nu^* \left[\frac{\tau_w^*}{\rho^*} + \frac{y^*}{\rho^*} \left| \frac{dP_e^*}{dx^*} \right| \right]^{-1/2} \tag{62}$$

In a more recent publication, Cebeci [ref. 13] suggested that the value of y^+ in equation (58) be replaced by a constant value of 11.8. This is an experimentally determined value for the laminar sublayer thickness and gives

$$A^+ = 26[1 - 11.8P^+]^{-1/2} \tag{63}$$

Cebeci [ref. 13] does not indicate a procedure for the case of a negative square root which occurs for $P^+ > 1/11.8$.

Reichardt [ref.24] considered the incompressible continuity equation for the fluctuating velocity components to demonstrate that ε_i^{+*} varies with y^{*3} and presented an expression which was obtained by curve fitting experimental data of flow in pipes. Reichardt's expression for the inner eddy viscosity is

$$\varepsilon_i^{+*} = \mu^* \, 0.4 \left[\frac{y^* u_f^*}{\nu^*} - 11 \tan h \left(\frac{y^* u_f^*}{11 \nu^*} \right) \right] \tag{64}$$

B. Eddy Viscosity Expression for the Case of a Porous Wall

For a porous wall with pressure gradient, the conservation of momentum, equation (44), is approximated for the region near the wall as, (Cebeci [ref. 13]):

$$\frac{d\tau^*}{dy^*} - \frac{v_w^*}{v^*} \tau^* = \frac{dP_e^*}{dx^*} \qquad (65)$$

Solving equation (65) for the shear stress gives

$$\tau^* = \frac{dP_e^*}{dx^*} \frac{v^*}{v_w^*} \left[\exp\left(\frac{v_w^*}{v_.^*} y^* - 1\right)\right] + \tau_w^* \exp\left(\frac{v_w^*}{v^*} y^*\right) \qquad (66)$$

The damping constant, A^+, for the porous wall is expressed as

$$A^+ = 26 \left\{ -\frac{P^+}{v_w^+} [\exp(v_w^+ y^+) - 1] + \exp(v_w^+ y^+) \right\}^{-1/2} \qquad (67)$$

Assuming that y^+ at the edge of the laminar sublayer for the case of a porous wall is approximately the same as that for a flat plate without mass transfer, Cebeci [ref. 13] used a value of 11.8 for y^+ and expressed A^+ as

$$A^+ = 26 \left\{ -\frac{P^+}{v_w^+} [\exp(11.8 \, v_w^+) - 1] + \exp(11.8 \, v_w^+) \right\}^{-1/2} \qquad (68)$$

For the case of no mass transfer, equation (68) reduces to equation (63), and for a porous flat plate becomes

$$A^+ = 26 \exp(-5.9 \, v_w^+) \qquad (69)$$

The nondimensional form of the inner eddy viscosity laws for no mass transfer at the wall are:

19

Van Driest [ref. 22]

$$\varepsilon_i^+ = X_1 \left\{ 1 - \exp\left[- X_2 \left(\frac{\hat{c}_{f_\infty}}{2}\right)^{1/2} \right] \right\} |F'| \tag{70}$$

Patankar and Spalding [ref. 23]

$$\varepsilon_i^+ = X_1 \left\{ 1 - \exp\left[- X_2 \left(\frac{\hat{c}_{f_\infty}}{2} - \frac{y}{\rho} \rho_e u_e \frac{du_e}{dx}\right)^{1/2} \right] \right\} |F'| \tag{71}$$

Cebeci and Smith [ref. 11]

$$\varepsilon_i^+ = X_1 \left\{ 1 - \exp\left[- X_2 \left(\left|\frac{\hat{c}_{f_\infty}}{2} - \frac{y}{\rho} \rho_e u_e \frac{du_e}{dx}\right|\right)^{1/2} \right] \right\} |F'| \tag{72}$$

Absolute Value of the Pressure Gradient

$$\varepsilon_i^+ = X_1 \left\{ 1 - \exp\left[- X_2 \left(\frac{\hat{c}_{f_\infty}}{2} + \frac{y}{\rho} \rho_e u_e \left|\frac{du_e}{dx}\right|\right)^{1/2} \right] \right\} |F'| \tag{73}$$

20

Cebeci [ref. 13]

$$\varepsilon_i^+ = X_1 \left\{ 1 - \exp\left[-\frac{y^+}{A^+} \right] \right\}^2 |F'| \tag{74}$$

where A^+ is given by equation (63). In equations (70)-(74), X_1 and X_2 are defined as:

$$X_1 = \frac{k_1^2 \, y^2 \, \rho^2 \, u_e^2 \, r^j}{\varepsilon_{VD} \, \mu \, (2\xi)^{1/2}} \tag{75}$$

and

$$X_2 = \frac{y\rho}{26\mu \, \sqrt{\varepsilon_{VD}}} \tag{76}$$

Reichardt [ref. 24]

$$\varepsilon_i^+ = \frac{0.4y}{\mu} \left(\frac{\hat{c}_{f_\infty} \rho}{2\varepsilon_{VD}} \right)^{1/2} - 4.4 \tan h \left[\frac{y}{11\mu} \left(\frac{\hat{c}_{f_\infty} \rho}{2\varepsilon_{VD}} \right)^{1/2} \right] \tag{77}$$

The inner eddy viscosity law for the case of mass injection is (Cebeci [ref. 13])

$$\varepsilon_i^+ = X_1 \left\{ 1 - \exp\left(-\frac{y^+}{A^+} \right) \right\}^2 |F'| \tag{78}$$

where A^+ is given by equation (68) or equation (69).

C. Outer Eddy Viscosity Expression

The above expressions for the inner eddy viscosity have been employed in combination with the Clauser outer eddy viscosity as modified by Klebanoff [ref. 25] and is expressed in nondimensional form as

$$\varepsilon_o^+ = k_2 \, u_e \, \frac{\delta_k^*}{a^*} \, \gamma \tag{79}$$

where δ_k^* is the incompressible boundary-layer displacement thickness

$$\frac{\delta_k^*}{a^*} = \varepsilon_{VD} \int_0^{y_e} \left(1 - \frac{u}{u_e}\right) dy \tag{80}$$

and γ is Klebanoff's intermittancy factor

$$\gamma = \left[1 + 5.5\left(\frac{y}{\delta}\right)^6\right]^{-1} \tag{81}$$

The inner eddy viscosity, ε_i^+, applies from the wall outward to the point where $\varepsilon_i^+ = \varepsilon_o^+$. For turbulent flow the enthalpy, viscosity, and equations of state are given by equations (20)-(24), and the thermodynamic and transport properties for an equilibrium gas are determined by the method given in Appendix A.

6.1.4 Turbulent Boundary-Layer

Equations Expressed in Levy-Lees Variables

Proceeding in the same manner as for the laminar boundary-layer equations (Section 6.1.2), the equations for turbulent flow are expressed in Levy-Lees variables as: (Cebeci, Smith, and Mosinskis

[ref. 12]):

Continuity

$$2\xi \ F_\xi + V' + F = 0 \tag{82}$$

Momentum

$$2\xi \ F \ F_\xi + V \ F_\eta = \beta\left(\frac{\rho_e}{\rho} - F^2\right) + (C(1 + \epsilon^+) \ F')' \tag{83}$$

Energy

$$2\xi \ Fg_\xi + Vg' = \frac{C}{Pr}\left(1 + \epsilon^+ \frac{Pr}{Pr_t}\right) g''$$

$$+ \left[\frac{C}{Pr}\left(1 + \epsilon^+ \frac{Pr}{Pr_t}\right)\right]' g' + \frac{u_e^2}{H_e}\left\{\left(1 - \frac{1}{Pr}\right)\ [C' \ FF'\right.$$

$$\left. + CF'^2 + CF''] + CFF'\left(1 - \frac{1}{Pr}\right)'\right\} \tag{84}$$

where

$$V = \frac{2\xi}{\rho_e \ u_e \ \mu_e \ r^{2j}}\left[f' \ \eta_x + \frac{(\rho v + \overline{\rho'v'}) \ r^j}{(2\xi)^{1/2}}\right] \tag{85}$$

or at the stagnation point

$$V = \frac{\rho v + \overline{\rho' v'}}{\left[\rho_e \, \mu_e \, \frac{du_e}{dx} \, (j+1) \right]^{1/2}} \qquad (86)$$

6.1.5 Boundary Conditions for the Governing Equations

The boundary conditions at the wall, $\eta = 0$, and at the outer edge of the boundary-layer, $\eta = \eta_e$, for equations (34)-(40) and (82)-(86) are:

$$\text{at } \eta = 0: \quad F = 0; \quad g = \frac{H_w}{H_e} = \frac{h_w}{H_e}; \quad V = V_w$$

and $\qquad\qquad\qquad (87)$

$$\text{at } \eta = \eta_e: \quad F = 1; \quad g = 1$$

6.2 Numerical Solution Procedure

The conservation equations for laminar or turbulent flow have been solved using an implicit finite-difference scheme. The numerical method is the one employed by Davis [ref. 9] and requires that the governing equations be expressed in the general parabolic form

$$W'' + A_1 W' + A_2 W + A_3 + A_4 W_\xi = 0 \qquad (88)$$

where W is the dependent variable and the coefficients are functions of ξ, η and W.

In the following sections, the conservation equations are expressed in the general parabolic form, equation (88), and the finite-difference scheme is described.

24

6.2.1 Standard Parabolic Form of the Governing Equations

The governing equations are expressed in the form of equation
(88) for a perfect gas or an equilibrium gas mixture as:

Momentum

$$F'' + A_1 F' + A_2 F + A_3 + A_4 F_\xi = 0 \qquad (89)$$

where

$$A_1 = \frac{C'}{C} + \frac{\overline{A_o'}}{\overline{A_o}} - \frac{V}{A_o}$$

$$A_2 = - \beta F / A_o$$

$$A_3 = \beta \frac{\rho_e}{\rho} / A_o$$

$$A_4 = - 2\xi F / A_o$$

A_o is defined for laminar and turbulent flow as

$$A_o = C \quad \text{(for laminar flow)}$$

$$A_o = C (1 + \epsilon^+) \quad \text{(for turbulent flow)}$$

and

$$\overline{A_o} = A_o / C$$

Energy

$$g'' + A_1 g' + A_2 g + A_3 + A_4 g_\xi = 0 \qquad (90)$$

where

$$A_1 = \frac{C'}{C} + \frac{\overline{A_o'}}{A_o} - \frac{V}{A_o}$$

25

$$A_2 = 0$$

$$A_3 = \frac{u_e^2}{H_e} \left(1 - \frac{1}{Pr}\right) \left[\frac{C'}{C\bar{A}_o} FF' + \frac{F'^2}{\bar{A}_o} + \frac{FF''}{\bar{A}_o}\right] \quad \text{(for a perfect gas)}$$

$$A_3 = \frac{u_e^2}{H_e} C_1 \left[\left[\left(\frac{C'}{C} + \frac{C_1'}{C_1}\right) FF' + F'^2 + FF''\right]\right] / \bar{A}_o \quad \text{(for an equilibrium gas)}$$

$$A_4 = - 2\xi F / A_o$$

$$A_o = \frac{C}{Pr} \quad \text{(for laminar flow)}$$

$$A_o = \frac{C}{Pr} \left(1 + \epsilon^+ \frac{Pr}{Pr_t}\right) \quad \text{(for turbulent flow)}$$

$$\bar{A}_o = \frac{A_o}{C}$$

and

$$C_1 = 1 - \frac{1}{Pr}$$

Continuity

The solution of the continuity equation is determined by numerical integration of the expression

$$V = V_w - \int_o^{\eta_e} (2\xi F_\xi + F) \, d\eta \tag{91}$$

after each iteration of the momentum and energy equations. The integration is performed using the trapizoid rule.

26

6.2.2 Derivation of the Finite-Difference Solution Procedure

The finite-difference scheme used to solve the boundary-layer equations is an implicit method of the Crank-Nicolson type [ref. 5], which has been applied successfully by a number of authors; for example, Davis [ref.9], Blottner [ref. 1] and Harris [ref. 3].

The boundary layer is considered as a network of nodal points with a varying step size in the normal coordinate direction as shown schematically in the figure below
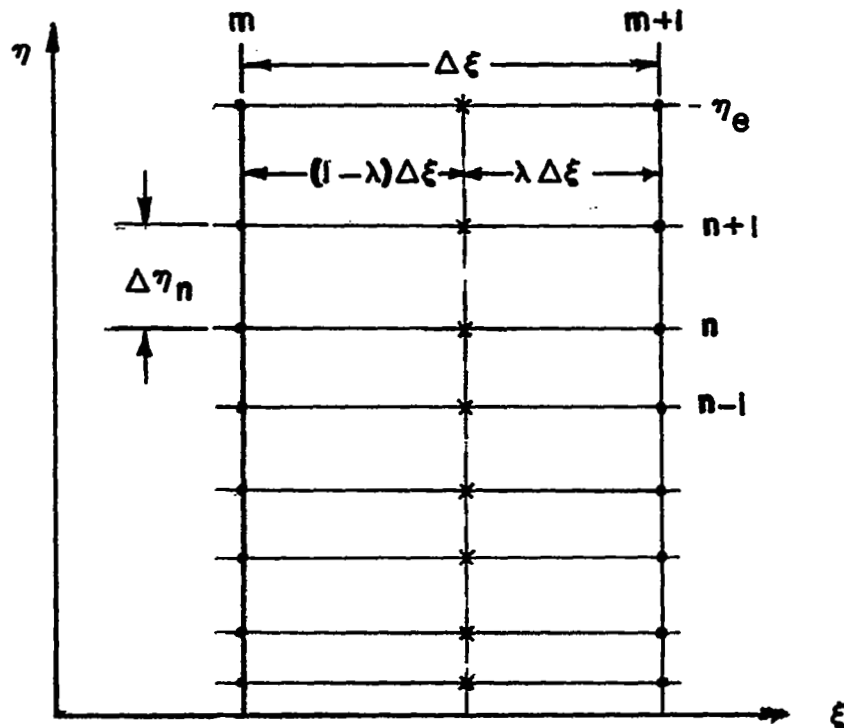
For convenience, equation (88) is expressed at (m,n) and (m+1,n) as

$$\left(\frac{\partial W}{\partial \xi}\right)^n_m = G^n_m \tag{92}$$

and

$$\Big|^n_{m+1} = G^n_{m+1} \tag{93}$$

If it is assumed that the dependent variable is known at the points (m,n) and (m+1,n), Taylor series expansions for $W^n_{m+(1-\lambda)}$ gives

$$W^n_{m+(1-\lambda)} = W^n_m + (1-\lambda) \, \Delta\xi \left(\frac{\partial W}{\partial \xi}\right)^n_m$$

$$+ \frac{(1-\lambda)^2 \, \Delta\xi^2}{2} \left(\frac{\partial^2 W}{\partial \xi^2}\right)^n_m$$

$$+ \frac{(1-\lambda)^3 \, \Delta\xi^3}{3!} \left(\frac{\partial^3 W}{\partial \xi^3}\right)^n_m + \cdots + \tag{94}$$

and

$$W^n_{m+(1-\lambda)} = W^n_{m+1} - \lambda\Delta\xi \left(\frac{\partial W}{\partial \xi}\right)^n_{m+1}$$

$$+ \frac{\lambda^2 \, \Delta\xi^2}{2} \left(\frac{\partial^2 W}{\partial \xi^2}\right)^n_{m+1} - \frac{\lambda^3 \, \Delta\xi^3}{3!} \left(\frac{\partial^3 W}{\partial \xi^3}\right)^n_{m+1} + \cdots + \tag{95}$$

where

$$0 \leq \lambda \leq 1$$

28

Noting that

$$\left(\frac{\partial^2 W}{\partial \xi^2}\right)^n_{m+1} = \left(\frac{\partial^2 W}{\partial \xi^2}\right)^n_m + \Delta\xi \left(\frac{\partial^3 W}{\partial \xi^3}\right)^n_m + \cdots +$$

and solving equations (94) and (95) for W^n_{m+1} gives

$$W^n_{m+1} = W^n_m + \Delta\xi \left[(1-\lambda)\left(\frac{\partial W}{\partial \xi}\right)^n_m + \lambda\left(\frac{\partial W}{\partial \xi}\right)^n_{m+1}\right]$$

$$+ \frac{\Delta\xi^2}{2}\left[(1-2\lambda)\left(\frac{\partial^2 W}{\partial \xi^2}\right)^n_m\right] + 0(\Delta\xi^3) \tag{96}$$

or using equations (92) and (93),

$$W^n_{m+1} = W^n_m + \Delta\xi[(1-\lambda) G^n_m + \lambda G^n_{m+1}]$$

$$+ \frac{\Delta\xi^2}{2}\left[(1-2\lambda)\left(\frac{\partial G}{\partial \xi}\right)^n_m\right] + 0(\Delta\xi^3) \tag{97}$$

Davis [ref. 9] approximated equation (97) as

$$W^n_{m+1} = W^n_m + \Delta\xi[(1-\lambda) G^n_m + \lambda G^n_{m+1}] \tag{98}$$

and evaluated the A_i in equation (88) at the points (m+1,n). Following Davis' formulation, the normal derivatives in equation (88) are replaced by Taylor series expansions for varying step sizes in the η direction at the point m+1,n as

29

$$(W')_{m+1}^{n} = \frac{\Delta\eta_{n-1}}{\Delta\eta_n(\Delta\eta_n + \Delta\eta_{n-1})} W_{m+1}^{n+1}$$

$$+ \frac{\Delta\eta_n - \Delta\eta_{n-1}}{\Delta\eta_n \, \Delta\eta_{n-1}} W_{m+1}^{n} - \frac{\Delta\eta_n}{\Delta\eta_{n-1}(\Delta\eta_n + \Delta\eta_{n+1})} W_{m+1}^{n-1}$$

$$+ 0(\Delta\eta^2) \tag{99}$$

and

$$(W'')_{m+1}^{n} = \frac{2}{\Delta\eta_n(\Delta\eta_n + \Delta\eta_{n-1})} W_{m+1}^{n+1} - \frac{2}{\Delta\eta_n \, \Delta\eta_{n-1}} W_{m+1}^{n}$$

$$+ \frac{2}{\Delta\eta_{n-1}(\Delta\eta_n + \Delta\eta_{n-1})} W_{m+1}^{n-1} + 0(\Delta\eta^2) \tag{100}$$

Evaluating the A_i at $m+1, n$ and letting

$$W_{1_n} = W_m^n$$

and

$$W_{2_n} = W_{m+1}^n$$

gives upon substituting equations (99) and (100) into equation (98)

$$A_n \, W_{2_{n-1}} + B_n \, W_{2_n} + C_n \, W_{2_{n+1}} = D_n; \quad 2 \leq n \leq N - 1 \tag{101}$$

where

$$A_n = \frac{2 - A_{1_n} \Delta\eta_n}{\Delta\eta_{n-1}(\Delta\eta_n + \Delta\eta_{n-1})} \lambda$$

$$B_n = \left[\frac{-2 + A_{1_n} (\Delta \eta_n - \Delta \eta_{n-1})}{\Delta \eta_n \Delta \eta_{n-1}} + A_{2_n} \right] \lambda + \frac{A_{4_n}}{\Delta \xi}$$

$$C_n = \frac{2 + A_{1_n} \Delta \eta_{n-1}}{\Delta \eta_n (\Delta \eta_n + \Delta \eta_{n-1})} \lambda$$

and

$$D_n = - [W_{1_n}'' + A_{1_n} W_{1_n}' + A_{2_n} W_{1_n}] (1 - \lambda) - A_{3_n} + \frac{A_{4_n} W_{1_n}}{\Delta \xi}$$

Assuming that

$$W_{2_n} = E_n W_{2_{n+1}} + F_n \tag{102}$$

is valid throughout the boundary-layer (Richtmyer [ref. 26]), then $W_{2_{n-1}}$ is given by

$$W_{2_{n-1}} = E_{n-1} W_{2_n} + F_{n-1} \tag{103}$$

Using equation (103) in equation (101) and solving for W_{2_n} and comparing with equation (102) gives

$$E_n = \frac{-C_n}{B_n + A_n E_{n-1}} \tag{104}$$

and

$$F_n = \frac{D_n - A_n F_{n-1}}{B_n + A_n E_{n-1}} \tag{105}$$

31

The values of E_1 and F_1 are determined by the boundary condition for W.

6.2.3 Spacing of Node Points in the Normal Coordinate Direction

The finite-difference solution procedure has been developed for a variable spacing of the node points in the normal (η) coordinate direction. This permits a close spacing of points in the region near the wall where the variation of fluid and dynamic properties is greatest. The procedure employed is that given by Cebeci, Smith, and Mosinskis [ref. 12].

Using this procedure, the ratio of the adjacent intervals is a constant expressed as

$$k = \frac{\Delta\eta_n}{\Delta\eta_{n-1}} \tag{106}$$

The distance to the nth point measured from the wall boundary is given by

$$\eta_n = \Delta\eta_1 \frac{k^n - 1}{k - 1} \tag{107}$$

where

$$\Delta\eta_1 = \eta_e \frac{k - 1}{k^N - 1} \tag{108}$$

N is the number of strips in the boundary-layer, and η_e is the location of the boundary-layer outer edge.

The values of the constant k for laminar or turbulent flow were determined by numerical experiments. A number of solutions were obtained for laminar and turbulent boundary layer flows at supersonic

conditions considering both adiabatic and cold wall cases. The value of k was varied over the range from 1 to 1.5 with η_e varied from 4 to 12 for laminar flow and from 75 to 200 for turbulent flow. The results of these test cases were compared with experimental data to determine a value of k which gave good agreement with experimental data and where the solution showed little change for different values of η_e.

The values selected were:

$$k = 1.04 \text{ and } \eta_e = 6 \text{ for laminar flow}$$

$$k = 1.09 \text{ and } \eta_e = 100 \text{ for turbulent flow}$$

The above values correspond to a value of N = 100 in equation (108).

Similar tests were made varying N from 50 to 500. An N of 50 was found to be unsatisfactory for most cases, but values of N greater than 100 did not improve the solutions which were obtained.

6.2.4 Convergence Criteria

A suitable convergence test may be established for laminar boundary-layer flows by comparing F_W' at successive iterates of the solution. This type of convergence test was employed by Davis [ref. 9] and Cebeci and Smith [ref. 11].

For turbulent flows, Cebeci and Smith found that a second requirement based on successive iterates of the boundary-layer displacement thickness was necessary to obtain satisfactory solutions. They continued the iteration procedure until both tests were satisfied.

For the present calculations provisions were made to establish convergence by comparison of successive iterates of both F_W' and g_W' or

33

by comparing successive iterates of both F and g at all points in the boundary layer. The convergence test are expressed as

Derivative Test

$$\left| 1 - \frac{F_W'^{(k+1)}}{F_W'^{(k)}} \right| \leq \epsilon_d$$

and

$$\left| 1 - \frac{g_W'^{(k+1)}}{g_W'^{(k)}} \right| \leq \epsilon_d$$

Function Test

$$\left| 1 - \frac{F_n^{(k+1)}}{F_n^{(k)}} \right| \leq \epsilon_f$$

and

$$\left| 1 - \frac{g_n^{(k+1)}}{g_n^{(k)}} \right| \leq \epsilon_f$$

where k is the iteration number and ϵ_d and ϵ_f are prescribed values. The function test with $\epsilon_f = 0.01$ and the additional requirement that the number of iterations at the new location be two or greater was found to be satisfactory for both laminar and turbulent flows. A value of $\epsilon_d = 0.001$ was used with the derivative test, but this test is in general not recommended for turbulent boundary-layer calculations.

6.3 Specification of Body Geometry

The geometry of a given configuration is considered as a series
of segments of fourth order and requires that the coordinates, z, x,
and r be given in tabular form. Since transverse-curvature effects
have been neglected in the governing equations, provisions have not
been made to distinguish between different body sections. Thus, some
inaccuracies are introduced in regions near the intersection points of
different contours. For problems requiring a specified pressure
and/or a wall temperature distribution, these data are entered in tab-
ular form at the same points as the geometry data. The temperature is
entered in °R and the pressure is given as P/P_o or P/P_o'.

To insure accurate interpolation and/or differentiation of the
temperature and pressure data in regions of large gradients, it is nec-
essary to have a close spacing of the coordinate data.

For nozzles, at least 30 points should be entered in the throat
region, and for blunt bodies, at least 50 points should be entered
for the nose section. A maximum of 500 points may be tabulated, and
the minimum number permitted is 5. Best results were obtained when
the maximum ratio of adjacent step sizes in z were not greater than
1.25.

The body shapes which have been considered are blunt bodies,
wedges, flat plates, and nozzles.

6.4 Fluid Properties at the Outer Edge of the Boundary-Layer

In the present method for solving the boundary-layer equations,
the effects of mass entrainment of the outer inviscid vortical stream-
line into the expanding boundary-layer on a blunt body is neglected.

35

Therefore, the edge conditions may be specified by conditions on the body surface for the inviscid flow of the gas. The procedures employed for specifying the outer edge conditions for the different geometries and gas models is discussed in the following sections.

6.4.1 Axisymmetric Nozzles

The edge conditions for nozzle flows of a perfect or an equilibrium gas may be specified by assuming a one-dimensional expansion or the expansion can be determined for a specified pressure distribution where the pressure is given in tabular form as indicated in Section 6.3. The procedures employed for the different cases are discussed below.

A. One-Dimensional Expansion of a Perfect Gas

For a one-dimensional expansion of a perfect gas, tables of Mach numbers and the corresponding area ratios are computed within the boundary-layer computer program using the relation

$$A/A_t = \frac{1}{M} \left[\frac{1 + \frac{\gamma-1}{2} M^2}{\frac{\gamma+1}{2}} \right]^{\frac{\gamma+1}{2(\gamma-1)}} \tag{109}$$

at intervals of 0.01 in Mach number for $M < 2$ and in intervals of 0.05 for $M \geq 2$.

After the above tables have been generated, the Mach number at the nozzle exit is determined by five point interpolation in the tables of area ratio and Mach number with the area ratio as the independent

variable. The exit Mach number is denoted by M_∞.

The free-stream pressure, temperature, velocity, density, viscosity, and Reynolds number are then computed using the relations

$$P_\infty^* = \frac{P_o^*}{\left[1 + \frac{\gamma-1}{2} M_\infty^2\right]^{\gamma/(\gamma-1)}} \tag{110}$$

$$T_\infty^* = \frac{T_o^*}{1 + \frac{\gamma-1}{2} M_\infty^2} \tag{111}$$

$$U_\infty^* = M_\infty \sqrt{\gamma \; RGAS \; T_\infty^*} \tag{112}$$

$$\rho_\infty^* = \frac{P_\infty^*}{RGAS \; T_\infty^*} \tag{113}$$

$$\mu_\infty^* = \mu_{ref_1}^* \left[\frac{T_{ref_1}^* + c^*}{T_\infty^* + c^*}\right] \left(\frac{T_\infty^*}{T_{ref_1}^*}\right)^{3/2} \tag{114}$$

and

$$R_{e_\infty} = \frac{\rho_\infty^* U_\infty^* L^*}{\mu_\infty^*} \tag{115}$$

37

where $\mu^*_{ref_1}$, $T^*_{ref_1}$ and L^* are reference values of viscosity, temperature and length.

Corresponding to the points in the geometry arrays, tables of the edge pressure and velocity are computed in nondimensionalized form using the expressions

$$P_e = \frac{P_o}{\left[1 + \frac{\gamma-1}{2} M_L^2\right]^{\gamma/(\gamma-1)}} \qquad (116)$$

$$u_e = \sqrt{(T_o - T_e)2} \qquad (117)$$

where

$$P_e = \frac{P^*_e}{P^*_{ref}} = \frac{P^*_e}{\rho^*_\infty U^{*2}_\infty} = \frac{P^*_e}{\gamma M^2_\infty P^*_\infty} \qquad (118)$$

$$T_o = \frac{T^*_o}{T^*_{ref}} = \frac{T^*_o c^*_p}{U^{*2}_\infty} = \frac{T^*_o}{(\gamma-1) M^2_\infty T^*_\infty} \qquad (119)$$

$$T_e = \frac{T_o}{1 + \frac{\gamma-1}{2} M_L^2} \qquad (120)$$

and M_L is the local Mach number determined for the area ratio at the given point in the geometry arrays.

At a local solution station $x = x_1 + \Delta x$, P_e, u_e and M_L are determined by interpolation, and T_e, ρ_e and μ_e are computed using

38

$$T_e = T_o - u_e^2/2 \qquad (121)$$

$$\rho_e = \frac{\gamma}{\gamma-1} \frac{P_e}{T_e} \qquad (122)$$

$$\mu_e = \frac{1 + \bar{c}}{T_e + \bar{c}} \, T_e^{3/2} \qquad (123)$$

or

$$\mu_e = T_e^{\omega} \qquad (124)$$

where

$$\rho_e = \frac{\rho_e^*}{\rho_{ref}^*} = \frac{\rho_e^*}{\rho_\infty^*}$$

and

$$\mu_e = \frac{\mu_e^*}{\mu_{ref}^*}$$

The velocity derivative $\dfrac{du_e}{dx}$ is evaluated numerically.

B. Pressure Distribution Specified for a Perfect Gas Solution

For solutions where the pressure distribution is input to the computer program, the outer edge conditions are computed in the same manner as for the one-dimensional expansion solution with the exception that the Mach number table is computed from the input pressure distribution using

$$M_L = \left[\frac{2}{\gamma-1} \left(\frac{P}{P_o} \right)^{-\frac{\gamma}{\gamma-1}} - 1 \right]^{1/2} \qquad (125)$$

39

After computing the Mach number array using equation (125), equations (116)-(124) are evaluated using the local Mach number data corresponding to the given pressure distribution, and $\frac{du_e}{dx}$ is evaluated numerically.

C. One-Dimensional Expansion of a Reacting
Gas in Chemical Equilibrium

The boundary-layer edge conditions for the equilibrium gas case were determined by the solution of the inviscid equations of motion for the given mixture of perfect gases. The data which must be given for the boundary-layer solution are:

$$A/A_t, \ M, \ U^*, \ \tilde{P}, \ \text{and} \ \tilde{h}$$

These data are tabulated for use with a table-look-up procedure. For a one-dimensional expansion of the gas mixture, the area ratio is used as the independent variable to determine the local edge conditions for the given body geometry. Since the area ratio is not a monotone function over the length of the nozzle, it was found to be more satisfactory to create a secondary expansion data set on a scratch unit expressed in terms of z or x. The locations of z and x were determined for a given A/A_t by interpolation and the secondary data set was written as unformatted records in the order

$$z, \ x, \ M, \ U^*, \ \tilde{P} \ \text{and} \ \tilde{h}$$

This operation is performed within the boundary-layer program and requires no additional preparation of the expansion data. In addition

40

to the expansion data tape, a tape unit is required for the tables of thermodynamic and transport properties of the equilibrium gas mixture. These tables are written at constant $\tilde{P}$ with the temperature decreasing. The data in each table are written as unformatted records in the form $(P; T^*, \tilde{h}, \tilde{\rho}, \mu^*, c_p, Pr)$. The expansion data and the tables of thermodynamic and transport properties were obtained using two modified versions of the computer program developed by Lordi et al. [ref. 20]. A description of these modifications are given in Appendix A.

After the secondary expansion data set has been written, local values of M, U^*, $\tilde{P}$ and $\tilde{h}$ are determined by interpolation with either z or x as the independent variable. With the local values of $\tilde{P}$ and $\tilde{h}$ as independent variables, the local values of T^*, $\tilde{\rho}$, μ^*, c_p and Pr are found by interpolation in the tables of thermodynamic and transport properties. The nozzle exit conditions are taken as the free-stream conditions and the reference conditions retain the same definitions in the dimensional form with the exception of μ^*_{ref}. The reference viscosity for the equilibrium cases may be chosen arbitrarily and does not necessarily correspond to the reference temperature and reference pressure. The reference viscosity employed is computed using Sutherland's law.

D. Equilibrium Gas Solutions with the Pressure Distribution Given

If the pressure distribution is given, the local value of $\tilde{P}$ is determined by interpolation in the given pressure distribution table. With this value of $\tilde{P}$ as the independent variable, local values of M, U^* and $\tilde{h}$ are determined by interpolation of the data on the expansion

41

data tape. It is not necessary for $\tilde{P}$ to be a monotone function. The remaining edge conditions are determined by interpolation in the tables of thermodynamic and transport properties with $\tilde{P}$ and $\tilde{h}$ as the independent variables as in paragraph C above.

6.4.2 Blunt Bodies

The solution of the boundary-layer equations for flows over blunt bodies requires that the pressure distribution be specified. The remaining edge conditions are determined for a perfect gas or an equilibrium mixture of perfect gases as discussed below.

A. Isentropic Expansion of a Perfect Gas Along
the Body Streamline From the Stagnation Point

For these solutions, the pressure distribution is entered in the table as P/P_o' where P_o' is the stagnation pressure behind a normal shock expressed in nondimensionalized form as

$$P_o' = \frac{\left[\dfrac{(\gamma+1)\, M_\infty^2}{2}\right]^{\frac{\gamma}{\gamma-1}} \left[\dfrac{\gamma+1}{2\gamma\, M_\infty^2 - (\gamma-1)}\right]^{\frac{1}{\gamma-1}}}{\gamma\, M_\infty^2}$$

The reference conditions are based on the flow properties ahead of the bow shock. Since the inviscid flow along the body streamline is isentropic, the edge conditions are computed in the same way as for a nozzle with the pressure distribution given and is described in paragraph C of Section 6.4.1 above. It is noted that the expansion is from the stagnation conditions behind the normal shock.

42

B. Isentropic Expansion of an Equilibrium Gas

Along the Body Streamline from the Stagnation Point

For this case, the equilibrium expansion data are determined for
the stagnation pressure and temperature behind a normal shock for the
given mixture of perfect gases and free-stream conditions. The free-
stream and reference conditions with the exception of the reference
viscosity are determined by the fluid properties ahead of the bow
shock. The edge conditions at local points along the body are deter-
mined in the same manner as for an equilibrium solution for a nozzle
with the pressure distribution given and is discussed in 6.4.1 D.

6.4.3 Wedges and Flat Plates

The edge conditions for wedges and flat plates are constants cor-
responding to conditions behind an oblique shock or the free-stream
conditions respectively. The computer program for the solution of the
boundary-layer equations is suitable for both wedges and flat plates
if a perfect gas is considered. The solution of wedges for an equili-
brium gas requires modification of the boundary-layer computer program.
Thus, only flat plates are considered for equilibrium chemistry solu-
tions. The procedure for determining the edge conditions for a per-
fect gas and an equilibrium gas mixture is discussed below.

A. Edge Conditions for Flat Plates and

Wedges for a Perfect Gas Solution

The pressure, temperature, and velocity at the outer edge of the
boundary-layer are computed from the oblique shock relations and are
expressed in nondimensional form by the relations

$$P_e = \frac{2\gamma M_\infty^2 \sin^2 \sigma - (\gamma-1)}{(\gamma+1) \ \gamma \ M_\infty^2} \qquad (126)$$

$$T_e = \frac{[2\gamma M_\infty^2 \sin^2 \sigma - (\gamma-1)][(\gamma-1) M_\infty^2 \sin^2 \sigma + 2]}{(\gamma-1) M_\infty^2 (\gamma+1)^2 M_\infty^2 \sin^2 \sigma} \qquad (127)$$

and

$$u_e = \left[\frac{[1 - 4(M_\infty^2 \sin^2 \sigma - 1)(\gamma M_\infty^2 \sin^2 \sigma + 1)]}{(\gamma+1)^2 M_\infty^4 \sin^2 \sigma} \right] \qquad (128)$$

The density and viscosity are computed using equations (122) and (123) or (124).

B. Flat-Plate Solutions for Equilibrium Gases

The solution of flat plates in an equilibrium gas requires the use of the tables of thermodynamic and transport properties for the given gas mixture (Appendix A). The free-stream pressure, temperature, and velocity are input data to the boundary-layer computer program. Using the free-stream pressure and temperature as independent variables, the values of h_∞^*, ρ_∞^*, μ_∞^*, and $c_{p_\infty}^*$ are determined by the use of interpolation in the tables of thermodynamic and transport properties.

6.4.4 Evaluation of the Longitudinal Coordinate-ξ

The coordinate ξ is evaluated by equation (26) numerically using a modified Simpson's rule (Davis [ref. 9]), and is expressed as

$$\xi_{m+1} = \xi_m + [U_{e_m} r_m^{2j} \rho_{e_m} \mu_{e_m}$$

$$+ 4(U_{e_{m+1/2}} r_{m+1/2}^{2j} \rho_{e_{m+1/2}} \mu_{e_{m+1/2}}) \qquad (129)$$

$$+ U_{e_{m+1}} r_{m+1}^{2j} \rho_{e_{m+1}} \mu_{e_{m+1}}] \Delta x/6$$

where the subscripts refer to the edge conditions at the points x_m, $x_m + \frac{\Delta x}{2}$, and $x_m + \Delta x$ respectively.

6.5 Solution for the Initial Profile Data

The equations governing the laminar or turbulent boundary-layer flow of a perfect gas or an equilibrium mixture of perfect gases reduce to a system of ordinary non-linear differential equations at $x = 0$. However, for fully developed turbulent flow, the eddy viscosity cannot be evaluated at $x = 0$, for flat plates or nozzles. The limiting form of the differential equations are employed at $x = 0$ for blunt body flows. The procedures used to obtain the starting profile data are discussed below.

6.5.1 Initial Profiles for the Solution
of the Laminar Boundary-Layer Equations

To start the solution of the boundary-layer equations, initial guesses of the profiles for the dependent variables F, g, and V are required. At the leading edge or stagnation point, the equations are ordinary differential equations, and the initial profile data are determined by an iteration procedure using the implicit finite-

difference scheme developed in 6.2.2.

Initial guesses are made for the profiles and for the first iteration. These estimates are denoted by the subscripts $(\ )_1$ and $(\ )_c$ respectively and the k+1 iterate is denoted by the subscript $(\ )_2$.

The initial guesses of the profile data are assumed to have the forms given below:

at $\eta < \eta_e$

$$F_1 = F_c = 1 - e^{-\eta}$$

$$F_1' = F_c' = e^{-\eta}$$

$$F_1'' = F_c'' = - e^{-\eta}$$

$$g_1 = g_c = g_w + (1 - g_w) F_1$$

$$g_1' = g_c' = (1 - g_w) F_1'$$

$$g_1'' = (1 - g_w) F_1''$$

at $\eta = \eta_e$

$$F_1 = 1$$

$$F_1' = 0$$

$$F_1'' = 0$$

$$g_1 = 1$$

$$g_1' = 0$$

$$g_1'' = 0$$

The solution of the continuity equation is assumed as

$$V_c = V_w - \eta$$

and the temperature distribution is computed from the g profile using the definitions

$$\theta = \frac{T}{T_e} = \frac{h}{h_e}$$

$$g = \frac{H}{H_e} = \frac{h + \frac{1}{2} u_e^2 \, F^2}{h_e + \frac{1}{2} u_e^2}$$

or

$$g = \frac{\theta + \frac{1}{2} \frac{u_e^2}{h_e} F^2}{1 + \frac{1}{2} \frac{u_e^2}{h_e}}$$

Solving for θ gives

$$\theta = \left(1 + \frac{1}{2} \frac{u_e^2}{h_e} \right) g_c - \frac{1}{2} \frac{u_e^2}{h_e} F_c^2$$

and

$$\theta' = \left(1 + \frac{1}{2} \frac{u_e^2}{h_e} \right) g_c' - \frac{u_e^2}{h_e} F_c F_c'$$

For a perfect gas

$$\frac{\rho}{\rho_e} = \frac{1}{\theta}$$

and the Chapman-Rubesin factor, C, is assumed unity across the boundary-layer.

Using the above guesses of the profile data, the governing equations are solved to determine F_2, F_2', F_2'', g_2, g_2', and g_2''. The subscripted variables $(\ )_1$ and $(\ )_c$ are set equal to the variables with

subscript $(\ )_2$ and new values of θ, θ', $\frac{\rho_e}{\rho}$, V_c, and C are then computed where

$$V_c = V_w \int_0^{\eta_c} (2\xi\ F_{c\xi} + F_c)\ d\eta$$

$$C = \frac{\rho\mu}{\rho_e\ \mu_e} = \theta^{1/2}\ \frac{(1 + \bar{c})}{(\theta + \bar{c})} \quad \text{(Sutherland's law)}$$

or

$$C = \theta^{(\omega-1)} \quad \text{(power law)}$$

$$C' = \frac{\partial C}{\partial \theta}\ \theta'$$

The procedure is repeated until the convergence criteria of section 6.2.4 is satisfied.

For an equilibrium gas, the initial guesses of the profile data are assumed to be the profile data corresponding to the converged solution for a perfect gas described above. Using the perfect gas profiles of F and g, the remaining thermodynamic and transport properties are determined by use of the table-look-up procedure. Derivatives of θ and C are evaluated numerically for the equilibrium gas. The iteration procedure is the same as for the perfect gas case.

6.5.2 Initial Profiles for the
Turbulent Boundary-Layer Equations

The solution of flat plates, wedges, or nozzle flows assuming fully developed turbulent flow assumes that the profiles at x = 0 and x = 0.001 are similar. This procedure has been adopted because the

48

values of ϵ^+ are zero at $x = 0$. With this exception and assuming an initial profile for ϵ^+ as zero, the starting procedure is the same as for the laminar boundary layer.

An alternate method for starting these solutions is to use the laminar starting profile at $x = 0$ and assume an instantaneous transition to turbulent flow at $x > 0.001$. Both methods have been used and the differences in the resulting solutions are insignificant.

For blunt body solutions, the turbulent starting profiles are determined at $x = 0$ using the limiting form of the governing equations.

The initial guesses of the starting profiles for the equilibrium solution is determined from the converged profiles for a perfect gas. Using these profiles, the iteration procedure is continued using the equilibrium gas properties until the convergence tests are satisfied.

6.6 Boundary-Layer Paramaters

The definitions of the boundary-layer thicknesses, skin-friction coefficient, heat transfer, heat transfer coefficients, and Stanton numbers which have been used in the boundary-layer calculations are presented in this section. Both the dimensional and nondimensional expressions are given.

Velocity or Boundary-Layer Thickness

The velocity thickness, δ, is assumed to be the value of y^* at $\frac{u^*}{u_e^*} = 0.995$, and is determined by interpolation in the velocity profile array.

Incompressible Displacement Thickness

The incompressible displacement thickness is computed using the

49

two-dimensional definition

$$\delta_k^* = \int_0^{y_e^*} \left(1 - \frac{u^*}{u_e^*}\right) dy^*$$

$$\frac{\delta_k^*}{a^*} = \varepsilon_{VD} \int_0^{y_e} \left(1 - \frac{u}{u_e}\right) dy$$

or

$$\frac{\delta_k^*}{a^*} = \frac{\varepsilon_{VD} (2\xi)^{1/2}}{\rho_e u_e r^j} \int_0^{\eta_e} \frac{\rho_e}{\rho} (1 - F) \, d\eta$$

Compressible Displacement Thickness

Two-dimensional

$$\delta^* = \int_0^{y_e^*} \left(1 - \frac{\rho^* u^*}{\rho_e^* u_e^*}\right) dy^*$$

$$\frac{\delta^*}{a^*} = \varepsilon_{VD} \int_0^{y} \left(1 - \frac{\rho u}{\rho_e u_e}\right) dy$$

or

$$\frac{\delta^*}{a^*} = \frac{\varepsilon_{VD} (2\xi)^{1/2}}{\rho_e u_e r^j} \int_0^{\eta_e} \left(\frac{\rho_e}{\rho} - F\right) d\eta$$

50

Axisymmetric:

The axisymmetric compressible displacement thickness is approximated as; (Cebeci and Mosinskis [ref. 27]):

$$\rho_e^* u_e^* [(r^* + y_e^*)^2 - (r^* + \delta_{Axi}^*)^2] = 2 \int_{r^*}^{r^* + y_e^*} \rho^* u^* r^* dr^*$$

or

$$\frac{\delta_{Axi}^*}{a^*} = r \left[\left(1 + \frac{2\delta^*/a^*}{r} \right)^{1/2} - 1 \right]$$

Momentum Thickness:

$$\theta^* = \int_o^{y_e^*} \frac{\rho^* u^*}{\rho_e^* u_e^*} \left(1 - \frac{u^*}{u_e^*} \right) dy^*$$

$$\frac{\theta^*}{a^*} = \varepsilon_{VD} \int_o^{y_e} \frac{\rho u}{\rho_e u_e} \left(1 - \frac{u}{u_e} \right) dy$$

or

$$\frac{\theta^*}{a^*} = \frac{\varepsilon_{VD} (2\xi)^{1/2}}{\rho_e u_e r^j} \int_o^{\eta_e} F(1 - F) \, d\eta$$

Heat Transfer Rate:

In dimensional variables

$$\dot{q}_w^* = - K_w^* \left[\frac{\partial T^*}{\partial y^*} \right]_w$$

or

$$\dot{q}_w^* = - \frac{\mu_w^*}{Pr_w} \left[\frac{\partial H^*}{\partial y^*} \right]_w$$

In nondimensional form

$$q_w = \frac{\dot{q}^*}{\varepsilon_{VD} \, \rho_{ref}^* \, u_{ref}^{*3}} = - \frac{\mu_w^* \, H_e}{Pr_w} \left(\frac{\partial H}{\partial y} \right)_w$$

or in Levy-Lees variables

$$\dot{q}_w = - \frac{\mu_e \, C_w \, H_e}{Pr_w} \frac{\rho_e \, u_e \, r^j}{(2\xi)^{1/2}} \left(\frac{\partial H}{\partial \eta} \right)_w$$

$\dot{q}_w$ is converted to BTU/ft^2-sec as

$$\dot{q}_w^* = \dot{q}_w \, \rho_{ref}^* \, u_{ref}^{*3} \, \varepsilon_{VD}/778$$

Film Coefficients:

$$hg_1 = \frac{\dot{q}_w^* \, c_p^*}{H_w^* - H_{Aw}^* \, (778)(144)} \quad BTU/in^2\text{-sec-}°R$$

or

$$hg_1 = \frac{\dot{q}_w \, \varepsilon_{VD} \, c_p^*}{(H_w - H_{Aw})} \frac{\rho_{ref}^* \, u_{ref}^*}{(778)(144)} \quad BTU/in^2\text{-sec-}°R$$

52

$$hg_2 = \frac{\dot{q}_w^*}{(H_w^* - H_{Aw}^*)} \frac{32.17}{144} \; lb_m/in^2\text{-sec}$$

or

$$hg_2 = \frac{\dot{q}_w \, \varepsilon_{VD}}{(H_w - H_{Aw})} \frac{\rho_{ref}^* \, u_{ref}^* \; 32.17}{144} \; lb_m/in^2\text{-sec}$$

Stanton Number Definitions:

A. Based on free-stream conditions

$$St_\infty = -\frac{\dot{q}_w^*}{\rho_\infty^* \, u_\infty^* \, (H_e^* - H_w^*)}$$

or

$$St_\infty = -\frac{\dot{q}_w \, \varepsilon_{VD}}{(H_e - H_w)}$$

B. Based on edge conditions

$$St_e = -\frac{\dot{q}_w^*}{\rho_e^* \, u_e^* \, (H_e^* - H_w^*)}$$

or

$$St_e = -\frac{\dot{q}_w}{\rho_e \, u_e \, (H_e - H_w)}$$

Heat Transfer Coefficients:

A. Based on free-stream conditions

53

$$C_{h_\infty} = - \frac{\dot{q}_w^*}{\rho_\infty^* u_\infty^* (H_{Aw}^* - H_w^*)}$$

or

$$C_{h_\infty} = - \frac{\dot{q}_w \, \varepsilon_{VD}}{(H_{Aw} - H_w)}$$

B. Based on edge conditions

$$C_{h_e} = - \frac{\dot{q}_w^*}{\rho_e^* u_e^* (H_{Aw}^* - H_w^*)}$$

or

$$C_{h_e} = - \frac{\dot{q}_w \, \varepsilon_{VD}}{\rho_e u_e (H_{Aw} - H_w)}$$

Skin-Friction Coefficients:

A. Based on free-stream conditions

$$C_{f_\infty} = \frac{2 \, \tau_w^*}{\rho_\infty^* u_\infty^{*2}}$$

or

$$C_{f_\infty} = \frac{2 \, \varepsilon_{VD} \, \mu_e \, C_w \, \rho_e \, u_e \, r^j}{(2\xi)^{1/2}} \left(\frac{\partial F}{\partial \eta} \right)_w$$

B. Based on edge conditions:

$$C_{f_e} = \frac{2 \, \tau_w^*}{\rho_e^* u_e^{*2}}$$

or

$$C_{f_e} = \frac{C_{f_\infty}}{\rho_e u_e^2},$$

VII. RESULTS AND DISCUSSION

The implicit finite-difference scheme developed in Chapter VI has been applied to obtain solutions of laminar and turbulent boundary-layer flows of perfect gases and equilibrium gas mixtures over flat plates, an hyperboloid, a spherically blunted cone, and in axisymmetric nozzles.

Solutions of perfect gas turbulent flows using different expressions for the inner eddy viscosity law are presented in Section 7.1, and are compared with experimental data and/or other numerical solutions for cases where these data were available. Solutions using the equilibrium gas option are presented in Section 7.2, and the solution of boundary-layer flows with mass injection are presented in Section 7.3.

The numerical solutions presented assume either fully developed turbulent or laminar flow; however the boundary-layer computer program described by Miner, Anderson, and Lewis [ref. 28] provides options for either an instantaneous or a continuous transition from laminar to turbulent flow. The continuous transition model is based on the experimental results of Owen [ref. 29] and is discussed in the report on the computer program.

7.1 Perfect Gas Turbulent Boundary-Layer Flows

Solutions of turbulent flows over flat plates and in axisymmetric nozzles using the inner eddy viscosity laws of Van Driest, equation (70), Cebeci and Smith, equation (72), absolute value of the pressure gradient, equation (73), and Reichardt, equation (77), are presented

in this section. The inner eddy viscosity law proposed by Patankar and Spalding, equation (71), was found to be unsatisfactory for flows having a significant favorable pressure gradient and is not considered.

7.1.1 Perfect Gas Solutions for Turbulent Flows Over Flat Plates

For flat-plate flows the inner eddy viscosity laws expressed by equations (70)-(74) are identical and are referred to as the Van Driest model. The inner eddy viscosity law given by equation (77) is referred to as the Reichardt model.

Three flat-plate solutions are presented corresponding to case numbers 20, 26, and 62 of the experimental data given by Coles [ref. 30]. The results of the present numerical method of solution are compared with Coles' experimental data and the solutions of Van Driest [ref. 22] and Dorrance [ref. 31]. The free-stream conditions for the three cases are given in Table I. The free-stream Mach numbers for cases 20, 26, and 62 were 3.701, 2.578, and 4.544 respectively, and the plates were assumed to be adiabatic.

Boundary-layer displacement thicknesses predicted using the Van Driest and Reichardt eddy viscosity models are compared with Coles' experimental data in Figure 2. The displacement thickness predicted using the Van Driest and Reichardt eddy viscosity model were found to differ by less than 3% for the three cases, but the predicted values of displacement thickness differ from Coles' experimental data by as much as 20%. The numerically determined displacement thickness is less than the experimental value in all three cases. The numerical result is in good agreement with experiment for Case 62.

57

The numerically determined velocity profiles at x = 21.48 in. for Case 20 are presented in Figures 3 and 4. The results using either eddy viscosity model are in good agreement with Coles' experimental data. Figure 4 shows the solution given by Van Driest [ref. 22]. Figure 5 shows the eddy viscosity profiles predicted using the Van Driest and Reichardt eddy viscosity models at x = 21.48. The difference in the two models is not significant.

The predicted skin-friction coefficients for the three cases are compared with the solution of Dorrance [ref. 31] and Coles' experimental data in Figure 6. The skin-friction predictions for Cases 20 and 26 are in excellent agreement with both the experimental data and Dorrance's solutions. For Case 62, the present method of solution is in good agreement with the experimental data points for Reynolds numbers greater than 3×10^6, but for $Re_\infty = 1.7 \times 10^6$ the present numerical solution predicts a skin-friction coefficient which is approximately 15% lower than the experimental value. The present method of solution is in better agreement with the experimental data for this case than the solution of Dorrance.

The above results are representative examples of turbulent flat-plate solutions and in all cases considered the numerical results were not significantly influenced by the choice of the inner eddy viscosity law. However, the use of the Reichardt inner law reduced the computing time by a factor of approximately 10 (see Section 7.1.3).

7.1.2 Turbulent Flow of Perfect Gases in Axisymmetric Nozzles

The present method of solution has been used to solve three axisymmetric nozzles, and the results are compared with the integral method

of solution developed by Elliott, Bartz, and Silver [ref. 15] and experimental data where the data were available. The inner eddy viscosity laws of Van Driest, equation (70), Cebeci and Smith, equation (72), absolute value of the pressure gradient, equation (73), and Reichardt, equation (77), have been considered for the sample case given by Elliott, Bartz, and Silver [ref. 15].

A. Elliott, Bartz, and Silver Sample Case

The problem considered consists of a 30° conical inlet section, a circular arc throat section with a throat radius of 0.885 in, and a 15° conical divergent section. The reservoir pressure and temperature were 300 psia and 4500°R respectively. The specific heat ratio, γ, was assumed to be 1.2 and the wall temperature was assumed to be a constant value of 1145°R. The data for this case are given in Table II, and the nozzle geometry is shown in Figure 7.

Eddy viscosity profiles predicted at the nozzle throat using the four eddy viscosity models are shown in Figure 8. In the region near the wall, $\eta < 0.4$, the eddy viscosity predicted using the four inner laws are essentially identical. The Cebeci and Smith inner law (72) predicts a second zero value of ε^+ at $\eta \simeq 1.2$ resulting from the pressure gradient term $y/\rho \frac{dP}{dx}$ being equal and opposite in sign to τ_w/ρ. It is noted that the solution using the Patankar and Spalding expression, equation (71), fails upstream of the throat as a result of the square root term being negative. By replacing the sum

$$\frac{\tau_w}{\rho} + \frac{y}{\rho} \frac{dP_e}{dx}$$

by

$$\left| \frac{\tau_w}{\rho} + \frac{y}{\rho} \frac{dP_e}{dx} \right|$$

Cebeci and Smith [ref. 11] were successful in obtaining solutions to problems having a significant pressure gradient. This model, equation (72), results in substantially smaller values of ε^+ for most of the boundary-layer than is given by the Van Driest Law, equation (70), the absolute value of the pressure gradient equation (73) and the Reichardt Law, equation (77). The values of ε^+ corresponding to the Van Driest expression and the expression using the absolute value of the pressure gradient differ by less than 3%, and the ε^+ corresponding to the outer law, equation (79), $\eta > 1.7$, also differs by less than 3%. In the sublayer, the Reichardt expression, equation (77), predicts values of ε^+ which are 10 to 20% larger than those given by equations (70) and (73), but above the match point with the outer law, $\eta = 1.4$, ε^+ is nearly the same as when using equation (70) or equation (73) for the inner law. It is emphasized that the outer eddy viscosity law is the same expression in all cases.

The resulting profiles of velocity and temperature differed by less than 5% for the solutions obtained using the different viscosity laws. The boundary-layer paramaters δ, δ^*, θ, c_{f_∞}, etc. also agreed to within 5%. If the inner law of Cebeci and Smith is excluded in the comparison, the resulting solutions differed by less than 3%. These results indicate that including the pressure gradient term in the inner law had little influence upon the eddy viscosity profiles, and had

60

essentially no influence upon the resulting solution.

As a result of the above, and the formulations of equations (71) and (72) for the inner law, these expressions were dropped from further consideration. The results which are discussed below were obtained using the Van Driest or Reichardt expression for the inner eddy viscosity law. However, as in the previous cases, use of the Reichardt inner law resulted in a substantial reduction of the computer time requirement (see Section 7.1.3). Since the differences in these solutions were insignificant, these data are shown as a single curve.

The heat transfer coefficient, boundary-layer, momentum, and displacement thicknesses predicted by the present numerical solutions are compared in Figures 9-12 with the results obtained by Elliott, Bartz, and Silver [ref. 15] using an integral method of solution. The solutions using the present numerical method and the integral method differ by up to 30%; however it should be noted, that the solutions using the integral method can be varied over a wide range by changing the assumptions which must be made relating to the nominal entrance conditions. Since the starting profiles for the present method are determined from the solution of the governing equations, direct comparison of the two methods is not possible, also it is not clear what assumptions should be made for the initial conditions necessary for the integral method if experimental data were not available before the calculations are made. Because of the arbitrariness of the solution using the integral method, the agreement of the two solution procedures is considered. to be adequate.

B. NASA-Lewis Case 2a (Boldman et al. [ref. 16])

The nozzle configuration consist of a 30° conical convergent section, a circular arc throat section, and a 15° conical divergent section. The throat radius is 0.746 in., and the stagnation pressure and temperature were 300 psia and 970°R respectively. The test conditions are given in Table III. The geometry is shown in Figure 13, and the pressure distribution corresponding to a one-dimensional expansion and the experimental data are shown in Figure 14. The experimentally determined wall temperature distribution is shown in Figure 15.

Solutions to this problem were obtained using the Van Driest and the Reichardt expressions, equations (70) and (77), for the inner eddy viscosity laws, and as in the previously discussed Elliott, Bartz, and Silver sample case, the differences in the solutions were insignificant. However, the solution using the Van Driest inner law required approximately 10 times more computing time than was necessary using the Reichardt inner law (see Section 7.1.3).

The predicted heat-transfer coefficient using the present method of solution is compared with the experimental data and the solutions obtained using the Elliott, Bartz, and Silver integral method in Figure 16. The present method of solution is in excellent agreement with the experimental data in the throat region and downstream. Differences of up to 20% between the predicted and experimentally determined heat-transfer coefficient are noted in the subsonic region of the nozzle. The near discontinuous change in the experimental value of the heat-transfer coefficient at $z = 1.97$ is the result of the temperature tabulated in this region (see Figure 15), and also the experimental pressure data were not smooth in this region. For the present calculations,

these data were smoothed in the region $1.9 \leq z \leq 2.5$. The integral method of solution is seen to reflect a strong dependence upon the starting condition assumptions. The two solutions presented using the integral method differ from each other by as much as 50%.

C. AEDC Hotshot Wind Tunnel Nozzle

The problem considered corresponds to the case referred to as "Hotshot 1" by Edenfield [ref. 17]. The nozzle geometry, wall enthalpy and pressure distribution are shown in Figures 17-19. The operating conditions are given in Table IV. In this section the experimental pressure distribution shown in Figure 19 was not used. The results presented assume a one-dimensional expansion of nitrogen and the specific heat ratio, γ, was taken as 1.4. The experimental wall enthalpy distribution, Figure 18, for 20 milliseconds of tunnel operation was used. The stagnation pressure and temperature were 11,500 psi and 5400°R. The nozzle consist of 10° and 5° converging conical inlet sections, a faired circular arc throat section, and a 5° conical divergent section. The throat radius is 0.055 in.

Attempts to solve this problem using the Van Driest expression, equation (70), for the inner eddy viscosity resulted in an instability at $z/r^* \approx 100$.* When the Reichardt inner eddy viscosity law, equation (77), was used a complete solution was obtained. The solutions obtained are compared for values of z/r^* up to 100 in Figures 20-23.

Figure 20 shows the eddy viscosity profiles for z/r^* in the range from 7 to 80. Differences in the eddy viscosity using the two models

---

*This applies only if the velocity derivative in equation (70) is evaluated implicitly (see Section 7.1.3).

differ from 5 to 20% with the larger differences being at stations near the nozzle throat. Heat-transfer rates predicted using the two eddy viscosity models are shown in Figure 21. For this problem, the Van Driest inner law resulted in heat-transfer rates which are approximately 10% higher than the predicted heating rates using the Reichardt inner law in the region near and upstream of the throat. Downstream of the throat, the Van Driest model oscillated about the solution obtained using the Reichardt inner eddy viscosity law. The displacement thickness predictions using the two inner eddy viscosity laws were nearly identical and are shown in Figure 22.

The computer time required to obtain a solution to a given axial position, z/r^*, is shown in Figure 23. The curves illustrate the time requirement in terms of the total number of iterations. The use of the Van Driest inner law required approximately five times as many iterations to obtain a solution to $z/r^* = 100$ as was necessary for the complete solution using the Reichardt inner law.*

The problems discussed in this section have demonstrated that the choice of the inner eddy viscosity law had little influence upon the resulting solution for cases where convergence was obtained, and that the computing time requirement was considerably less when the Reichardt expression was used for the inner law (see Section 7.1.3). For the cases where experimental data were available, the results obtained with the present method of solution were in good agreement with these data.

---

*This applies only if the velocity derivative in equation (70) is evaluated implicitly (see Section 7.1.3).

7.1.3 Revised Evaluation of the Inner Eddy Viscosity Laws

After the solutions discussed in Section 7.1 and 7.2 were obtained, the more recent expression for the inner eddy viscosity law given by Cebeci [ref. 13] became available. This relation, equation (74), was used in the boundary-layer computer program with and without including the pressure gradient term; equation (74) is the same as that given by Van Driest, equation (70), when the pressure gradient term is neglected. The results obtained using equation (74) with the pressure gradient term included were essentially the same as that given by the Van Driest expression and resulted in instability at $z/r^* \approx 100$ for the AEDC nozzle.

In all of the results which have been presented up to this point using Van Driest's and Cebeci's expressions for the inner eddy viscosity, the velocity derivative was evaluated at the station $x + \Delta x$. It was noted that in the cases which resulted in converged solutions, the solutions obtained were relatively unaffected by the inner eddy viscosity law which was used, and that a large number of iterations were necessary if viscosity laws based on Van Driest's [ref. 22] modification of Prandtl's mixing length were used. The difficulty appeared to be in the evaluation of $\left(\frac{\partial F}{\partial \eta}\right)_{x+\Delta x}$. To determine the influence of the implicit evaluation of the velocity derivative, the approximation

$$\left(\frac{\partial F}{\partial \eta}\right)_{x+\Delta x} \approx \left(\frac{\partial F}{\partial \eta}\right)_{x}$$

was made. With this replacement, the Van Driest inner law, equation (70), resulted in solutions which were essentially identical to the

65

solutions obtained using the Reichardt expression, equation (77), and the computer time requirement was nearly the same for both eddy viscosity laws. When the pressure gradient was included in equation (74), the results obtained showed that the pressure gradient term had little influence upon the solution. For the cases considered, the use of equations (70), (74), and (77) resulted in solutions which agreed to within $\pm$ 3%. Therefore, the results comparing the eddy viscosity laws presented in Section 7.1 should be considered as the influence of the implicit evaluation of $\frac{\partial F}{\partial \eta}$ rather than the differences in the eddy viscosity expressions.

The results presented in Section 7.2 have been obtained using the Reichardt expression for the inner eddy viscosity, and as mentioned above, the solutions are not significantly affected by the choice of the inner eddy viscosity expression. Equations (71) and (72) were not considered in this evaluation.

7.2 Laminar and Turbulent Boundary-Layer Flows of Reacting Gas Mixtures in Chemical Equilibrium

For the perfect gas solutions presented in Section 7.1, it was possible to obtain experimental data for most of the problems considered. However, it has not been possible to obtain experimental data in the range of pressure and/or temperature where the departure from the perfect gas condition is significant. For the problems considered in this section, both the perfect and the equilibrium gas solutions are given for the cases where significant differences were found to exist.

To check the accuracy of the table-look-up procedure, a number of

problems were solved at conditions corresponding to the range of pressure and temperature where the perfect gas relations are correct. For the cases considered the solutions with the table-look-up and the perfect gas options agreed to within ± 3%.

7.2.1 Equilibrium Gas Solutions for
Laminar and Turbulent Flows Over Flat Plates

Two flat plate cases were considered corresponding to the experimental data given by Hironimus [ref. 32]. The free-stream Mach number and temperature for Case 1 were 7.391 and 533°R and for Case 2, were 7.58 and 339°R respectively. The wall temperature was 533°R for Case 1 and 355°R for Case 2. The test conditions are given in Table V. Plots of Stanton number based on edge conditions are shown for both fully developed turbulent and laminar flow for Case 1 and Case 2 in Figures 24 and 25. The solutions shown were obtained with the table-look-up procedure. The perfect gas solutions for these cases differed from the equilibrium solution by less than 3% and are not presented.

Downstream of the transition from laminar to turbulent flow the agreement of the predicted and the experimentally determined Stanton number data is within 10%, and in the region of laminar flow the agreement between the numerical and experimental data is good.

7.2.2 Equilibrium and Perfect Gas Solutions for
Laminar Flow Over a Hyperboloid

A 10° half-angle hyperboloid at an altitude of 100,000 ft. with a wall temperature of 1400°K was considered for a free-stream Mach number and temperature of 20.178 and 226.98°K. This case corresponds

to Case A of the AGARD test cases (Lewis [ref. 33]). The flight conditions are given in Table VI. The body geometry and pressure distribution are shown in Figures 26 and 27.

The solutions of both perfect air and equilibrium air have been obtained for the laminar case only. The perfect gas solution is compared with the results of Adams [ref. 34], and the equilibrium solution is compared with Blottner's and Smith's results as presented by Lewis [ref. 33].

Figure 28 shows the boundary-layer displacement thickness predictions for the perfect and equilibrium air cases. The present method of solution is seen to be in excellent agreement with Adams' solution for the perfect gas case. The present equilibrium air solution is in good agreement with the results given by Keltner and Smith [ref. 35] but differs by a factor of two from the solution given by Blottner [ref. 1]. It is noted that Blottner used finite rate chemical reactions and complete multi-component diffusion whereas Keltner and Smith used a finite-rate binary air model.

Plots of the skin-friction coefficient and Stanton number distributions are shown in Figures 29 and 30. For the perfect gas case the skin friction predicted by the present method of solution is in excellent agreement with Adams' solution for $S/r_n \geq 0.4$, but the solutions differ by up to 10% near the stagnation point. The Stanton number distribution given by the present method is in good agreement with Adams' results for all S/r_n.

For the equilibrium air solution, the present method is in excellent agreement with Blottner's solution for both skin-friction and

Stanton number distributions.

The maximum differences between Blottner's, Keltner and Smith's, and the present results are less than 5%.

7.2.3 Equilibrium and Perfect Gas Solutions for Laminar and Turbulent Flow Over a Spherically-Blunted Cone

A 5° half-angle spherically-blunted cone at an altitude of 70,000 ft. is considered in this section.* The free-stream Mach number and temperature were 19,564 and 226.98°K respectively. The wall temperature was assumed to be constant at 1000°R. The problem data are presented in Table VII. The geometry and pressure distribution are shown in Figures 31 and 32. The pressure distribution for this case was determined for perfect air, $\gamma = 1.4$, using the computer program developed by Inouye, Rakich, and Lomax [ref. 36].

This problem is included to illustrate the solution of a weak adverse pressure gradient resulting from an overexpansion and recompression of the gas. Solutions are given for both laminar and fully developed turbulent flow for specific heat ratios, γ, of 1.4 and 1.165 and equilibrium air.

The boundary-layer displacement thickness, skin-friction, Stanton number, and heat-transfer rate distributions for these solutions are presented in Figures 33-37. Since experimental data or other numerical solutions are not available for comparison, it is not possible to assess the accuracy of the results. However, because of the similarity

---

*This case was provided by Mr. Randy Graves of the NASA Langley Research Center as representative of a body of unpublished free-flight experimental data available for this body.

with the hyperboloid discussed in Section 7.2.2, these results appear to show the correct trends.

7.2.4 Turbulent Flow of Equilibrium Gases in Axisymmetric Nozzles

The data for this case are given in Section 7.1.2.C of this Chapter. Edenfield [ref. 17] considered the nozzle discussed in this section for preliminary investigations leading to the design of contoured nozzles for hypersonic hotshot wind tunnels with a test section Mach number of about 20. Edenfield used a number of theories to predict the downstream boundary-layer displacement thickness, but the available methods of prediction either failed to give a complete solution for the nozzle or the results were found to be unacceptable. Attempts to solve the problem using the Elliott, Bartz, and Silver [ref. 15] integral method failed at $z/r^* = 1350.$* This failure was attributed to the assumed power law total enthalpy profiles used in the integral method. All other attempts to predict the displacement thickness used the momentum equation only with the Crocco enthalpy distribution or correlation formulas.

Before discussion of the present results, a brief description of the physical nozzle contour and the contour used in the calculations is given. The physical nozzle consists of a subsonic region composed of a 10° conical section followed by a 5° conical section. The throat is cylindrical with a length of one throat diameter and the supersonic portion is a 5° conic section. For the calculations, the nozzle contour was smoothed as shown in Figure 17.

---

*In this section r^* denotes the non-dimensional throat radius.

It should also be noted that the total length of the nozzle was given as 92.087 inches (Edenfield [ref. 17]. Using a throat radius of 0.055 inches results in a maximum value of z/r^* of approximately 1684. However, experimental pressure measurements are given in Figure 19 for values of z/r^* up to approximately 1850. The pressure data used upstream of $z/r^* = 100$ corresponds to an isentropic expansion of the gas (nitrogen). The transition from the isentropic expansion pressure data to the experimental data is particularly noticeable in the larger scale plots of the boundary-layer thicknesses computed using the present method of solution for z/r^* between 100 and 400. With reference to the above comments, it is not clear what conclusions should be made in the comparison of the predicted and experimental displacement thickness. However, the same conditions have been used for all prediction methods and the results of the different solutions may be compared.

The momentum thickness distribution corresponding to the Elliott, Bartz, and Silver integral method of solution and the present method is shown in Figure 38. The velocity or boundary-layer and displacement thickness are shown in Figure 39, and the predicted heat-transfer rates are given in Figure 40. The results presented in Figure 40 from the integral method were obtained by solving both the momentum and energy equations with a power law for the total enthalpy profiles.

The differences in the boundary-layer thickness predictions vary from 10% for the velocity thickness to a factor of 2 for the momentum and displacement thicknesses. The heat-transfer rates predicted by the integral method are from 30 to 60% lower than the rates predicted by

71

the present method. The results obtained with the integral method do not appear to be realistic, and as noted previously the method failed at z/r^* ≃ 1350. The assumed power law total enthalpy profiles together with the assumed velocity profiles in the integral method resulted in solutions which predicted large densities near the outer edge of the boundary layer in the downstream region of the nozzle. The density profiles predicted by the integral method, the method of Enkenhus and Maher [ref. 37] using the Crocco enthalpy distribution, and the present method are shown in Figure 41 for z/r^* = 984. As noted by Edenfield [ref. 17], pitot pressure measurements would detect the presence of these peaks in density if they exist, but the measurements made indicate that such peaks do not exist. The density profile predicted with the present method shows a decrease in density near the wall which is characteristic of boundary layers for cold wall cases.

Figure 42 shows the boundary-layer displacement thickness predicted by Enkenhus and Maher [ref. 37], Burke and Bird [ref. 38], Lee [ref. 39], Elliott, Bartz, and Silver [ref. 15], and the present method of solution. The present two-dimensional displacement thickness prediction is in general agreement with Burke's calculation based on the edge Reynolds number. The axisymmetric value of the displacement-thickness prediction is in general agreement with the solution of Lee. Burke's solution based on a reference Reynolds number (the reference Reynolds number is computed using Eckert's reference conditions) gave the best agreement with the data presented near the nozzle exit, but as noted at the beginning of this section, the experimental data presented at z/r^* = 1825 is outside of the nozzle dimensions.

The methods of Enkenhus and Maher, and Elliott, Bartz, and Silver are in poor agreement with the experimental data presented and the other solutions.

Figure 43 shows the displacement thickness predictions of the Elliott, Bartz, and Silver method for both an assumed power law and the Crocco enthalpy distribution. For the Crocco enthalpy distribution only the momentum equation is solved by the integral method. Two solutions are given corresponding to different skin-friction laws using the method of Enkenhus and Maher. The present two-dimensional and axisymmetric solutions are in good agreement with the other solution procedures which use the momentum equation only. It is not clear why these prediction methods should be in good agreement with experiment for z/r^* up to 1100 and overpredict the displacement thickness by a factor of two at the nozzle exit.

To demonstrate the feasibility of obtaining solutions to problems with more severe conditions than the cases presented, the nozzle geometry, wall enthalpy distribution and reservoir density for the above case have been retained and the reservoir pressure and temperature were changed to 58, 522 psia and 18,000°R respectively. Solutions were obtained for perfect nitrogen, equilibrium nitrogen, and equilibrium air for fully developed turbulent flow. The pressure distribution corresponds to a one-dimensional expansion of the gas and is shown for the three cases in Figure 44. The exit Mach numbers for perfect nitrogen, equilibrium nitrogen, and equilibrium air were 21.64, 13.69, and 10.62 respectively.

The predicted heat-transfer rate and Stanton number distribution

are shown in Figures 45 and 46. The heat-transfer rates predicted for the equilibrium gases were from two to five times greater than the perfect gas solution for the region near and downstream of the nozzle throat. As a result of the different edge conditions, the Stanton number distribution shows less variation.

7.3 Perfect Gas Solutions for Laminar and Turbulent
Flow Over a Flat Plate With Normal Mass Injection

Three flat-plate solutions are presented for air into air mass transfer and one case with no mass transfer corresponding to the experimental data referred to as run no's. 8, 11, 15, and 19 by Danberg [ref. 40]. The free-stream Mach number for these cases was approximately 6.3 and the temperature was approximately 59°K. The injection paramater, $c_q = \rho_w v_w / \rho_e u_e$, varied from 0 to 25.8 x 10^{-4}. The ratio of the wall-to-edge static temperature was approximately 4.0. More complete data are given in Table VIII.

The velocity profiles obtained numerically are compared with Danberg's experimental data for the four cases in Figure 47. The numerical solutions correspond to fully developed turbulent flow where the inner eddy viscosity law is the modified Van Driest expression given by Cebeci [ref. 13]. For $y^* < \delta$, the predicted velocity is consistently lower than the experimental data, and except for the case with no mass injection, run no. 19, the velocity derivative at the wall given by the numerical solution is considerably less than the corresponding experimental value. The computed velocity profiles are not in good agreement with the experimental data for any of the cases considered having mass transfer.

The predicted skin-friction and heat-transfer distributions are

shown in Figures 48 and 49. The predicted heat-transfer distribution
is in good agreement with the experimental data. However, as would be
expected from the poor agreement of the predicted and experimental
velocity profiles, the agreement between the predicted and experi-
mental skin-friction data is unsatisfactory. It is noted that the
experimental heat-transfer data were determined indirectly by the use
of thermocouples imbedded in the plate. The experimental skin-friction
data were determined by two-point differentiation of the experimental
velocity profile and are more likely to be influenced by the presence
of the probes within the boundary layer. Tabulations of the predicted
and experimental data for heat transfer and skin-friction are given in
Table IX for the turbulent solution.

7.4 Convergence Test and Computing Time Requirements

The solutions presented above have been obtained with $\epsilon_f = 0.01$
using the function test and the additional requirement that the mini-
mum number of iterations at the new station be 2 or greater. The last
requirement was found to be necessary to insure a smooth distribution
of the displacement thickness when considering turbulent flow problems
with weak pressure gradients.

To determine the influence of ϵ_f upon the computing time and the
resulting solution, a number of the above cases were computed with
$\epsilon_f = 0.001$. The flat plate Case I considered in Section 7.2.1 re-
quired approximately ten times more computing time with $\epsilon_f = 0.001$
than with $\epsilon_f = 0.01$. The results of the two solutions differed by
less than 2%. Essentially the same results were obtained for other
body shapes where the flow was turbulent and the ratio of wall to

stagnation enthalpy was small. The computing time was not significantly influenced by ε_f for laminar flows with zero pressure gradient, since these flows are self similar.

Representative computing time requirements for an IBM 360-65 computer are given in the table below. The times given are for solutions where a large number of stations were solved and should be regarded as maximum computing times rather than the optimum. The tabulated times for turbulent flows are for the use of the Reichardt inner eddy viscosity law. The solution times would be increased by approximately 20 to 30% using the Van Driest inner law for the same number of stations as when using the Reichardt law.

Body Shape	Section Number	Execution Time (Min:Sec)			
		Laminar		Turbulent	
		Perfect Gas	Equilibrium Gas	Perfect Gas	Equilibrium Gas
Flat Plate	7.2.1 (Case 1)	0 : 33	–	1:32	2:4
	7.2.1 (Case 2)	0 : 32	–	1:9	2:36
Hyperboloid	7.2.2	0 : 51	15:1	–	–
Blunt Cone	7.2.3	2 : 27	11:22	4:9	19:3
Nozzle	7.1.2 (B)	–	–	2:26	–
	7.2.4	–	–	7:3	22:50

VIII. CONCLUSIONS AND REMARKS

The results which have been presented demonstrate that the Crank-Nicolson type implicit finite-difference scheme can be used successfully to obtain solutions of the turbulent boundary-layer equations for nozzle flows of perfect gases or mixtures of perfect gases in chemical equilibrium. For the low Mach number perfect gas solutions considered for nozzle flows, the present method of solution was in excellent agreement with the experimental data. For the hypervelocity nozzle, the present solutions were in good agreement with other numerical solutions which used only the momentum equation and the Crocco enthalpy distribution. However, these solutions were not in good agreement with the available experimental data, but these experimental data did not match with the given geometry near the nozzle exit. The equilibrium solution for the hypervelocity nozzle was found to be essentially the same as that for a perfect gas at the same reservoir conditions. Thus, the data which were available do not appear to be sufficient to establish the accuracy of the numerical method.

The results presented for equilibrium laminar flow over a hyperboloid were found to be in excellent agreement with other numerical solutions for the predictions of heat transfer and skin friction, but the displacement thickness calculations differed by a factor of two or more among the different numerical solutions which were available for comparison.

Solutions of flat-plate laminar and turbulent boundary-layer flows of an equilibrium gas were obtained, but these solutions were also essentially the same as for a perfect gas. The solutions obtained were

in good agreement with the experimental data.

In all of the turbulent boundary-layer calculations considered without mass transfer at the wall, the solutions obtained were found to be essentially independent of the expression used for the inner eddy viscosity law. That is the pressure gradient term appearing in the inner eddy viscosity law may be included or excluded without significantly influencing the results.

For flat-plate turbulent flows with mass injection at the wall, the numerical results were in good agreement with the indirectly determined experimental data for heat transfer, but the predictions of skin friction and velocity profiles, determined from direct measurements, were not in satisfactory agreement with the experimental data. Thus, these results are also inconclusive.

The present method of solution has been demonstrated to be accurate for both internal and external flows of perfect gases for both laminar and turbulent flows for the case of no mass injection. More experimental data are needed to verify the method for the case of mass transfer.

For the equilibrium chemistry calculations, the present method of solution for the laminar flow of the gas is in good agreement with other numerical solutions. For turbulent flow of an equilibrium gas the present method of solution was found to be stable and the solutions show the expected trends, but the experimental data which were available were in a range of pressure and/or temperature which showed little departure from the perfect gas condition. With the exception of the Elliott, Bartz, and Silver [ref. 15] integral method of solution for equilibrium chemistry turbulent boundary-layer flows in nozzles, other

numerical solutions were not available for comparison. For the case of a hypervelocity nozzle, the integral method failed to converge for a stagnation pressure and temperature of 11,511 psia and 3000°K. Whereas, the present method was found to be stable for nozzle calculations with reservoir pressures and temperatures up to 58,522 psia and 10,000°K respectively.

IX. APPENDIX A

Thermodynamic and Transport Properties and one Dimensional

Expansion of a Reacting Gas Mixture in Chemical Equilibrium

In order to solve the conservation equations for laminar or turbulent boundary-layer flow of an arbitrary mixture of perfect gases in thermodynamic equilibrium, it is necessary to specify the boundary-layer edge conditions and to provide a method for determining the local thermodynamic and transport properties for the gas mixture considered.

The thermodynamic and transport properties and the inviscid expansion data which have been used in the present solution of the boundary-layer equations have been obtained by modifying the basic computer program developed by Lordi, Mates, and Moselle [ref. 20], which was developed to determine the inviscid expansion of arbitrary gas mixtures assuming either frozen chemistry, equilibrium chemistry, or finite-rate chemistry. Only the equilibrium chemistry option is considered in the sections below.

A.1 Equilibrium Gas Properties

A brief description of the procedure for determining the equilibrium chemistry solution is included in this appendix. The notation is the same as that employed by Lordi, Mates and Moselle, and is included in a separate list of symbols presented at the end of this appendix. The analysis presented below is essentially the same as that given in Sections 2.1, 2.2, and 4.1 of their report.

A.1.1 Thermodynamic and Transport Properties

The enthalpy of a given gas mixture in thermodynamic equilibrium is a function of the internal energies of the species and the chemical composition of the mixture, which are related to the local thermodynamic properties, pressure, density, and temperature. The composition of a specified gas mixture at a given equilibrium state is determined for c chemical elements and s chemical species as follows. The chemical equation for the ith species may be expressed as

$$M_i = M_i(\alpha_{i1}, \alpha_{i2}, \ldots \alpha_{ic}), \quad i = 1, 2, \ldots, s \quad (A1)$$

The species to be included in the mixture are specified through the matrix α_{ij}.

The equilibrium formation reactions for the species in terms of the elements may be expressed by (s − c) linearly independent relations of the form

$$M_i = \sum_{j=1}^{c} \alpha_{ij} M_j, \quad i = 1, 2, \ldots s \quad (A2)$$

where the rank of the α_{ij} matrix is c. Lordi, Mates and Moselle note that in some cases it is necessary to choose species other than the chemical elements as components. The formation reactions for the (s − c) dependent species are expressed in terms of the c components as

$$M_i = \sum_{j=1}^{c} \bar{\nu}_{ij} M_j, \quad i = c + 1, c + 2, \ldots, s \quad (A3)$$

The number of gram-atoms of each chemical element, Q_k, contained in the mixture must be given in addition to the chemical species and

chemical elements. The total number of gram-moles of the components which are present in the mixture is given by

$$\sum_{j=1}^{c} \alpha_{jk} \, q_j = Q_k \qquad (A4)$$

This relation specifies the element composition in terms of the components rather than the chemical elements.

Enforcing mass conservation in each of the formation reactions and a global mass conservation gives the mole fractions of the components as

$$X_j = q_j - \sum_{i=c+1}^{s} [\bar{\nu}_{ij} - q_j (\bar{\nu}_i - 1)] \, X_i, \quad j = c + 1, \, c + 2, .., s \qquad (A5)$$

where

$$q_j = \frac{q_j'}{\sum_j q_j'} \, , \quad \bar{\nu} = \sum_j \bar{\nu}_{ij}$$

The dependent species concentrations are related to the component concentrations through the equilibrium constants for the formation reactions, equation (A3), by

$$X_i = K_{P_i} \, P'^{(\bar{\nu}_i - 1)} \prod_{j=1}^{c} X_j^{\bar{\nu}_{ij}}, \quad i = c + 1, \, c + 2, \ldots, s \qquad (A6)$$

where

$$K_{P_i} = \exp \left[\sum_{j=1}^{s} \bar{\nu}_{ij} \frac{\mu_i^o}{T} - \frac{\mu_i^o}{T} \right] \qquad (A7)$$

82

The concentrations of the independent species or components are determined by solving equation (A5) and using a Newton-Raphson iteration procedure to solve equation (A4). The molecular weight at the specified pressure and temperature is calculated from

$$M = \sum_{j=1}^{s} X_j M_j \qquad (A8)$$

The density is then determined from the equation of state for a mixture of perfect gases

$$P' = \rho' \frac{R_o}{M} T' \qquad (A9)$$

and the specific enthalpy is given by

$$H = \sum_{j=1}^{s} X_j h_j \qquad (A10)$$

For a mixture of perfect gases, the molar enthalpy, h_j, chemical potential, μ_j^o, at one atmosphere of pressure, and molar entropy, s_j^o, are functions of temperature only. These data are specified by either a simple-harmonic-oscillator model, or by polynomial curve fits to more accurate calculations of the species properties. The latter method is called the thermo-fit method. In both methods, the species are assumed to be vibrationally and electronically excited, in equilibrium with the local translational temperature. The translational and rotational degrees of freedom are assumed to be fully excited.

For the harmonic-oscillator model, the specific enthalpy for a monatomic or diatomic species is expressed as

$$\frac{h_j - h_{j_o}^o}{T} = \frac{5 + 2(n_j - 1)}{2}$$

$$+ (n_j - 1) \frac{\theta_{v_j}}{T} \frac{1}{\exp(\theta_{v_j}/T) - 1} + \frac{\sum\limits_{\ell=1}^{L_j} \epsilon_{\ell_j} g_{\ell_j} \exp[-\epsilon_{\ell_j}/T]}{T \sum\limits_{\ell=1}^{L_j} g_{\ell_j} [-\epsilon_{\ell_j}/T]} \qquad (A11)$$

and the chemical potential at standard pressure is given by

$$\frac{\mu_j^o - h_{j_o}^o}{T} = - \left\{ a_j + \frac{5 + 2(n_j - 1)}{2} \ln T \right.$$

$$+ (n_j - 1) \ln \frac{\exp[\theta_{v_j}/T]}{\exp[(\theta_{v_j}/T) - 1]}$$

$$\left. + \ln \sum\limits_{\ell=1}^{L_j} g_{\ell_j} \exp[-\epsilon_{\ell_j}/T] \right\} \qquad (A12)$$

where

$$a_j = b_j + \frac{5 + 2(n_j - 1)}{2} \ln T_o' \qquad (A13)$$

and

$$b_j = \frac{3}{2} \ln \frac{2\pi M_j' k}{h^2} + \ln \frac{k}{p^{o'}} - (n_j - 1) \ln \theta_{r_j}' \qquad (A14)$$

84

For the thermo-fit method, these data are given by

$$\frac{\mu_j^o - h_{j_o}^o}{T} = a_j(1 - \ln T') - b_j T' \frac{c_j}{2} (T')^2 - \frac{d_j}{3} (T')^3 - \frac{e_j}{4} (T')^4 - k_j \tag{A15}$$

and by differentiation of equation (A15)

$$\frac{h_j - h_{j_o}^o}{T} = a_j + b_j T' + c_j (T')^2 + d_j (T')^3 + e_j (T')^4 \tag{A16}$$

For both methods s_j^o is determined from

$$s_j^o = \frac{h_j - \mu_j^o}{T} \tag{A17}$$

and the specific heat of the individual species is determined by differentiation of equation (A12) or equation (A16).

The local thermodynamic and transport properties which must be specified for use in the boundary-layer computer program are: T', $\tilde{H} = \log_{10}\left(\frac{H'}{RGAS}\right)$, $\tilde{P} = \log_{10}(P')$, $\tilde{\rho} = \log_{10}(\rho^*/\rho_s^*)$, μ^*, $c_p = \frac{c_p}{RGAS}$, Pr.

Tables of these data are generated for the desired range of temperatures in decreasing T' at constant pressure. The procedure is repeated for decreasing in $\tilde{P}$ to span the desired range in pressure.

Conversion of the data to the required form is as follows

$$\tilde{H} = \log_{10}\left(\frac{HT' M_s}{M_o}\right) = \log_{10}(H'/RGAS)$$

$$\tilde{\rho} = \log_{10} \frac{\rho_o'(2.205 \times 10^{-3})}{(3.531 \times 10^{-5})(32.176)(\rho_g')}$$

$$c_P = \left(\frac{\partial \tilde{H}}{\partial T}\right)_P 10^{\tilde{H}}/\log_{10}(e)$$

The derivative is computed using a five point Lagrangian differentiation polynomial.

The Prandtl number is obtained by interpolation in the tables of data given by Hansen [ref. 41] for air and Ahtye and Peng [ref. 42] for nitrogen.

The viscosity of the gas mixture is computed using Wilke's [ref. 43] semi-empirical formula

$$\mu^* = \sum_{i=1}^{ISS} \left[\frac{\gamma_i \mu_i^*}{\sum_{j=1}^{ISS} \gamma_j \phi_{ij}} \right] \qquad (A18)$$

where

$$\phi_{ij} = \frac{1}{\sqrt{8}} \left(1 + \frac{\overline{M}_i}{\overline{M}_j}\right)^{-1/2} \left[1 + \left(\frac{\mu_i^*}{\mu_j^*}\right)^{1/2} \left(\frac{\overline{M}_i}{\overline{M}_i}\right)^{1/4}\right] \qquad (A19)$$

Species viscosities, μ_i^*, are approximated by curve fit data of the form

$$\mu_i^* = e^{C_i} T^{(A_i \ln T + B_i)} \text{ gm/cm-Sec} \qquad (A20)$$

The constants A_i, B_i, and C_i are obtained from curve fitting the μ_i^* data given by use of the method of Yun and Mason [ref. 44]. The data which have been used in the boundary-layer calculations were given by Blottner [ref. 7].

The frozen values of thermal conductivity and Prandtl number, and the compressibility factor are also computed, but these quantities were not used.

A description of the modifications made to the computer program of Lordi, Mates and Moselle (for computing the thermodynamic properties) and the mixture transport property calculations are given by Miner, Anderson and Lewis [ref. 28] with listings of the added or modified subroutines, and a description of the necessary input data is given.

A.1.2 Boundary-Layer Edge Conditions for a

Gas Mixture in Thermodynamic Equilibrium

The boundary-layer edge conditions for the equilibrium gas case are obtained from the isentropic expansion of the gas from a given stagnation or reservoir state. To obtain the inviscid expansion of the gas it is necessary to conserve momentum and energy in addition to the requirements given in Section A.1.1. The procedure for determining the inviscid expansion discussed below is essentially that given in Section 2.2 of Lordi, Mates and Moselle [ref. 20].

For a quasi-one-dimensional inviscid flow of a gas the conservation of mass, momentum, and energy is expressed as

$$\rho u A = \dot{M} = \text{constant} \tag{A21}$$

$$u\,du + \frac{1}{\rho}\,d\rho = 0 \tag{A22}$$

$$H + \frac{u^2}{2} = H_o = \text{constant} \tag{A23}$$

For a chemically reacting gas mixture the entropy is expressed as

$$\frac{s'_o}{R_o} = \frac{1}{M_o} \sum_{j=1}^{s} X_j\, s_j = \frac{1}{M_o} \left\{ \sum_{j=1}^{s} X_j\, s_j^o \right.$$

$$\left. - \sum_{j=1}^{s} X_j \ln X_j - \ln \rho' \right\} = \text{constant} \tag{A24}$$

for an isentropic path. The governing equation which must be satisfied by the c components and the pressure is

$$F_j = 0, \quad j = 1, 2, \ldots, c+1$$

where from (A5)

$$F_j = q_j - \sum_{i=c+1}^{s} [\bar{\nu}_{ij} - q_j\,(\bar{\nu}_i - 1)]\, X_i - X_j, \quad j = 1, 2 \ldots c \tag{A25}$$

and from (A24)

$$F_{c+1} = \sum_{i=1}^{s} X_i(s_i^o - M_i\, S'_o - \ln X_i) - \ln \rho' \tag{A26}$$

The expansion is obtained by taking successive temperature steps

88

from the reservoir value and solving equations (A25) and (A26) by a Newton-Raphson method to determine the composition and pressure at the specified temperature and entropy.

To express the solution in terms of area ratio, the critical mass flow is first determined by computing the maximum value of ρu. This maximum value with the corresponding temperature determines the throat conditions for nozzle flows. The solution is then restarted from the reservoir and the area ratio is determined from equation (A21). At each point in the expansion, the density and Mach number are computed from

$$P' = \rho' \frac{R_o}{\bar{M}} T'$$

and

$$\tilde{M} = u/[(P - P_b)/(\rho - \rho_b)]^{1/2}$$

where the subscript b refers to the values at the previous step.

The area ratio is computed using

$$A = \frac{(\rho u)_{max}}{\rho u}$$

The velocity, pressure, and enthalpy are converted to the form required by the boundary layer program as follows

$$u^* = u(R_o (778.158)(1.8)(32.176) \ T_o'/M)^{1/2}$$

$$\tilde{P} = \log_{10}(PP_o')$$

$$\hat{H} = \log_{10}(H\ T'_o\ M_s/M)$$

Lordi, Mates and Moselle's computer program [ref. 20] was modified and is described by Miner, Anderson, and Lewis [ref. 28] where the additional input data are given.

a_j constant in thermo-fit and harmonic oscillator expressions for chemical potential.

A ratio of local cross-sectional area to minimum cross-sectional area.

b_j coefficient of T' in thermo-fit expression for species enthalpy, or defined by Eq.(A14) for harmonic-oscillator description.

c number of elements in mixture.

c_j coefficient of $(T')^2$ in thermo-fit expression for species enthalpy, or mass fraction.

c_p^* specific heat of mixture (ft^2/sec^2-°K).

c_p dimensionless specific heat (c_p^*/RGAS).

d_j coefficient of $(T')^3$ in thermo-fit expression for species enthalpy.

e_j coefficient of $(T')^4$ in thermo-fit expression for enthalpy.

g_{ℓ_j} degeneracy of the lth electronic state of the jth species.

h Plank's constant.

h_j molar enthalpy of the jth species ($h_j = h_j'/R_o T_o'$)

H specific enthalpy of mixture $\left(H = \dfrac{H' M_o}{R_o T_o'} \right)$.

$\hat{H}$ $\log_{10}\left(\dfrac{HT' M_s}{M_o} \right)$ or $\log_{10}(H'/RGAS)$

k Boltzmann's constant

91

k_j	constant in thermo-fit expression for the chemical potential of the jth species.
K_{P_i}	equilibrium constant for the ith reaction based on partial pressure
M_j	mass of the jth particle (gm).
$\overline{M}$	molecular weight (gms/mole).
$\widetilde{M}$	Mach number
$\overline{M}_s$	molecular weight of the gas mixture at standard atmospheric conditions.
n_j	number of atoms in the jth species.
P	pressure ($P = P'/P_o'$), P' in atmospheres.
$\widetilde{P}$	$\log_{10}(PP_o')$
q_j	mole fraction of jth component when only independent species are present in mixture.
Q_k	number of gram atoms of kth element in mixture.
R_o	universal gas constant $\left(1.98647 \; \dfrac{\text{gm-cal}}{\text{gm-mole}^\circ \text{K}} \right)$
RGAS	gas constant ($\text{ft}^2/\text{sec}^2\text{-}^\circ\text{K}$)
s	number of species in mixture
s_j	molar entropy of jth species ($s_j = s_j'/R_o$)
T	temperature (T'/T_o'); T' in $^\circ$K
u^*	velocity (ft/sec)
u	velocity $\left[u = u' \Big/ \sqrt{R_o \, T_o'/\overline{M}_o} \right]$
X_i	mole-fraction of jth species

α_{i_j} matrix specifying the elements and species in the chemical model of the mixture

γ_i mass concentration of the ith species, lb-mole/lb

ε_{ℓ_j} energy of the ℓth electronic state of the jth species $(\varepsilon_{\ell_j} = \varepsilon'_{\ell_j} / R_o T'_o)$

θ_{r_j} characteristic relational temperature of the jth species

θ_{v_j} characteristic vibrational temperature of the jth species $(\theta_{v_j} = \theta'_{v_j} / T'_o)$

μ_j chemical potential of the jth species $\left(\mu_j = \dfrac{\mu'_j}{R_o T'_o} \right)$

μ_i^* species viscosity (gm/cm-sec)

$\bar{\nu}_{ij}$ stoichiometric coefficients of the equilibrium formation reactions

$\bar{\nu}_i = \sum\limits_j \nu_{ij}$

ρ density $(\rho = \rho'/\rho'_o)$

ρ^* density (slugs/ft^3)

$\tilde{\rho}$ $\log_{10}(\rho^*/\rho_s^*)$

Subscripts

o reservoir condition

s standard atmospheric condition

i pertaining to the ith reaction

j pertaining to the jth species

k pertaining to the kth element

l pertaining to the lth electronic level

Superscripts

( )'   dimensional quantity

( )^o refers to standard pressure condition

REFERENCES

1. Blottner, F. G., "Finite Difference Solution of the First-Order Boundary Layer Equations," <u>Nonreacting and Chemically Reacting Viscous Flows Over a Hyperboloid at Hypersonic Condition.</u> Lewis, C. H., ed., AGARDograph No. 147, NATO, Paris, Sept. 1970, PP. 13-36.

2. Kline, S. J., Morkovin, M. V., Sovran, G., and Cockrell, D. J. eds.: <u>Computation of Turbulent Boundary Layers</u> - 1968 AFOSR-IRP-Stanford Conference Vol. 1 - <u>Methods, Predictions, Evaluation and Flow Structure,</u> Aug. 1968.

3. Harris, J. E., "Numerical Solution of the Compressible Laminar, Transitional, and Turbulent Boundary Layer Equations," PhD Dissertation, VPISU, Blacksburg, Virginia, 1970.

4. Pletcher, R. H., "On a Calculation Method for Compressible Turbulent Boundary Layer Flows with Heat Transfer," AIAA Paper 71-165, Jan. 1971.

5. Crank, J., and Nicolson, P., "A Practical Method for Numerical Evaluation of Solutions of Partial Differential Equations of the Heat Conduction Type," <u>Proc. Camb. Phil. Soc.</u> Vol. 43, 1947, P. 50.

6. Blottner, F. G., and Lenard, M., "Finite Rate Plasma Generation in the Laminar Air Boundary Layer of Slender Reentry Bodies," <u>Transactions of the Eighth Symposium on Ballistic Missile and Space Technology,</u> San Diego, California, 16-18 Oct. 1963, PP. 3-33.

7. Blottner, F. G., "Non-Equilibrium Laminar Boundary Layer Flow of Ionized Air," General Electric Report R64SD56. Also AIAA Journal Vol. 2 No. 11, Nov. 1964, PP. 1921-1927.

8. Davis, R. T., and Flugge-Lotz, I., "Second-Order Boundary-Layer Effects in Hypersonic Flow Past Axisymmetric Blunt Bodies," <u>J. Fluid Mechanics,</u> Vol. 20, Part 4, 1964, PP. 593-623.

9. Davis, R. T., "The Hypersonic Fully Viscous Shock-Layer Problem," Sandia Laboratories Report SC-RR-68-840, Dec. 1968.

10. Davis, R. T., "Solution of the Viscous Shock-Layer Equations for a Binary Mixture," <u>Nonreacting and Chemically Reacting Viscous Flows Over a Hyperboloid at Hypersonic Condition.</u> Lewis, C. H., ed., AGARDograph No. 147, NATO, Paris, Sept. 1970, PP. 55-67.

11. Cebeci, T., and Smith, A. M. O., "A Finite-Difference Solution of the Incompressible Turbulent Boundary-Layer Equations by an Eddy-Viscosity Concept," Douglas Aircraft Co., Report No. DAC-67130, Oct. 1968.

12. Cebeci, T., Smith, A. M. O., and Mosinskis, G., "Calculation of Compressible Adiabatic Turbulent Boundary Layers," AIAA Paper 69-687, June, 1969.

13. Cebeci, T., "Behavior of Turbulent Flow Near a Porous Wall with Pressure Gradient," AIAA Journal, Vol. 8, No. 2, Dec. 1970, pp. 2152-2156.

14. DuFort, E. C., and Frankel, S. P., "Stability Conditions in the Numerical Treatment of Parabolic Differential Equations," Math. Tables Aids Comput., 7, 1953, pp. 135-152.

15. Elliott, D. G., Bartz, D. R., and Silver, S., "Calculation of Turbulent Boundary Layer Growth and Heat Transfer in Axisymmetric Nozzles," JPL TR-32-387, 1963.

16. Boldman, D. R., Newmann, H. E., and Schmidt, J. F., "Heat Transfer in 30° and 60° Half-Angle of Convergence Nozzles with Various Diameter Uncooled Pipe Inlets," NASA TN D-4177, 1967.

17. Edenfield, E. E., "Contoured Nozzle Design and Evaluation for Hotshot Wind Tunnels," AIAA Paper 68-369, April 1968.

18. Hirschfelder, J. O., Curtiss, C. F., and Bird, R. B., Molecular Theory of Gases and Liquids, John Wiley and Sons, New York, 1954.

19. Van Dyke, M., "Second-Order Compressible Boundary-Layer Theory with Application to Blunt Bodies in Hypersonic Flow," Stanford University Report SUDAER No. 112, June, 1961.

20. Lordi, J. A., Mates, R. E., and Moselle, J. R., "Computer Program for the Numerical Solution of Nonequilibrium Expansions of Reacting Gas Mixtures," Cornell Aeronautical Laboratory, Inc., CAL Report No. AD-1689-A-6, Oct. 1965.

21. Boussinesq, J., "Theory de l'ecoulement tourbillant," Mem. pre. par. Siv Sav. XXIII, Paris, 1877.

22. Van Driest, E. R., "On Turbulent Flow Near a Wall," J.A.S., Vol. 23, No. 11, Nov. 1956, pp. 1007-1011, 1036.

23. Patankar, S. V., and Spalding, D. B., Heat and Mass Transfer in Boundary Layers, C.R.C. Press, 1967.

24. Reichardt, H., "Vollständige Darstellung der turbulenten Geschwindigkeitsverteilung in glatten Lutungen," ZAMM 31, 1951, pp. 208-219.

25. Klebanoff, P. S., "Characteristics of Turbulence in a Boundary Layer with Zero Pressure Gradient," NASA TN-3178, 1954.

26. Richtmyer, R. D., <u>Difference Methods for Initial-Value Problems</u>, Interscience Publishers, Inc., New York, 1957.

27. Cebeci, T., and Mosinskis, G., "Prediction of Turbulent Boundary Layers with Mass Addition, Including Highly Accelerating Flows," ASME Paper 70-HT/SpT-19, June, 1970.

28. Miner, E. W., Anderson, E. C., and Lewis, C. H., "A Computer Program for 2-D and Axisymmetric Non-Reacting Perfect Gas and Equilibrium Chemically Reacting Laminar, Transitional, and Turbulent Boundary-Layer Flows," College of Engineering Report, VPISU, Blacksburg, Virginia, to be published, 1971.

29. Owen, F. K., [1970] "Transition Experiments on a Flat Plate at Subsonic and Supersonic Speeds," <u>AIAA J.</u>, Vol. 8, No. 3, March, 1970, pp. 518-523.

30. Coles, D., "Measurements of Turbulent Friction on a Smooth Flat Plate in Supersonic Flow," <u>J. Aero. Sci.</u> Vol. 21, No. 7, July, 1954, pp. 433-448.

31. Dorrance, W. H., <u>Viscous Hypersonic Flow</u> (McGraw-Hill, New York) Chapter 7, 1962.

32. Hironimus, G. A., "Hypersonic Shock Tunnel Experiments on the W7 Flat Plate Model-Expansion Side Turbulent Flow and Leading Edge Transpiration Data," CAL Dept. AA-1953-y-2, Feb. 1966.

33. Lewis, C. H. ed. [1970]: <u>Nonreacting and Chemically Reacting Viscous Flows Over a Hyperboloid at Hypersonic Condition.</u> AGARDograph No. 147. NATO, Paris, Sept. 1970.

34. Adams, J. C., "Higher Order Boundary-Layer Effects for the AGARD Engineering Applications Body and Flow Conditions," <u>Nonreacting and Chemically Reacting Viscous Flows Over a Hyperboloid at Hypersonic Condition.</u> Lewis, C. H. ed, AGARDograph No. 147, NATO, Paris, Sept. 1970, pp. 121-134.

35. Keltner, G. L., and Smith, A. M. O., [1970] "Laminar Boundary-Layer Calculations on Bodies of Revolution in Hypersonic Flow," <u>Nonreacting and Chemically Reacting Viscous Flows Over a Hyperboloid at Hypersonic Condition.</u> Lewis, C. H. ed., AGARDograph No. 147, NATO, Paris, Sept. 1970, pp. 37-54.

36. Inouye, M., Rakich, J. V., and Lomax, H., "A Description of Numerical Methods and Computer Programs for Two-Dimensional and Axisymmetric Supersonic Flow Over Blunt-Nosed and Flared Profiles." NASA-TN D-2970, 1965.

37. Enkenkus, K. R., and Maher, E. F., "The Aerodynamic Design of Axisymmetric Nozzles for High-Temperature Air," NOL-R-7395, Feb. 1962.

38. Burke, A. F., and Bird, K. D., "The Use of Conical and Contoured Expansion Nozzles in Hypervelocity Facilities," CAL Report No. 112, Revised-July, 1962.

39. Lee, J. D., "Axisymmetric Nozzles for Hypersonic Flows," WADC TN-228, June, 1960.

40. Danberg, J. E., "Characteristics of the Turbulent Boundary Layer with Heat Transfer: Data Tabulation," NOLTR 67-6, Jan. 1967.

41. Hansen, C. F., "Approximations for the Thermodynamic and Transport Properties of High Temperature Air." NASA TR-R-50, 1959.

42. Ahyte, W. F., and Peng, T. C., "Approximations for the Thermodynamic and Transport Properties of High-Temperature Nitrogen with Shock-Tube Applications." NASA TN D-1303, 1962.

43. Wilke, C. R., "A Viscosity Equation for Gas Mixtures." J. Chem. Physics, Vol. 18, No. 4, April 1950, pp. 517-519.

44. Yun, K. S., and Mason, E. A., "Collision Integrals for the Transport Properties of Dissociating Air at High Temperatures," Physics of Fluids, Vol. 5, No. 4, April, 1962. pp. 380-386.

TABLE I

Test Conditions for Cole's Flat Plate Experiments

Case	P_o (cm Hg)	T_o (°R)	u_∞ (ft/sec)	M_∞	$Re_\infty \times 10^{-6}$/ft	T_w
20	103	561	2219	3.701	0.1642	Adiabatic
26	131	568	1972	2.578	0.387	Adiabatic
62	302	563	2327	4.544	0.322	Adiabatic

TABLE II

Elliott, Bartz, and Silver Test Case Nozzle Data

P_o = 300 psia P_∞ = 11.54 psia

T_o = 4500 °R T_∞ = 2614 °R

Re_∞ = 0.2 x 10^6/in. ρ_∞ = 3.7 x 10^{-4} slugs/ft^3

M_∞ = 2.685 T_w = 1125 °R

u_∞ = 6231 ft/sec. Pr = 0.83

γ = 1.2

TABLE III

Test Conditions for NASA-Lewis Nozzle – Case 2a

$P_O = 299.3$ psia

$P_\infty = 0.56$ psia

$T_O = 970$ °R

$T_\infty = 161$ °R

$Re_\infty = 0.588 \times 10^6/in.$

$\rho_\infty = 2.9 \times 10^{-4}$ slugs/ft^3

$M_\infty = 5.01$

$u_\infty = 3118$ ft/sec

$\gamma = 1.4$

T_w variable

TABLE IV

Test Conditions for AEDC Hotshot-Nozzle

Perfect Gas (N_2)

P_o = 11511.57 psia P_∞ = 4.34 x 10^{-4} psia

T_o = 5400 °R T_∞ = 78.87 °R

Re_∞ = 5.3 x 10^4/in. ρ_∞ = 4.46 x 10^{-6} slugs/ft^3

M_∞ = 18.37 u_∞ = 8132 ft/sec

γ = 1.4 T_w, variable

Equilibrium N_2

P_o = 11511.57 psia P_∞ = 4.33 x 10^{-3} psia

T_o = 5400 °R T_∞ = 108 °R

Re_∞ = 3.0 x 10^4/in. P_∞ = 3.41 x 10^{-6} slugs/ft^3

M_∞ = 17.24 u_∞ = 8732 ft/sec

T_w, variable

TABLE V

Test Conditions for Hironimus' Flat Plate Experiments

Case 1

$P_o = 8498$ psia

$T_o = 4913$ °R

$Re_\infty = 4.46 \times 10^5/\text{in}$

$M_\infty = 7.391$

$T_w = 533$ °R

$P_\infty = 1.53$ psia

$T_\infty = 546$ °R

$\rho_\infty = 2.49 \times 10^{-4}$ slugs/ft^3

$u_\infty = 8157$ ft/sec

Case 2

$P_o = 14670$ psia

$T_o = 3691$ °R

$Re_\infty = 1.33 \times 10^6/\text{in}$

$M_\infty = 7.58$

$T_w = 355$ °R

$P_\infty = 2.46$ psia

$T_\infty = 339$ °R

$\rho_\infty = 6.1 \times 10^{-4}$ slugs/ft^3

$u_\infty = 6843$ ft/sec

TABLE VI

Flight Conditions for AGARD Test Case A

P'_o = 6.035 atms $\qquad\qquad$ P_∞ = 1.0997 x 10^{-2} atms

T'_o = 6996 °K $\qquad\qquad$ T_∞ = 226.98 °R

Re_∞ = 2157943/ft $\qquad\qquad$ ALT = 100,000 ft

M_∞ = 20.178 $\qquad\qquad$ r_n = 1 in

u_∞ = 20,000 ft/sec $\qquad\qquad$ T_w = 1400 °K

TABLE VII

Flight Conditions for Sphere-Cone Sample Case

$P_0'/P_\infty = 513.994$ $P_\infty = 4.429 \times 10^{-2}$ atms

$T_0'/T_\infty = 33.065$ $T_\infty = 217.9$ °K

$\rho_0'/\rho_\infty = 11.783$ $\rho_\infty = 5.555 \times 10^{-2}$ AMAGAT

$M_\infty = 19.564$ Alt = 70,000 ft

$Re_\infty = 8.898 \times 10^6$/ft $T_W = 1000$ °R

$u_\infty = 19,000$ ft/sec $\gamma_0' = 1.1655$

TABLE VIII

Test Conditions for Flat Plate Flows with Mass Injection

Run No.	x, mm	$Re_x \times 10^{-6}$	M_e	T_w/T_e	$T_e \, °K$	$\dfrac{\rho_w v_w}{\rho_e u_e} \times 10^4$
5	377.8	2.925	6.38	4.102	60.4	9.23
6	428.6	3.446	6.49	4.132	58.1	9.07
7	479.4	4.160	6.60	4.263	56.3	8.85
8	530.2	4.261	6.48	4.167	58.3	9.21
9	377.8	3.249	6.39	4.102	59.5	16.86
10	479.4	3.950	6.42	3.991	59.1	16.24
11	530.2	4.264	6.37	3.808	60.0	17.81
12	377.8	3.185	6.28	3.864	61.9	24.91
13	428.6	3.619	6.20	3.640	62.4	24.52
14	479.4	3.945	6.22	3.759	62.5	24.90
15	530.2	4.298	6.22	3.662	62.5	25.80
16	377.8	3.057	6.52	4.418	57.6	0.0
17	428.6	3.163	6.32	4.171	61.0	0.0
18	479.4	3.679	6.44	4.346	59.0	0.0
19	530.2	4.260	6.45	4.297	58.6	0.0

TABLE IX

Comparison of Numerical Predictions and Experimental Data for Flat Plate Flows with Mass Injection

Danberg Run No.	Exp. or Calc.	x (mm)	Re/mm	$\rho_w v_w / \rho_e u_e$	$C_f \times 10^4$	$C_h \times 10^4$	θ (mm)	δ^* (mm)	δ (mm)	Re_θ	δ^*/θ
	exp.				12.54	6.33	0.376	5.68	10.0	3023	15.11
19		530.2	8034.7	0.0							
	calc.				11.95	7.77	0.409	5.75	10.1	3284	14.06
	exp.				8.39	3.17	0.658	7.86	14.1	5288	11.94
8		530.2	8036.6	9.21							
	calc.				4.902	3.77	0.665	9.57	15.4	5341	14.40
	exp.				5.17	1.90	0.934	10.7	18.0	7511	11.46
11		530.2	8042.2	17.81							
	calc.				2.59	2.37	0.996	14.2	21.8	8009	14.23
	exp.				3.40	1.29	1.25	14.2	22.7	10166	11.36
15		530.2	8106.4	25.8							
	calc.				1.50	1.54	1.34	19.2	28.5	10820	14.39
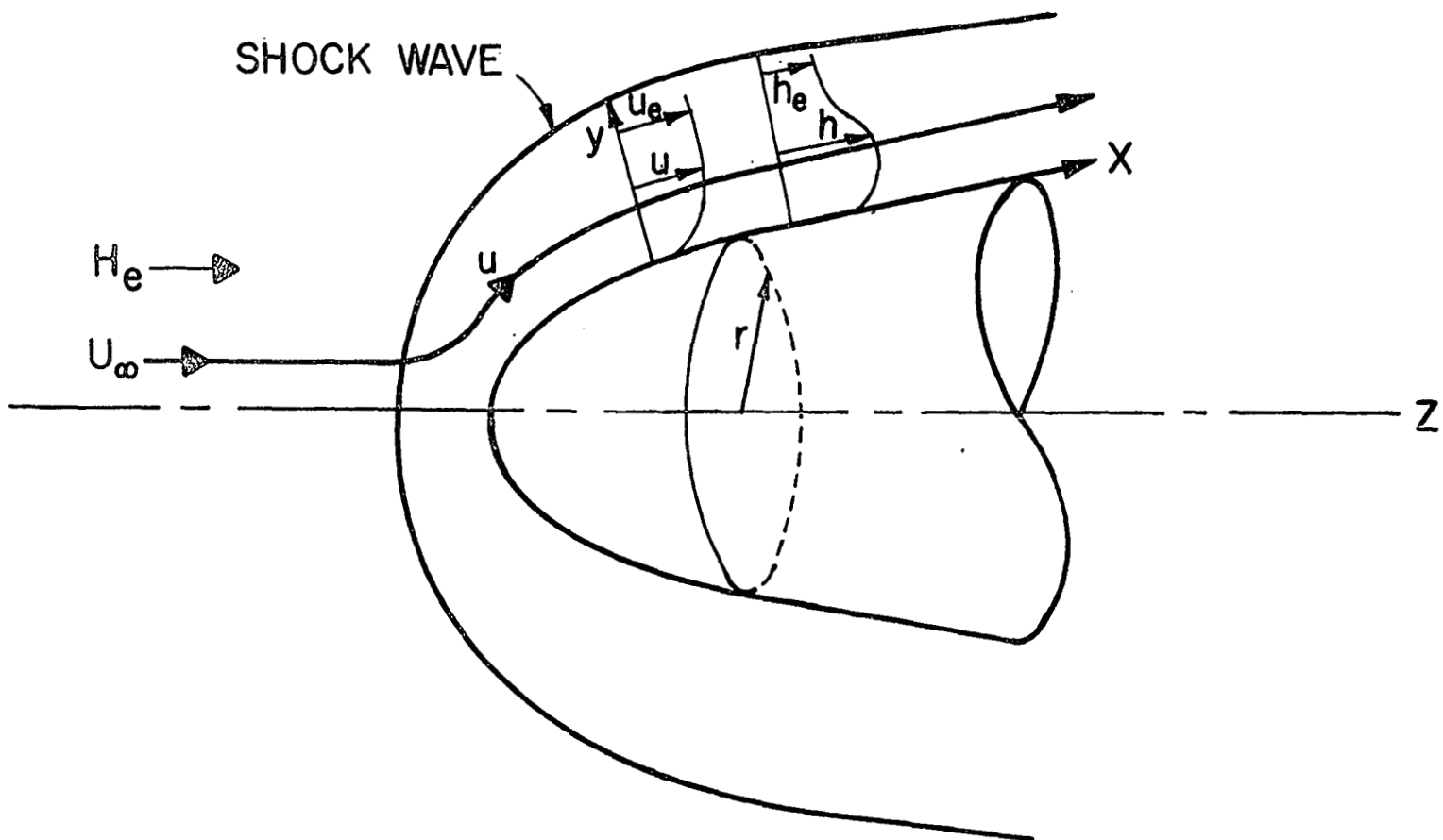
Figure 1: Boundary Layer Coordinate System
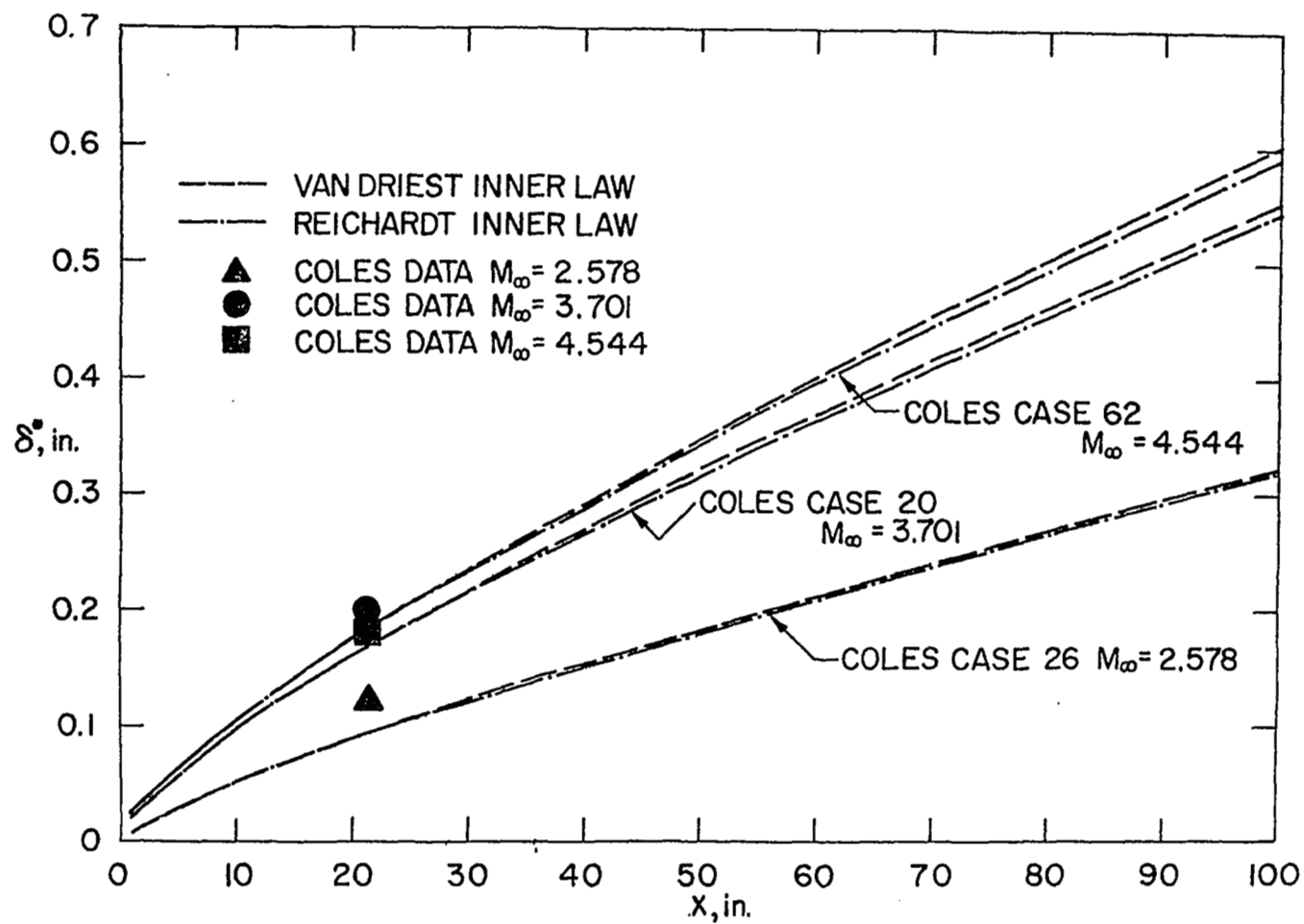
Figure 2: Displacement Thickness for Flat Plates—Coles Data
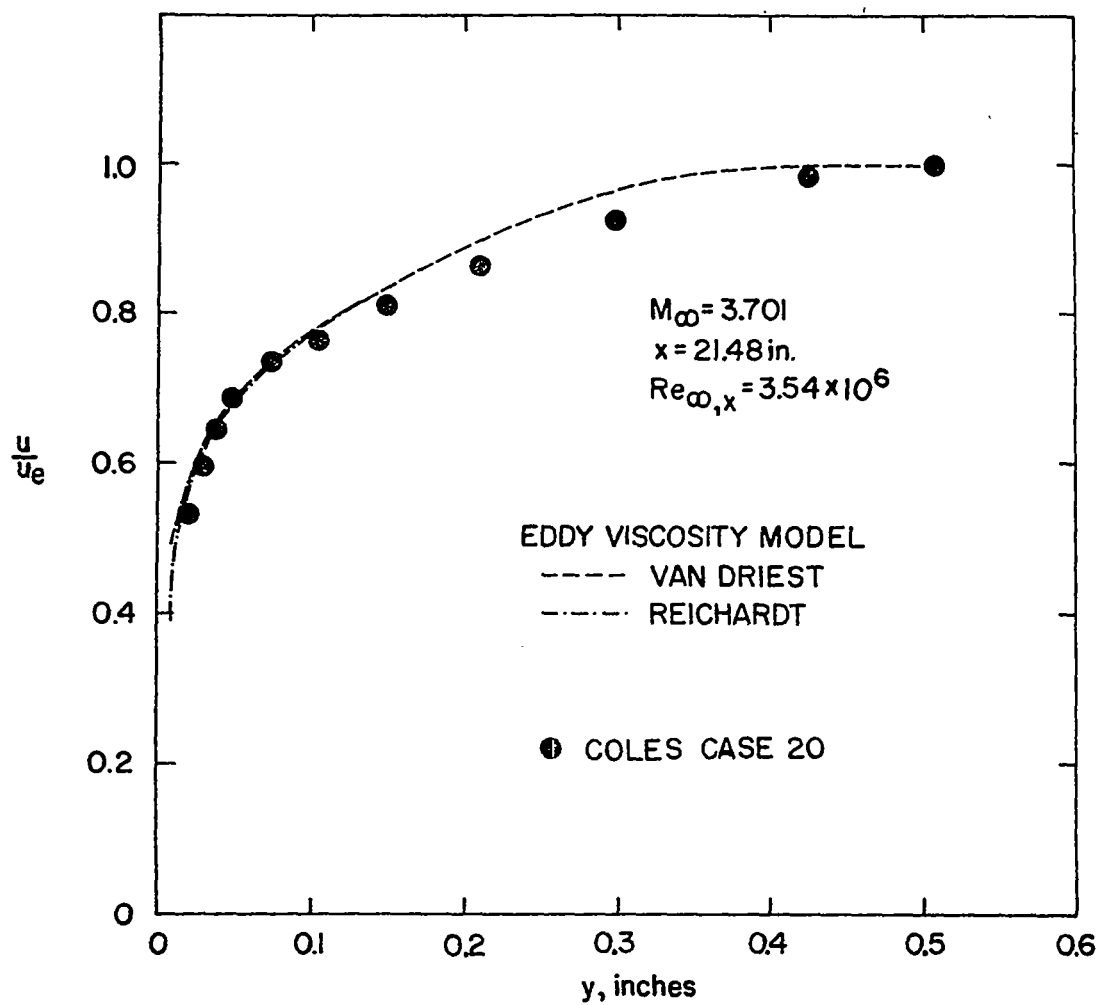
Figure 3: Velocity Profiles for a Flat-Plate-Coles Data
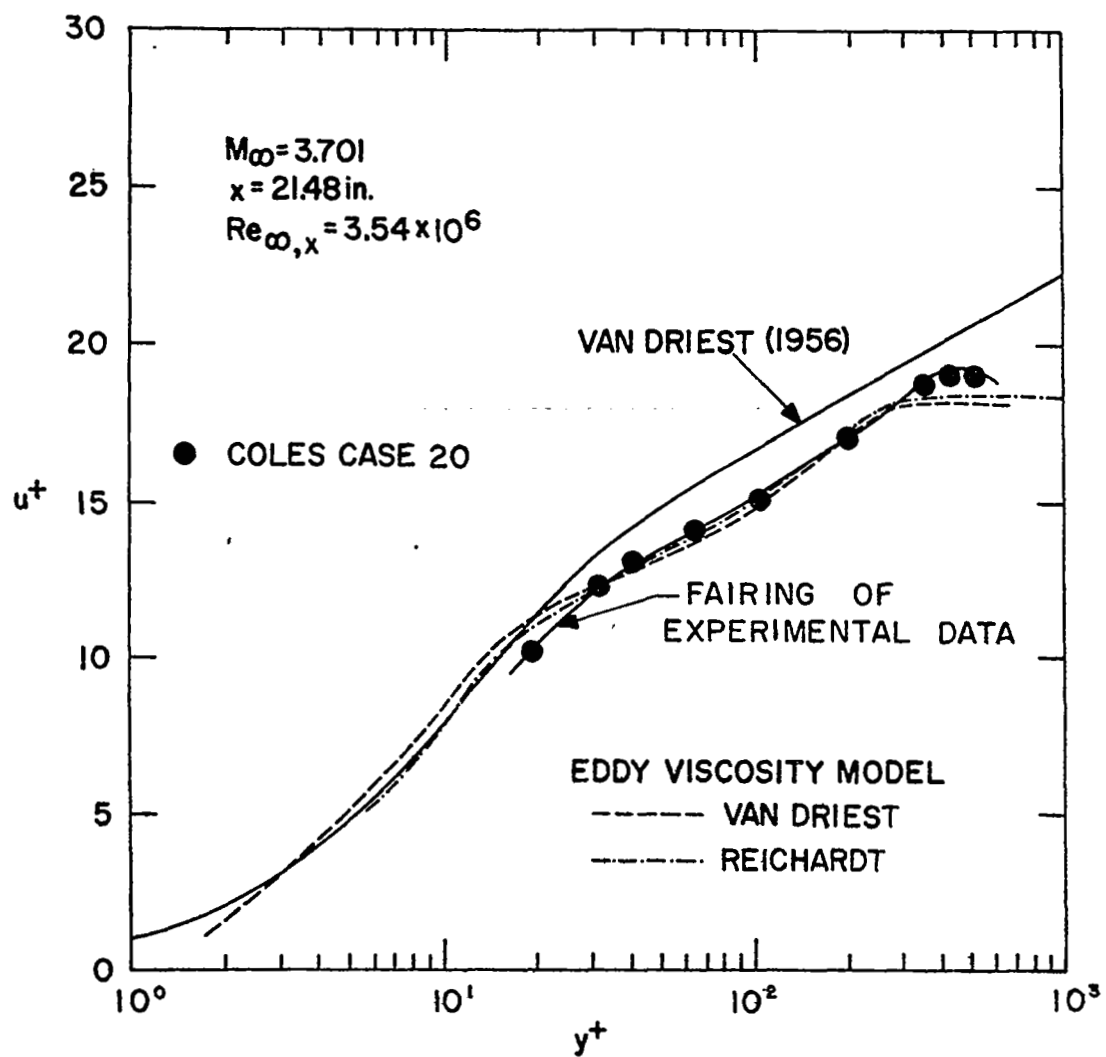
Figure 4: Velocity Profiles for a Flat Plate-Law of the Wall Variables-Coles Data

111
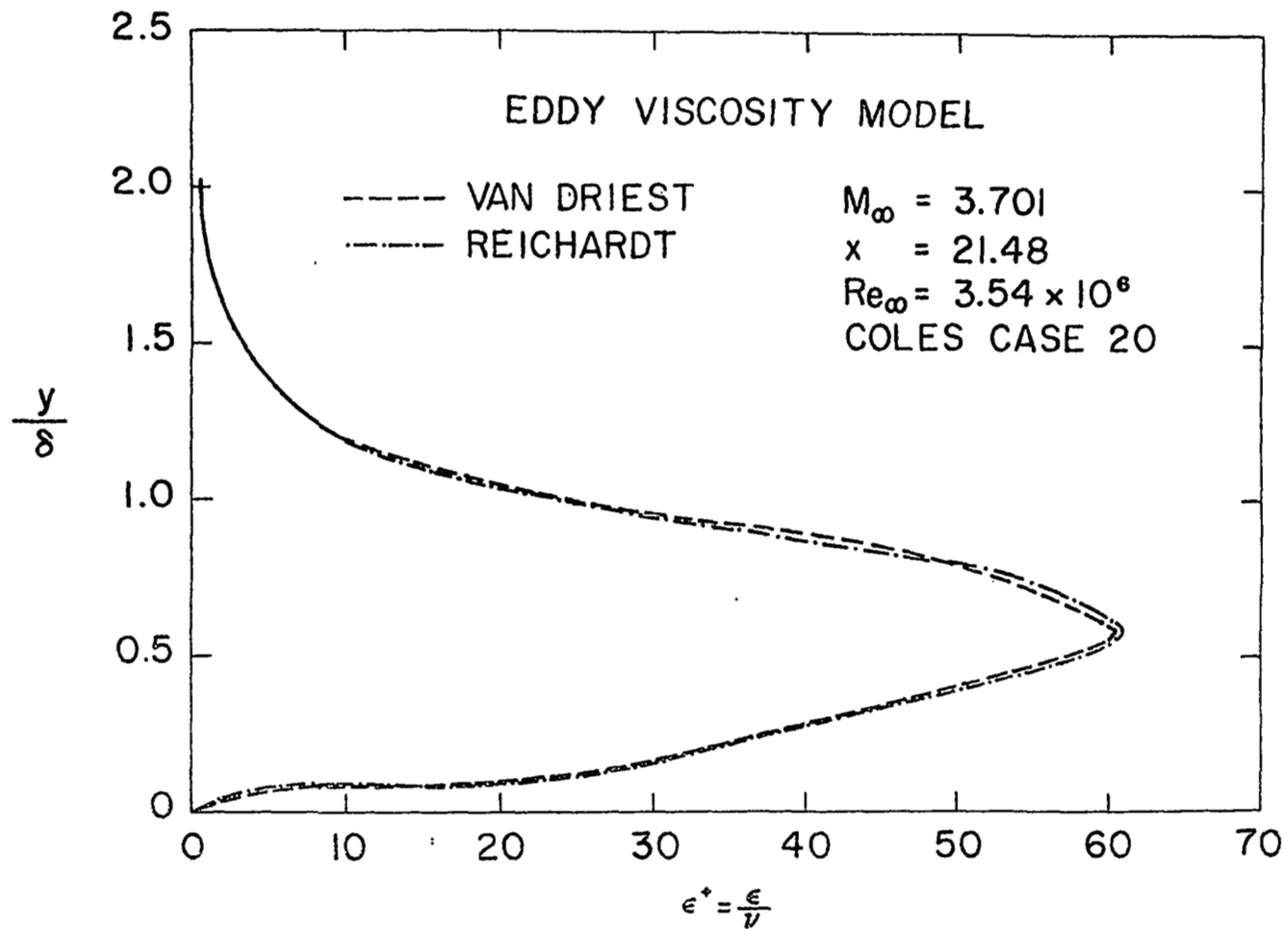
Figure 5: Comparison of Eddy Viscosity Profiles for a Flat Plate-Coles Data
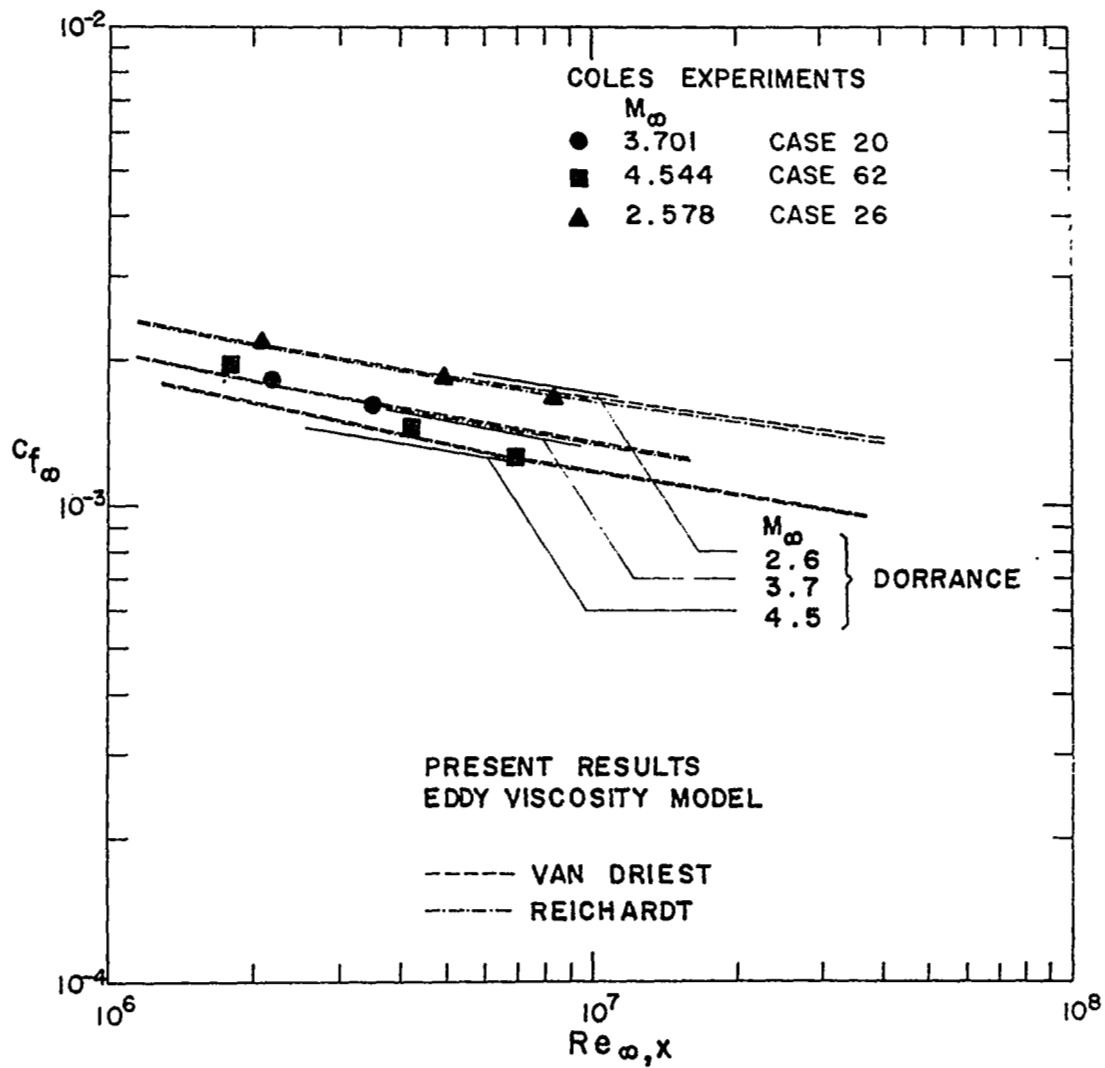
Figure 6: Skin-Friction Distribution for a Flat Plate-Coles Data

113
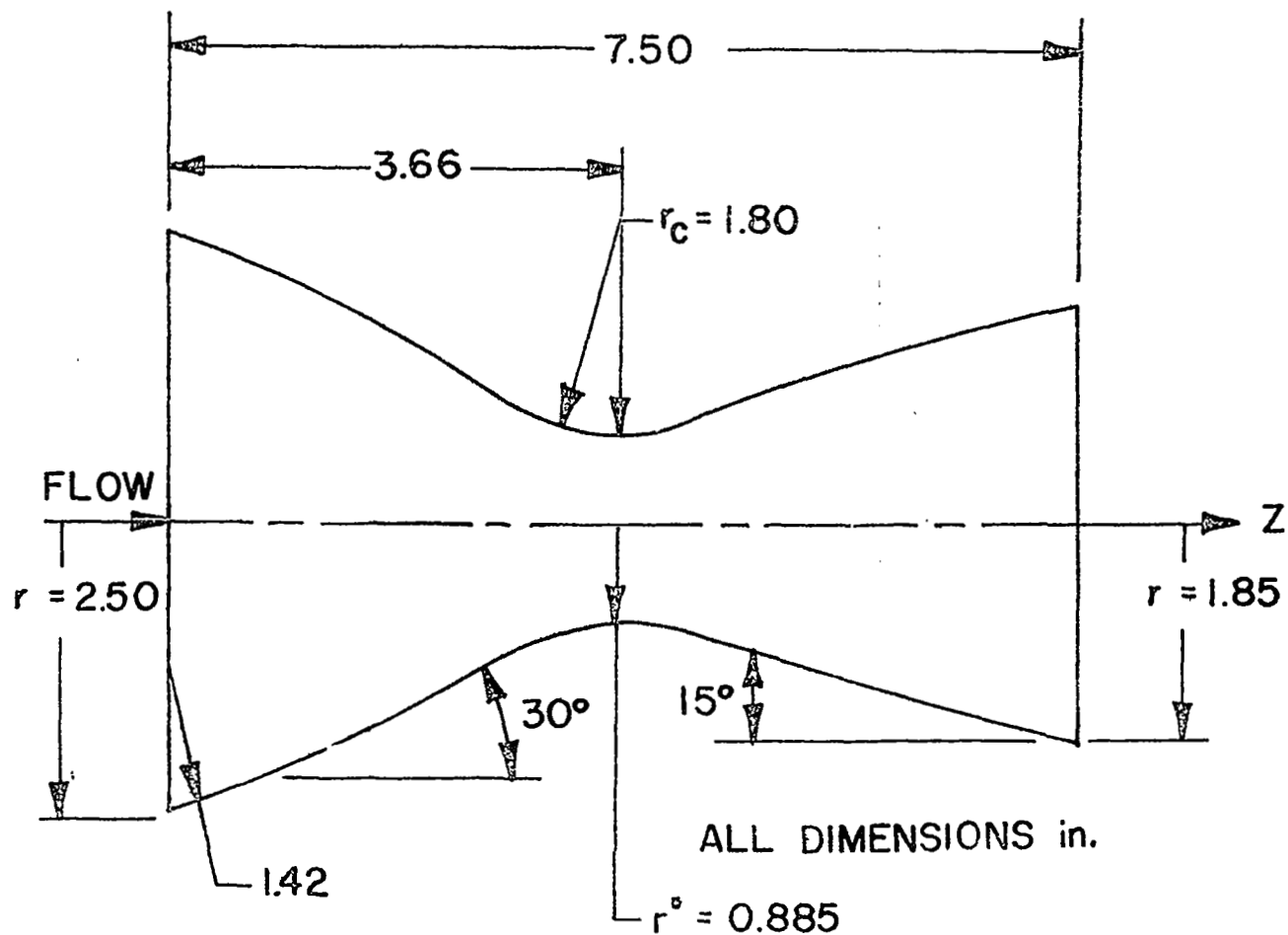
Figure 7: Nozzle Geometry-Elliott, Bartz, and Silver Test Case

$P_o = 300psi$, $T_o = 4500°R$, $\beta = 6.5$

CURVE	ϵ^+MODEL
1	CEBECI & SMITH
2	VAN DRIEST
3	$|DP/DX|$
4	REICHARDT

Figure 8: Eddy Viscosity Profiles at Nozzle Throat-Elliott, Bartz, and Silver Test Case

115

$P_o = 300\,psi$, $T_o = 4500°R$

NOMINAL ENTRANCE CONDITIONS					
CASE	δ	Λ	θ	ϕ	ζ
1	0	0	0	0	1.00
2a	0.188	0.201	0.022	0.024	1.01
2b	0.188	0	0.018	0	0
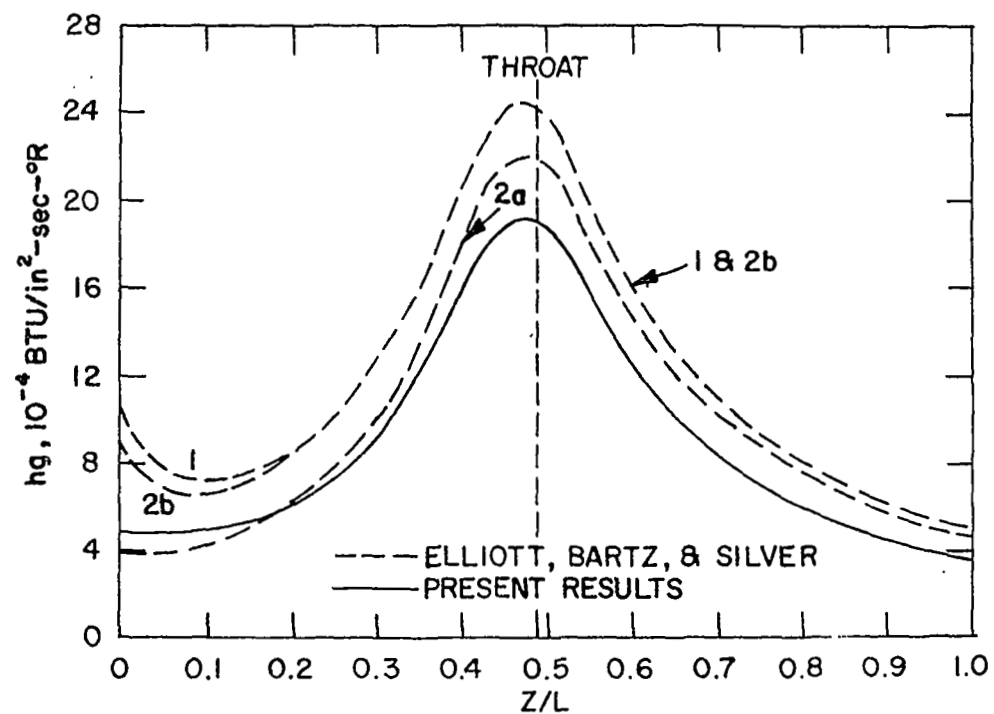
Figure 9: Heat Transfer Distribution Along Nozzle Wall-Elliott, Bartz, and Silver Test Case

$P_0 = 300psi$, $T_0 = 4500°R$

NOMINAL ENTRANCE CONDITIONS					
CASE	δ	Δ	θ	ϕ	ζ
1	0	0	0	0	1.00
2a	0.188	0.201	0.022	0.024	1.01
2b	0.188	0	0.018	0	0
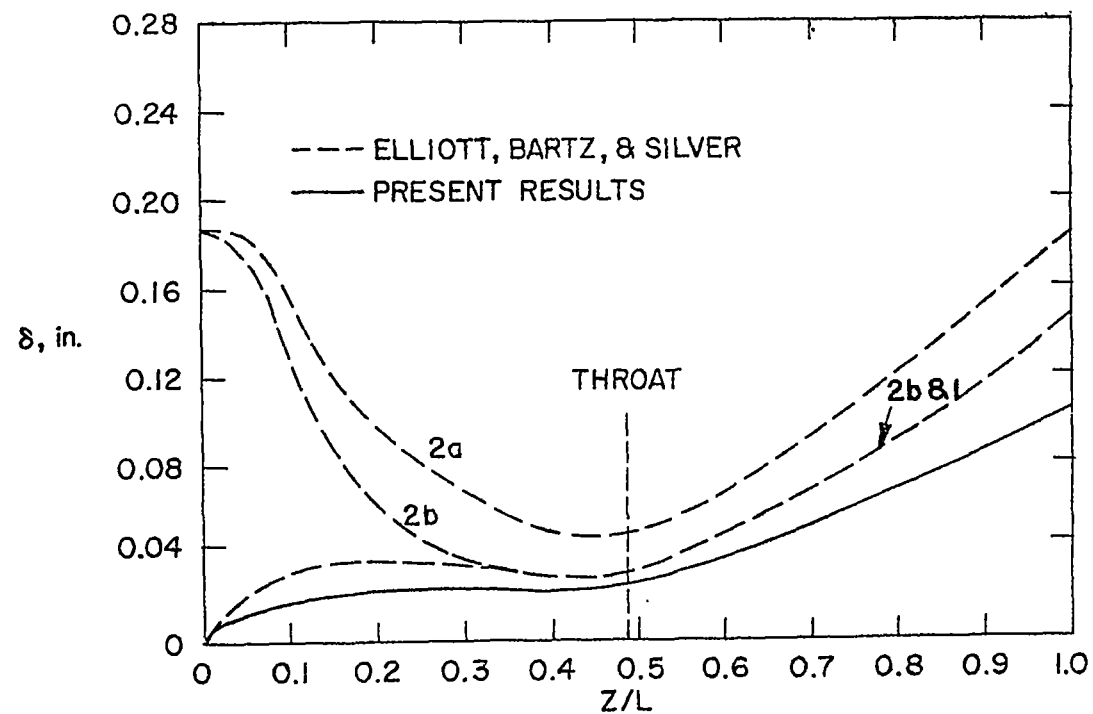
Figure 10: Boundary Layer Thickness Distribution for a Nozzle-Elliott, Bartz, and Silver Test Case

NOMINAL ENTRANCE CONDITIONS					
CASE	δ	Δ	θ	ϕ	ζ
1	0	0	0	0	1.00
2a	0.188	0.201	0.022	0.024	1.01
2b	0.188	0	0.018	0	0

——— PRESENT RESULTS

– – – ELLIOT, BARTZ & SILVER

P_0 = 300 psi

T_0 = 4500° R

THROAT

δ^*, in

Z/L
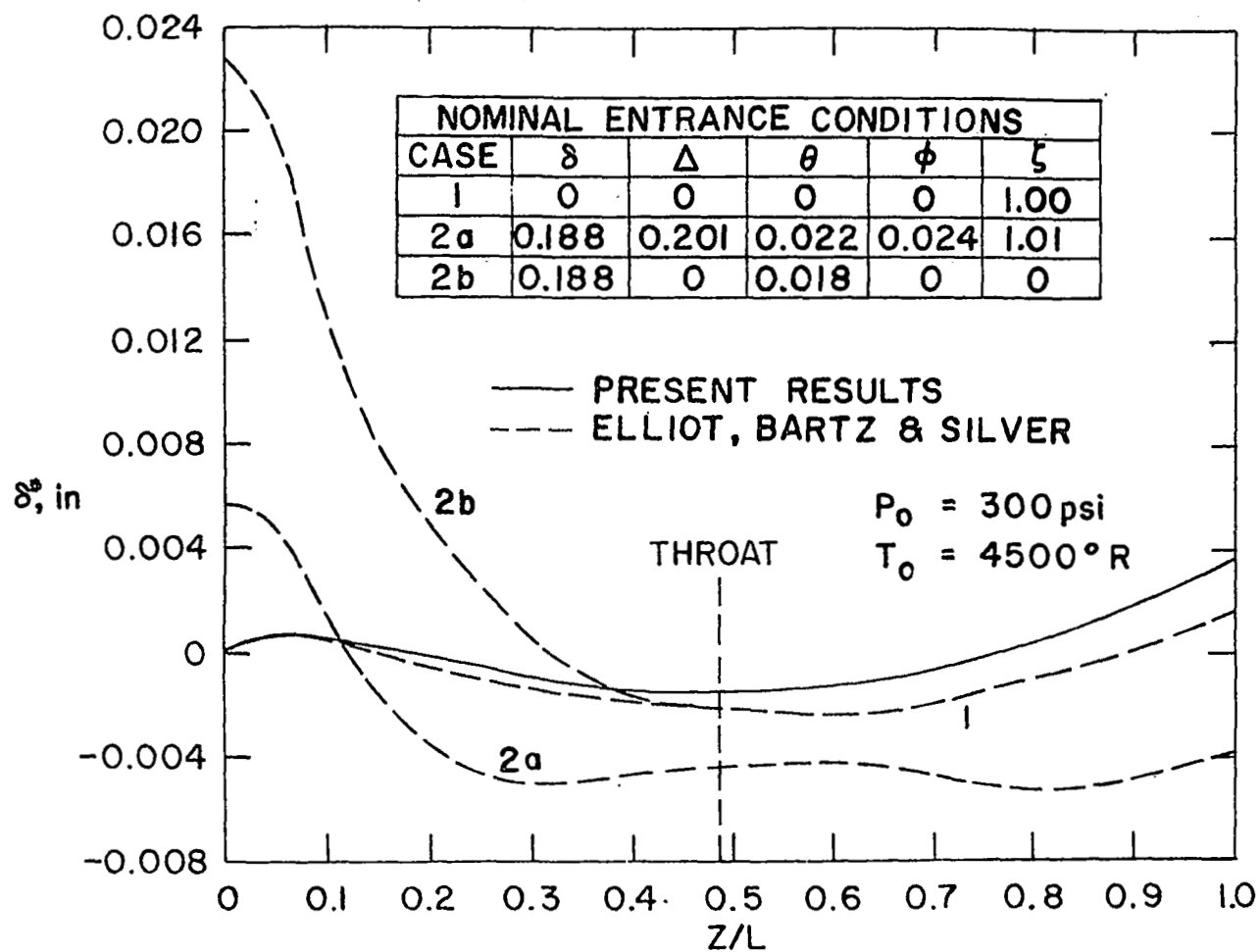
Figure 11: Displacement Thickness Distribution for a Nozzle-Elliott, Bartz, and Silver Test Case
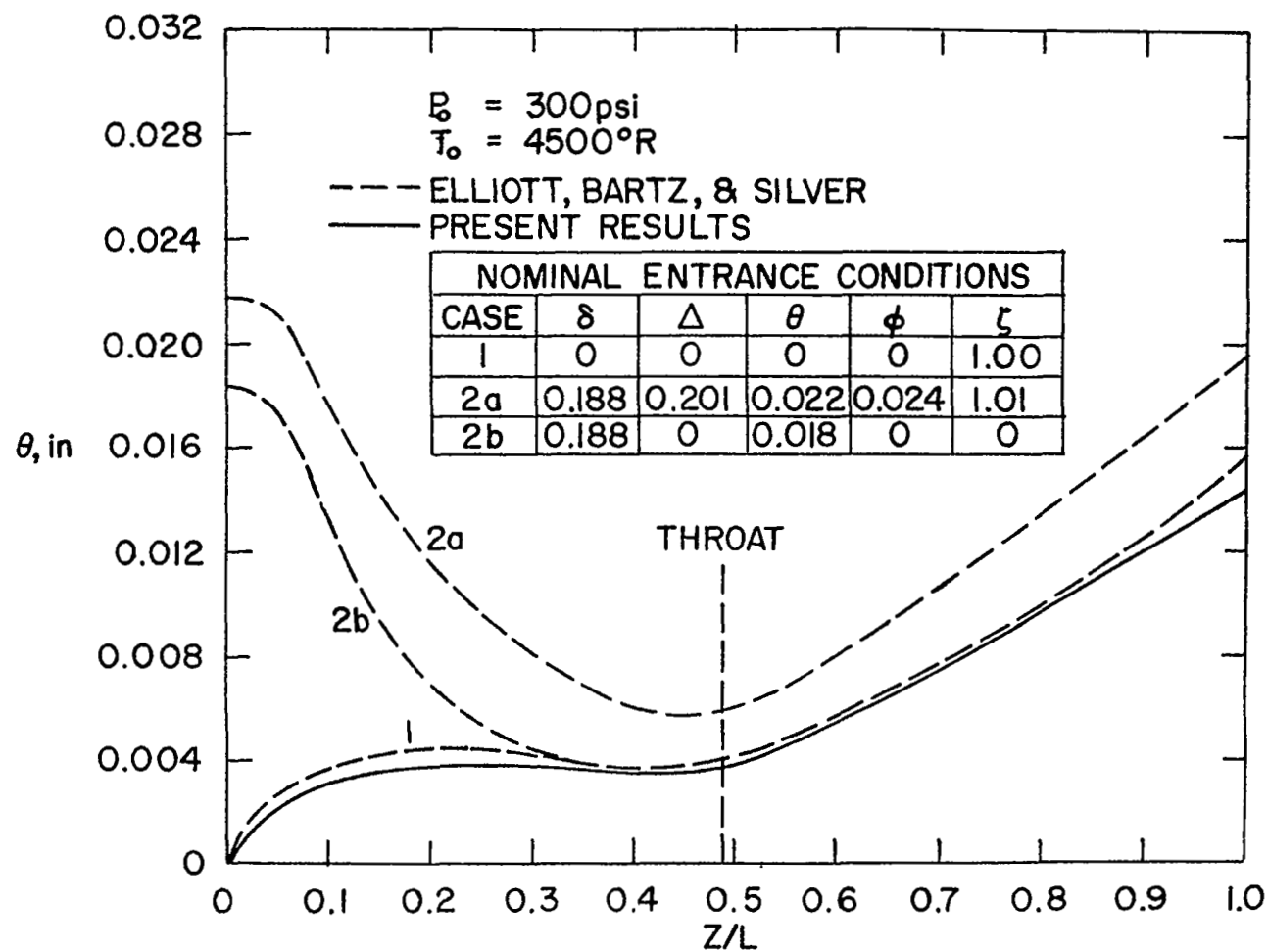
Figure 12: Momentum Thickness Distribution for a Nozzle-Elliott, Bartz, and Silver Test Case
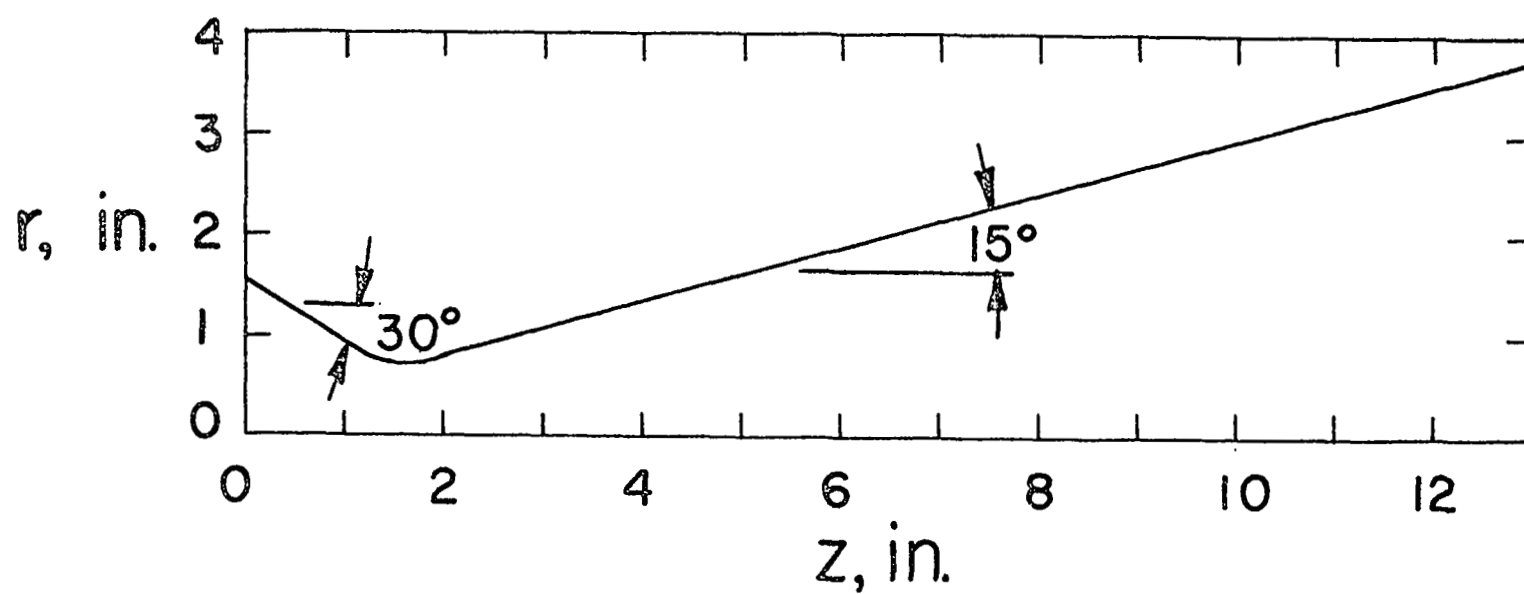
Figure 13: Geometry for the NASA-Lewis Nozzle
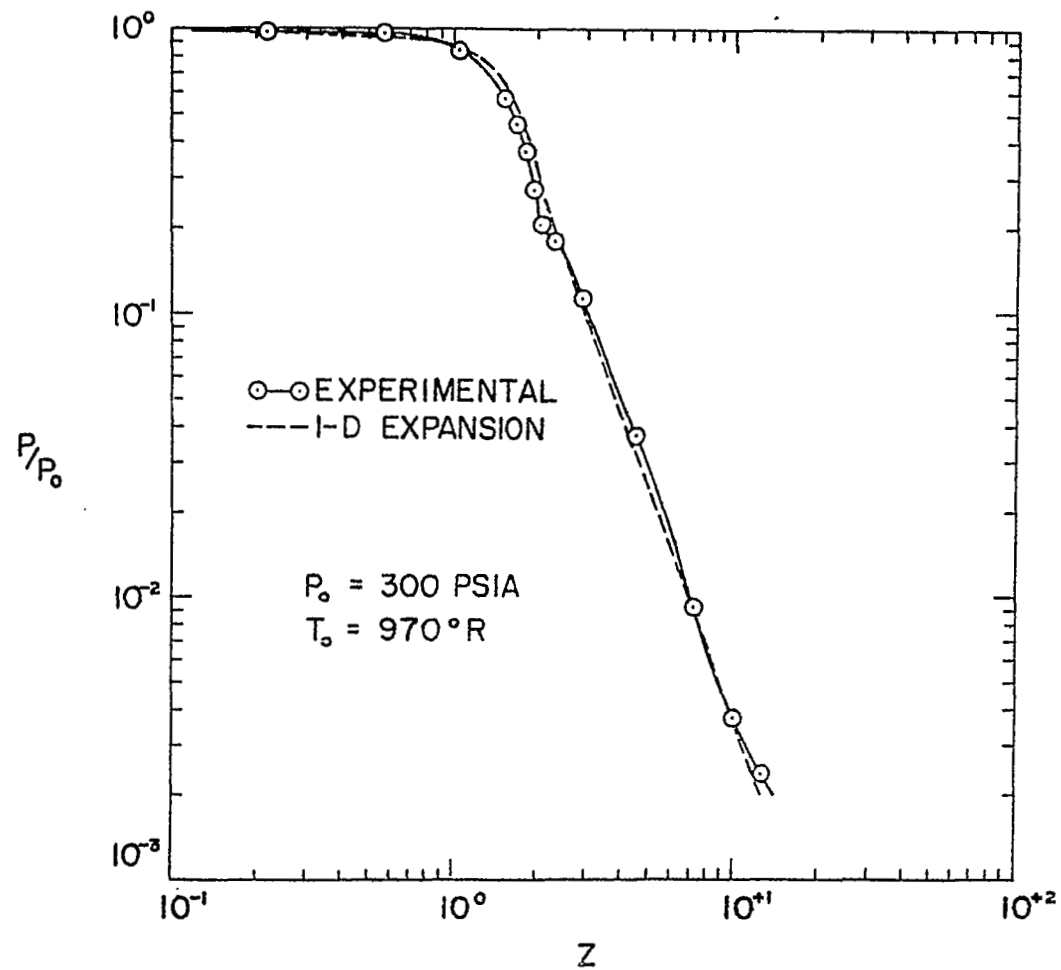
Figure 14: Pressure Distribution for the NASA-Lewis Nozzle
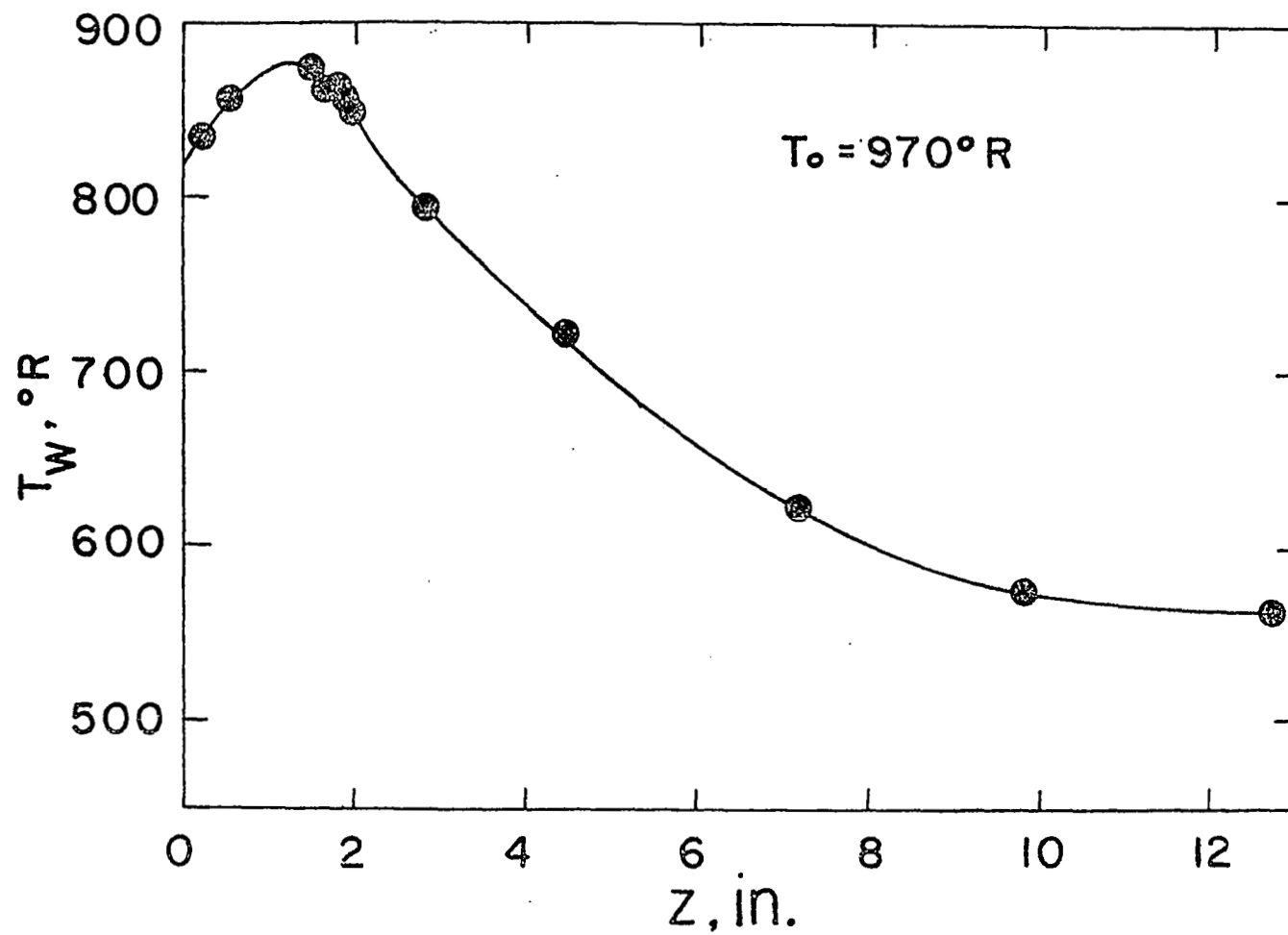
Figure 15:   Wall Temperature Distribution for the NASA-Lewis Nozzle
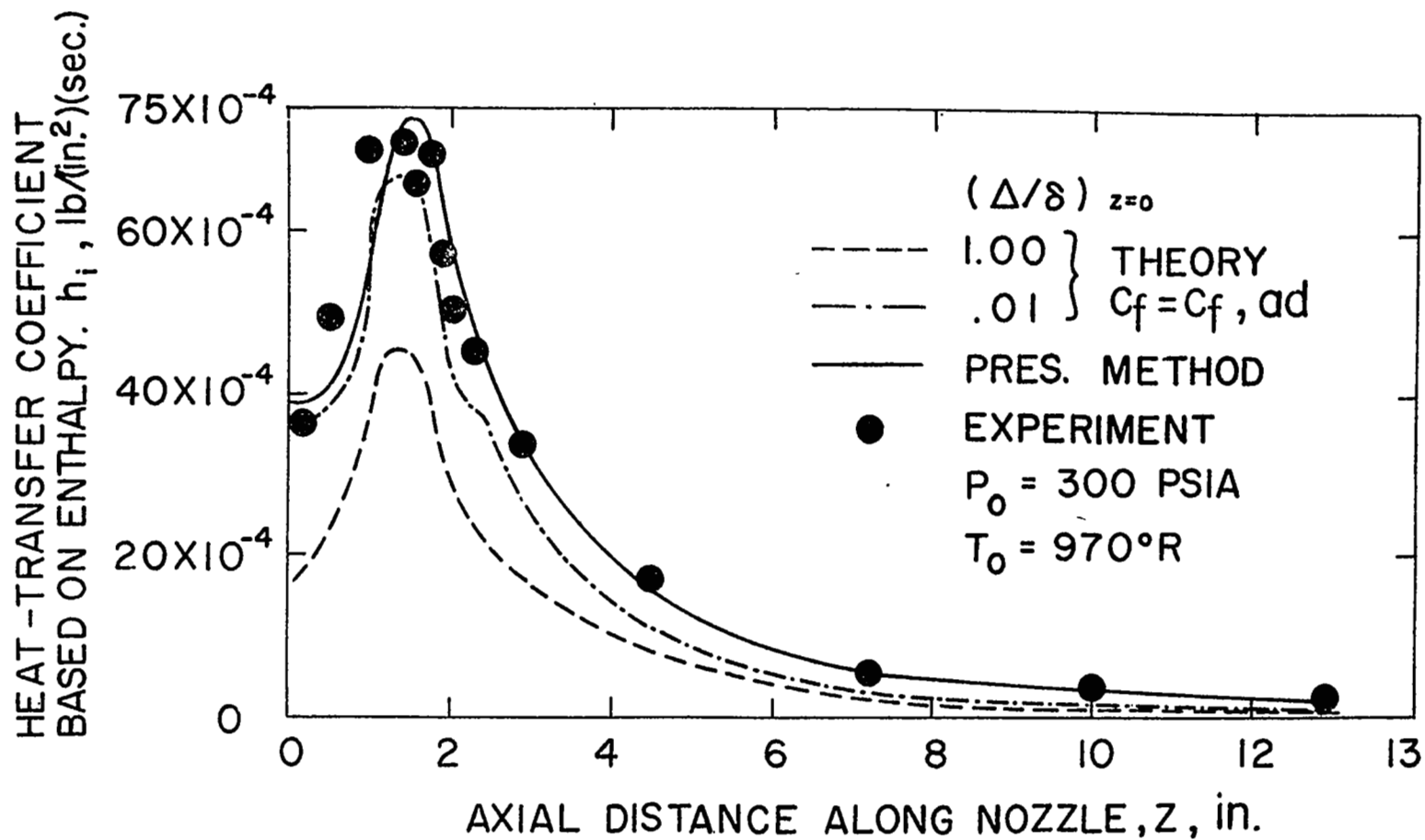
Figure 16: Heat Transfer Distribution for the NASA-Lewis Nozzle
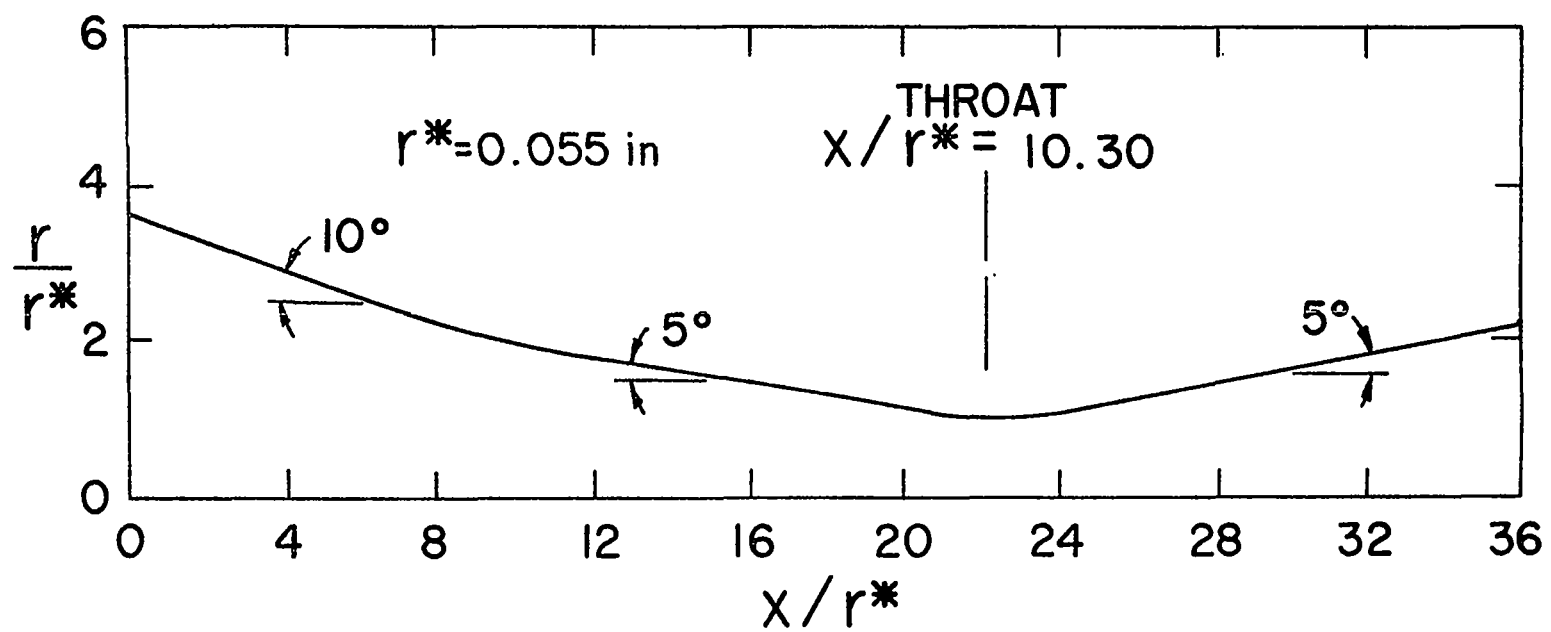
Figure 17: Geometry for the AEDC Hotshot-Nozzle
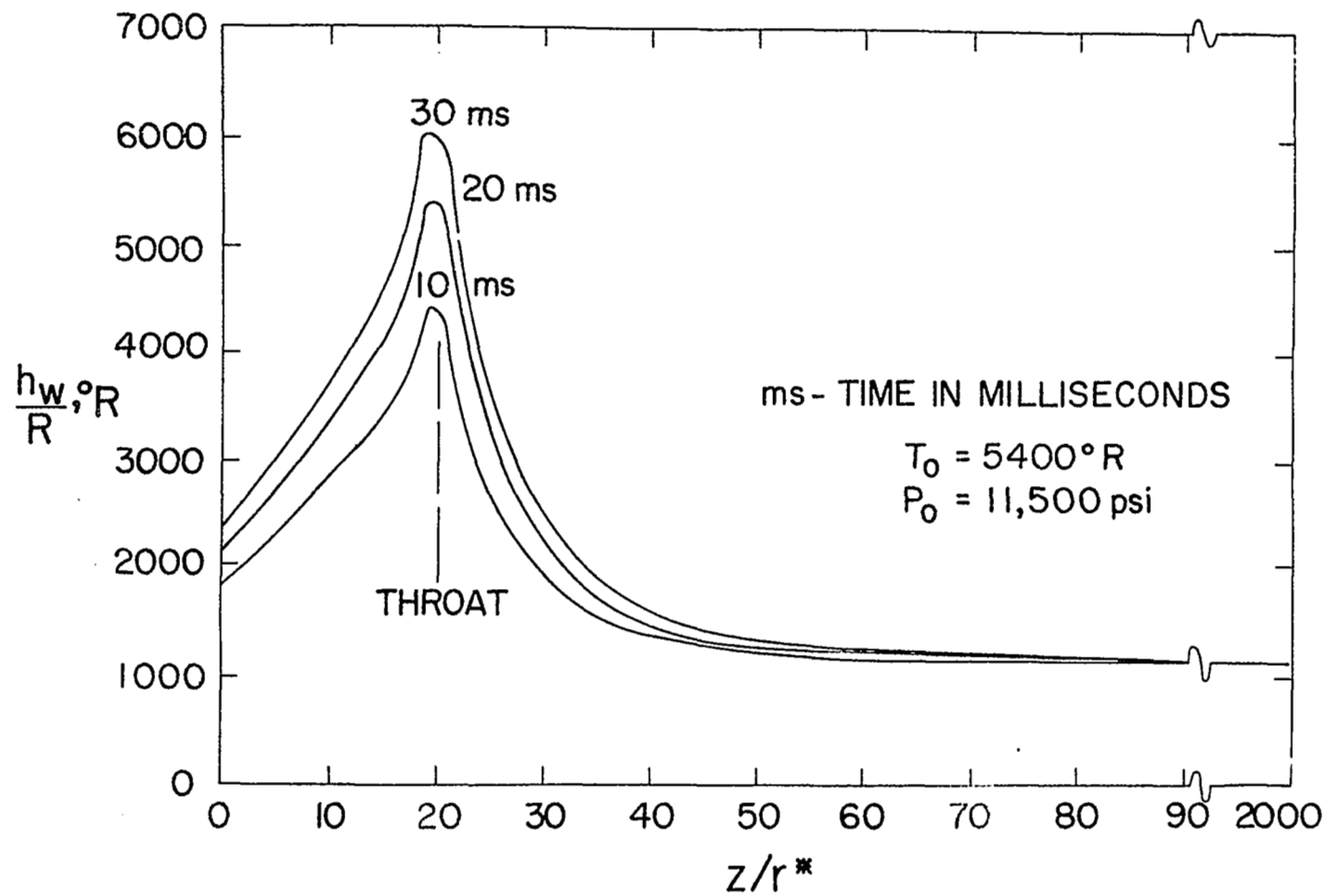
Figure 18: Wall Enthalpy Distribution for the AEDC Hotshot-Nozzle
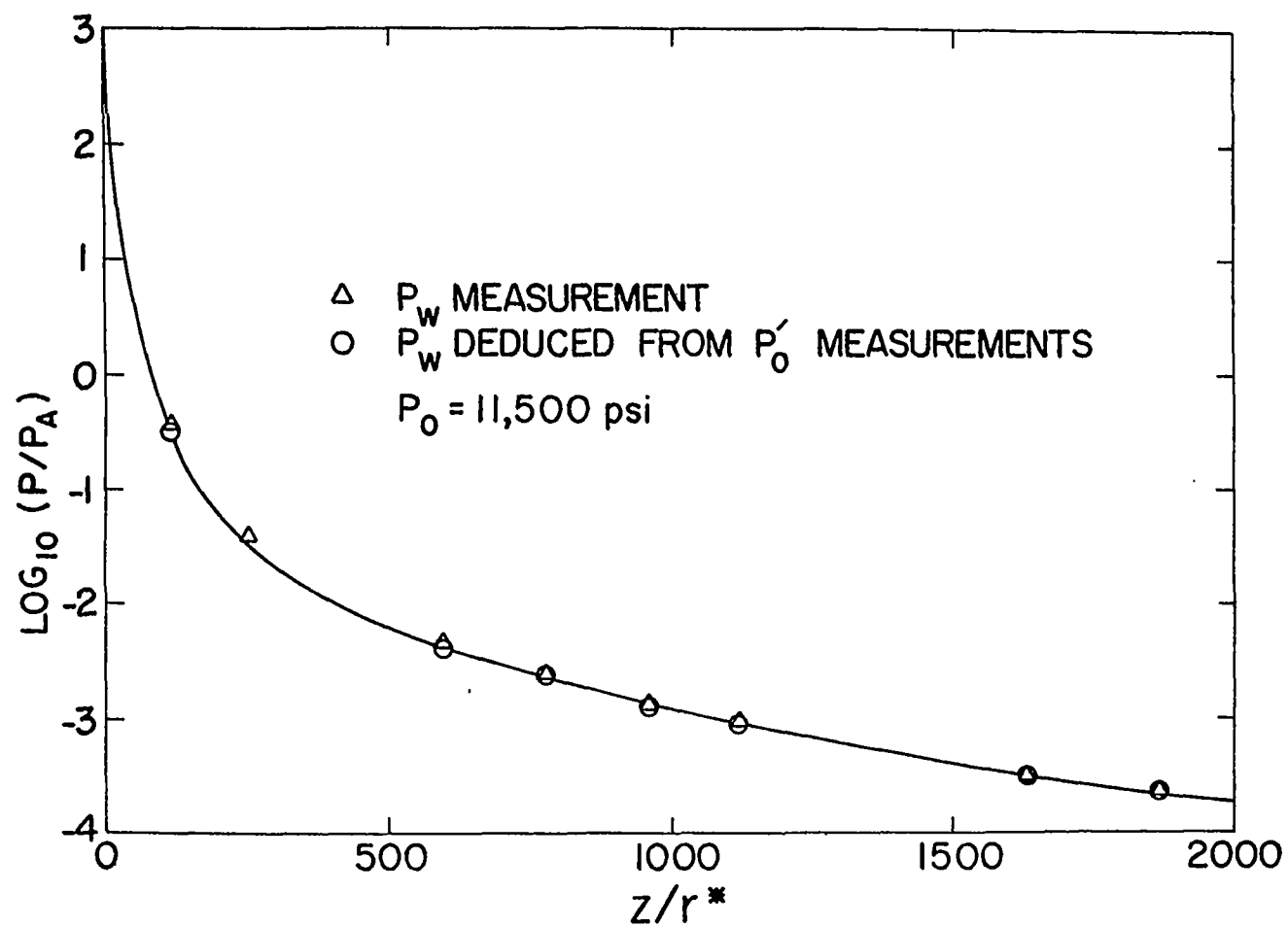
Figure 19: Pressure Distribution for the AEDC Hotshot-Nozzle
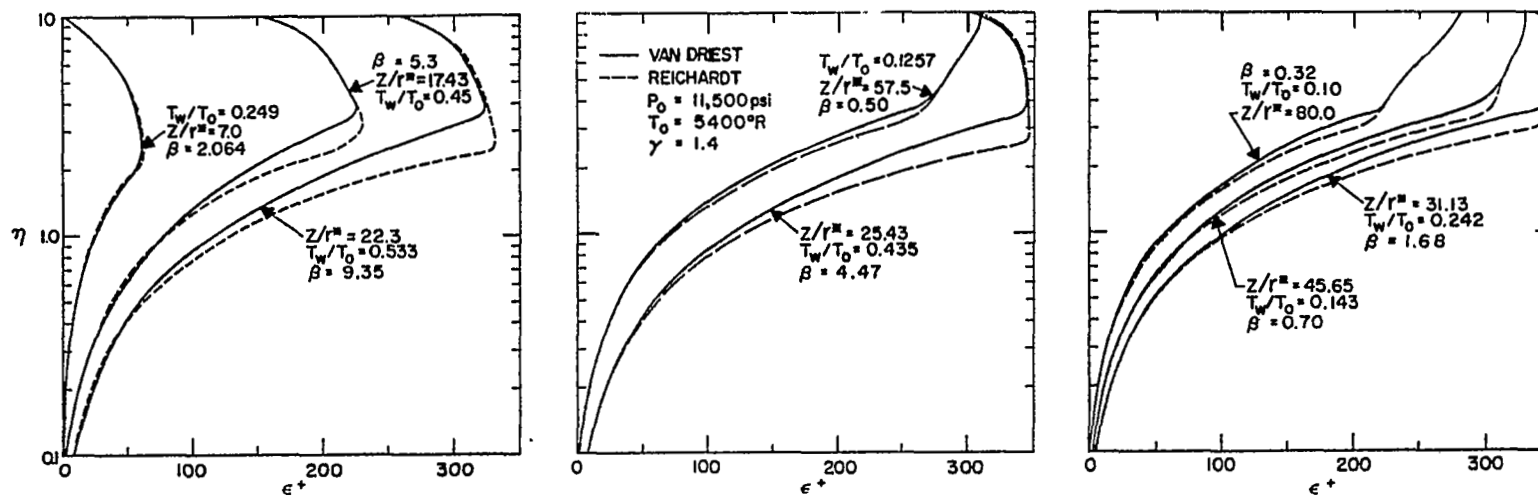
Figure 20: Eddy Viscosity Profiles for the AEDC Hotshot-Nozzle
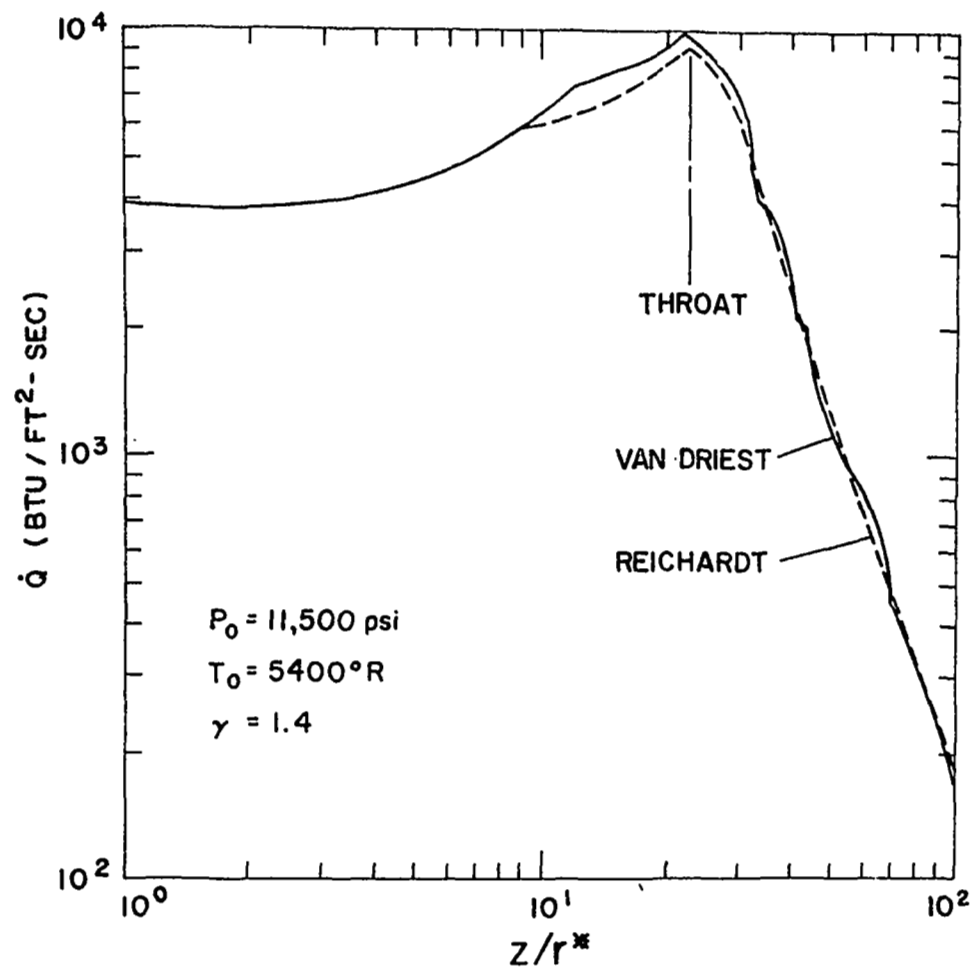
Figure 21: Heat Transfer Distribution for the AEDC Hotshot-Nozzle
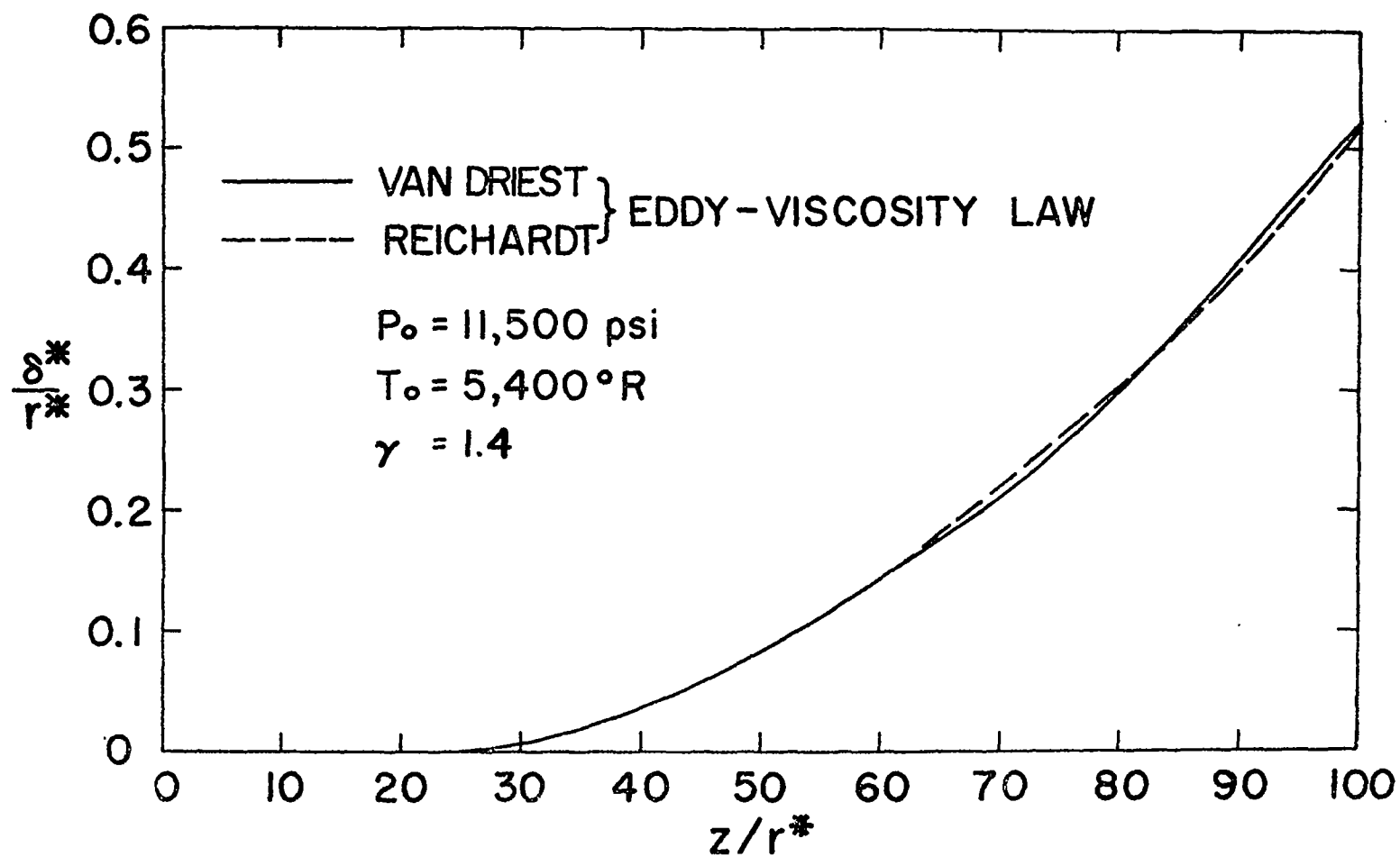
Figure 22: Displacement Thickness Distribution for the AEDC Hotshot-Nozzle
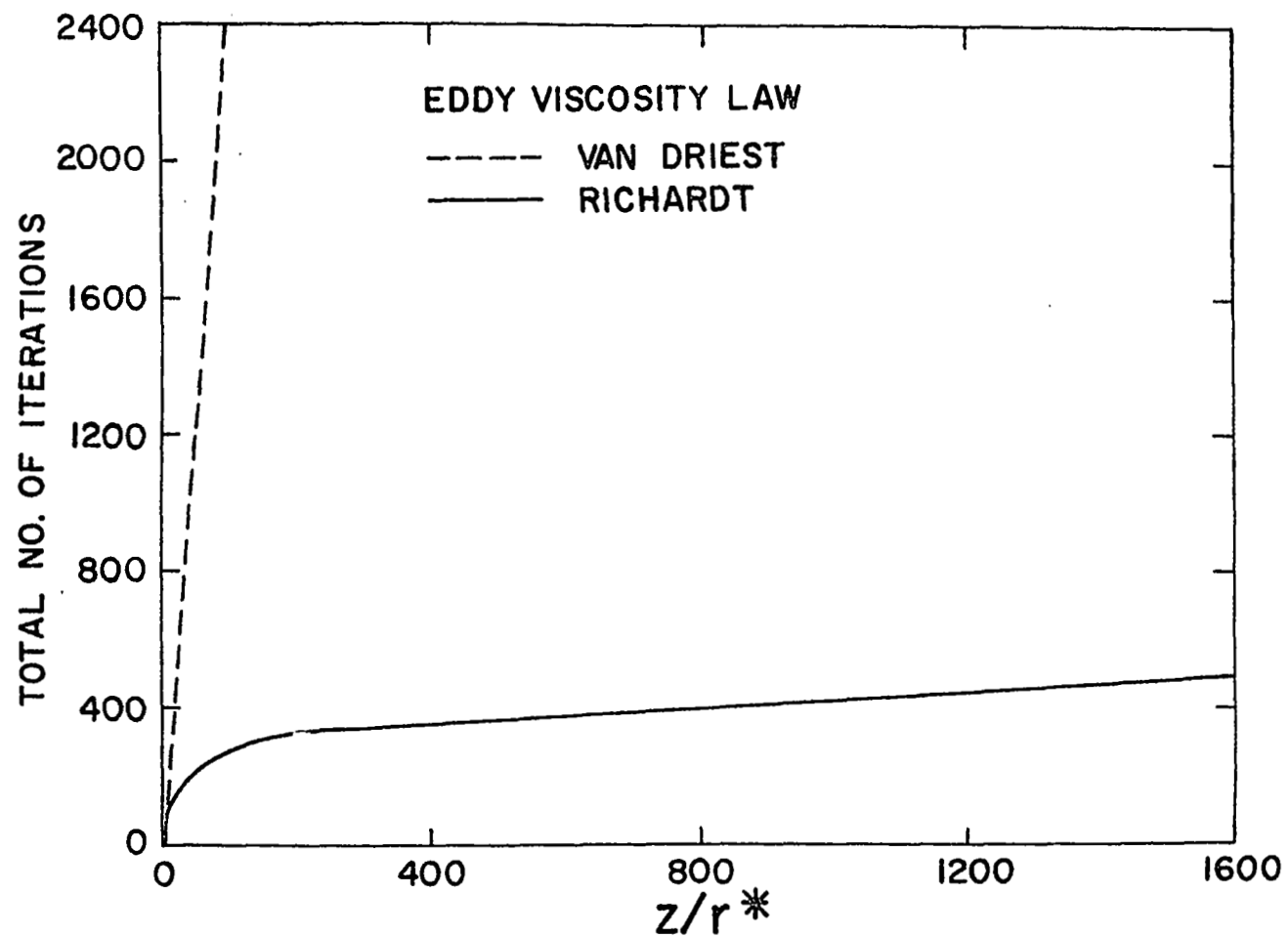
Figure 23: Number of Iterations Required to Obtain a Converged Solution
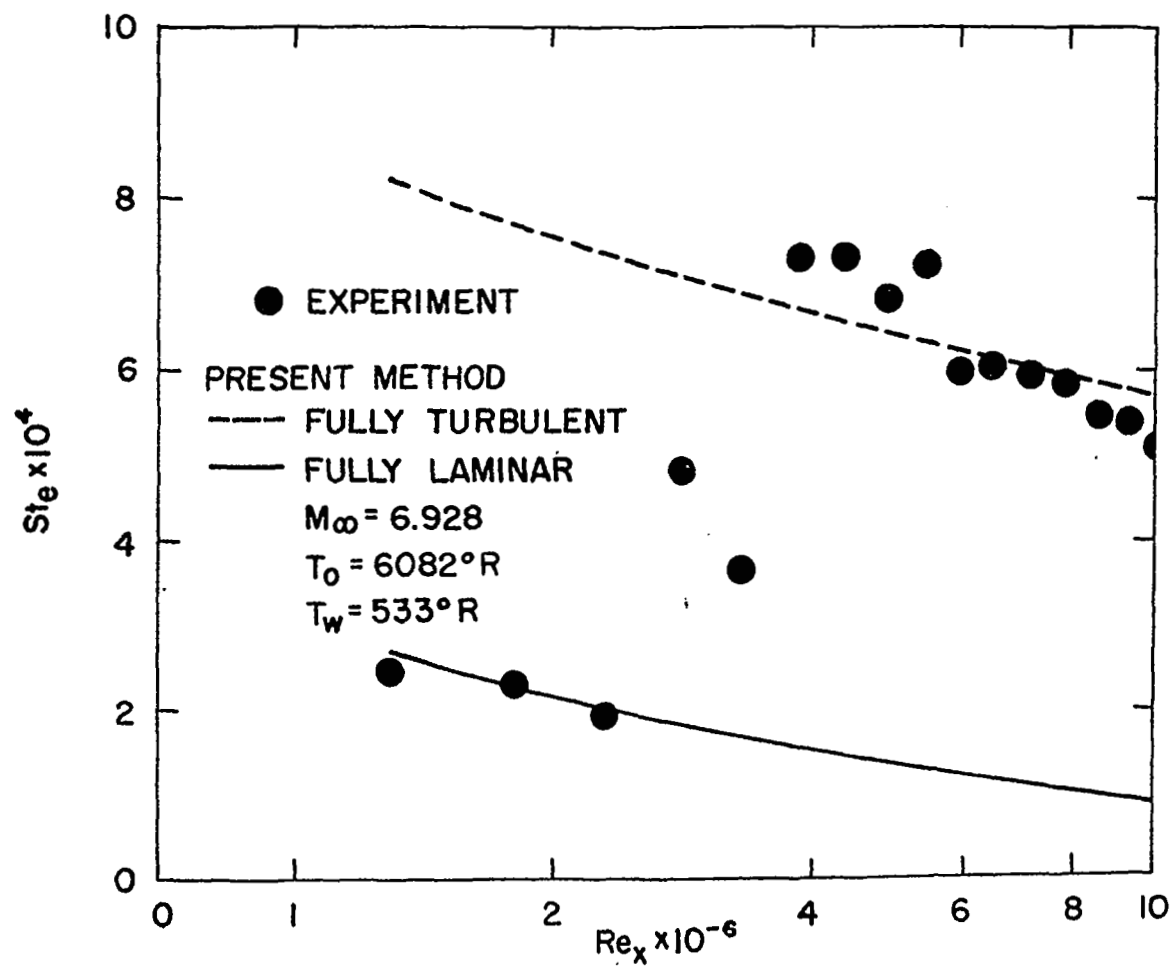
Figure 24: Skin Friction Distribution for a Flat Plate-Hironimus' Data Case I
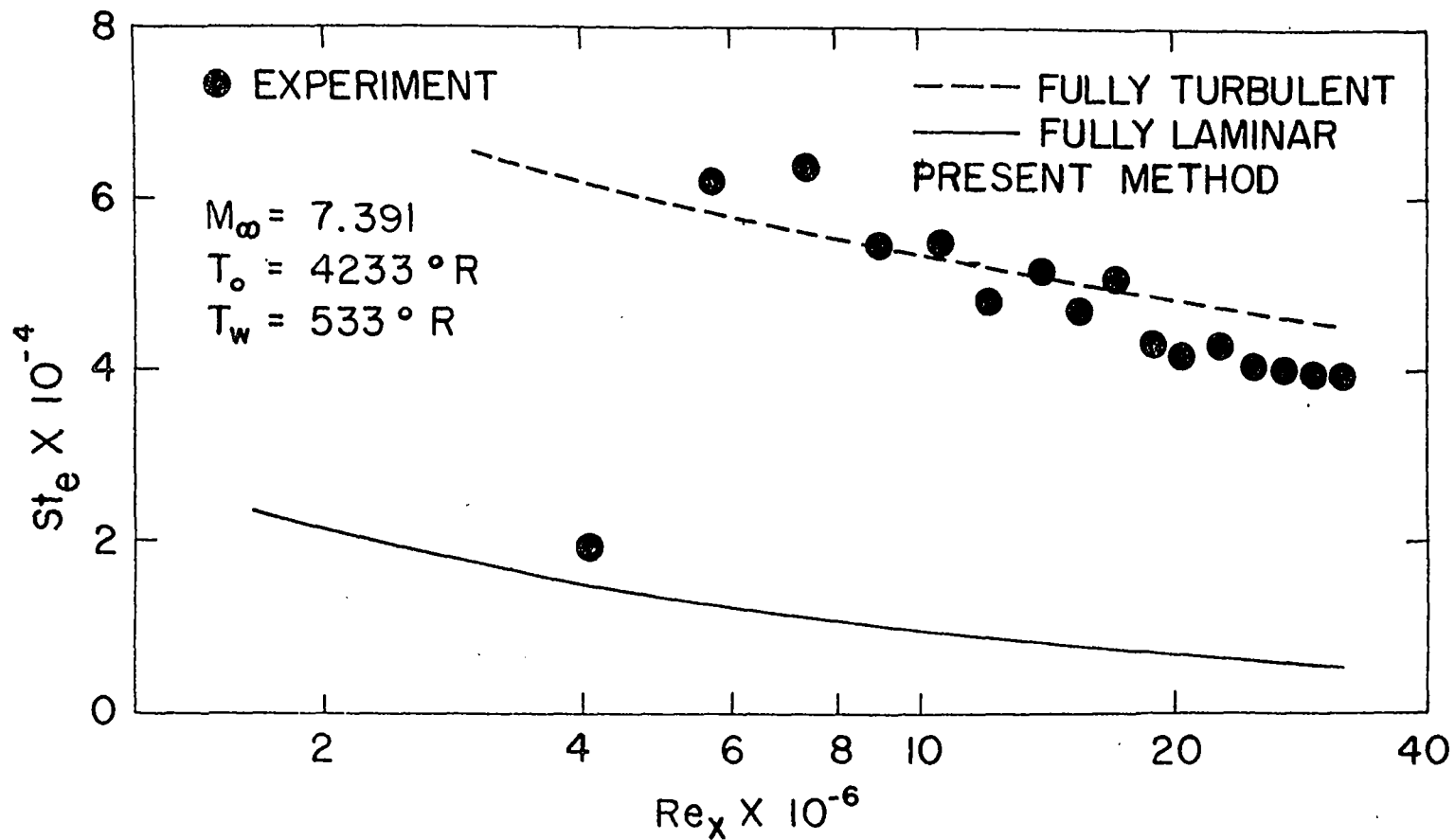
Figure 25: Skin Friction Distribution for a Flat Plate-Hironimus' Data Case II
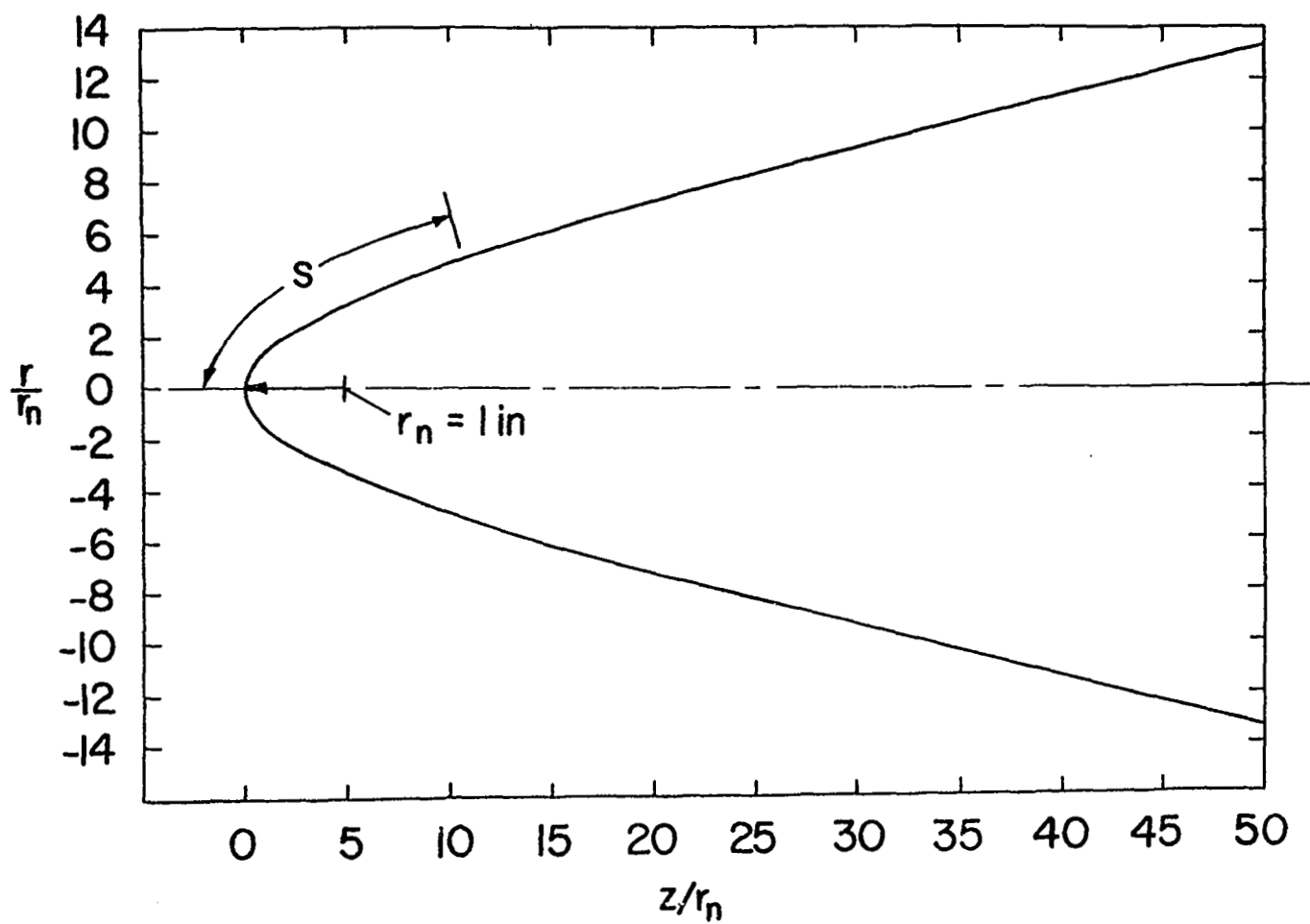
Figure 26: Geometry for a 10° Half-Angle Hyperboloid-AGARD Case A
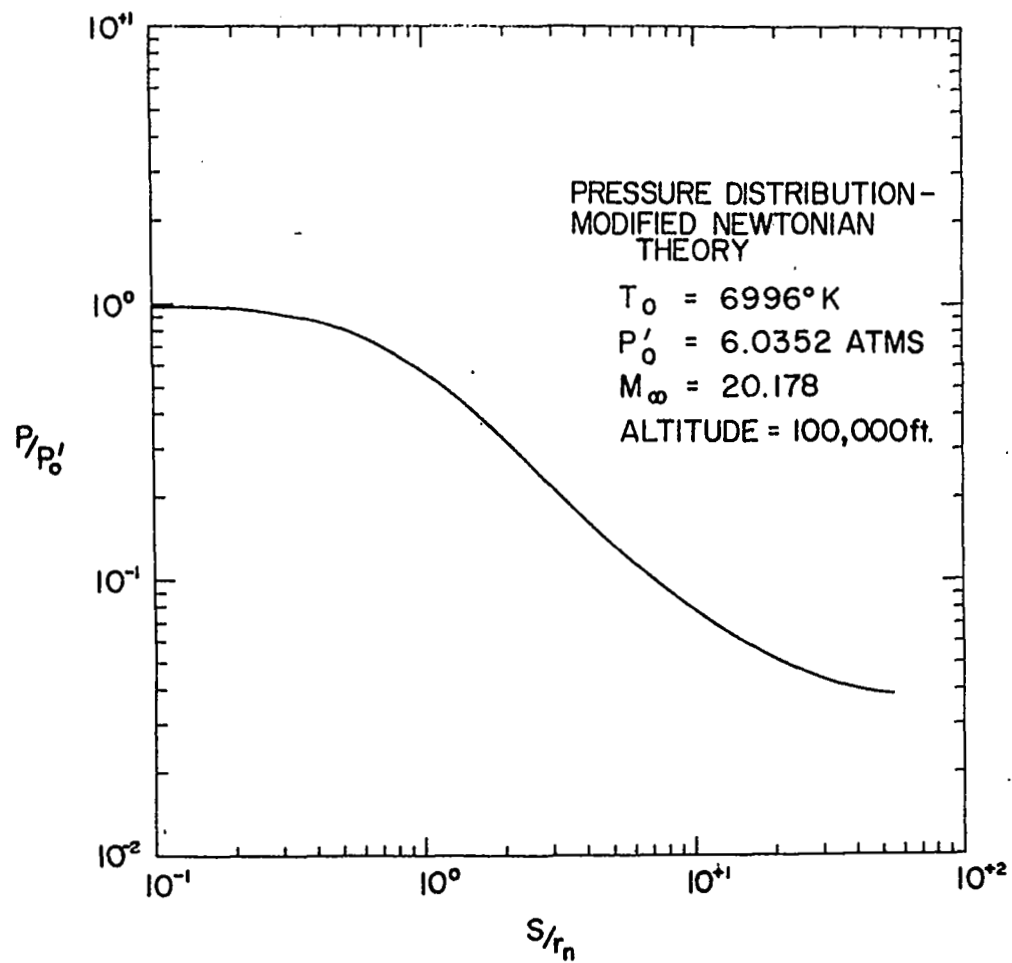
Figure 27: Pressure Distribution for a 10° Half-Angle Hyperboloid-AGARD Case A
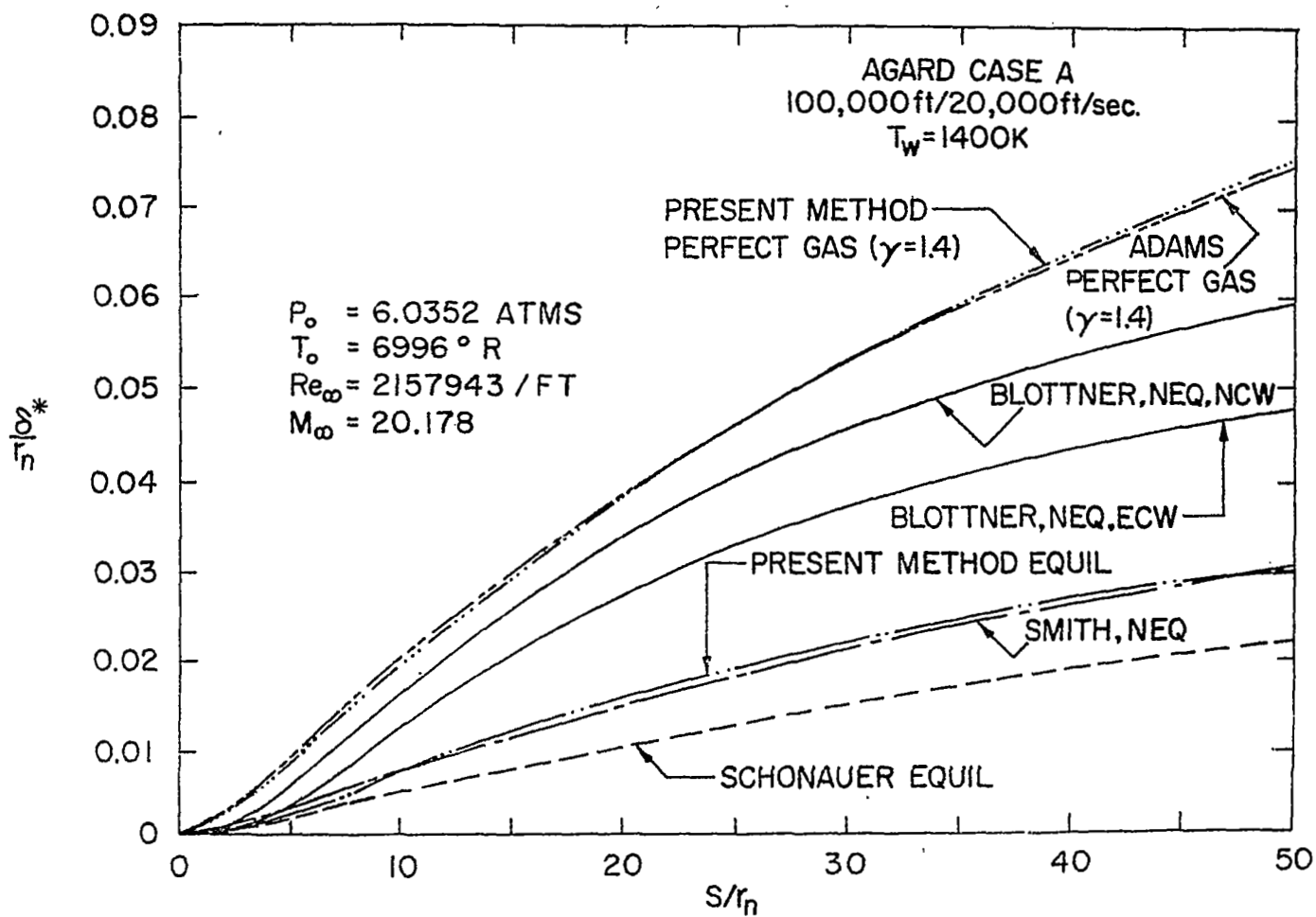
Figure 28: Displacement Thickness Distribution for a 10° Half-Angle Hyperboloid-AGARD Case A
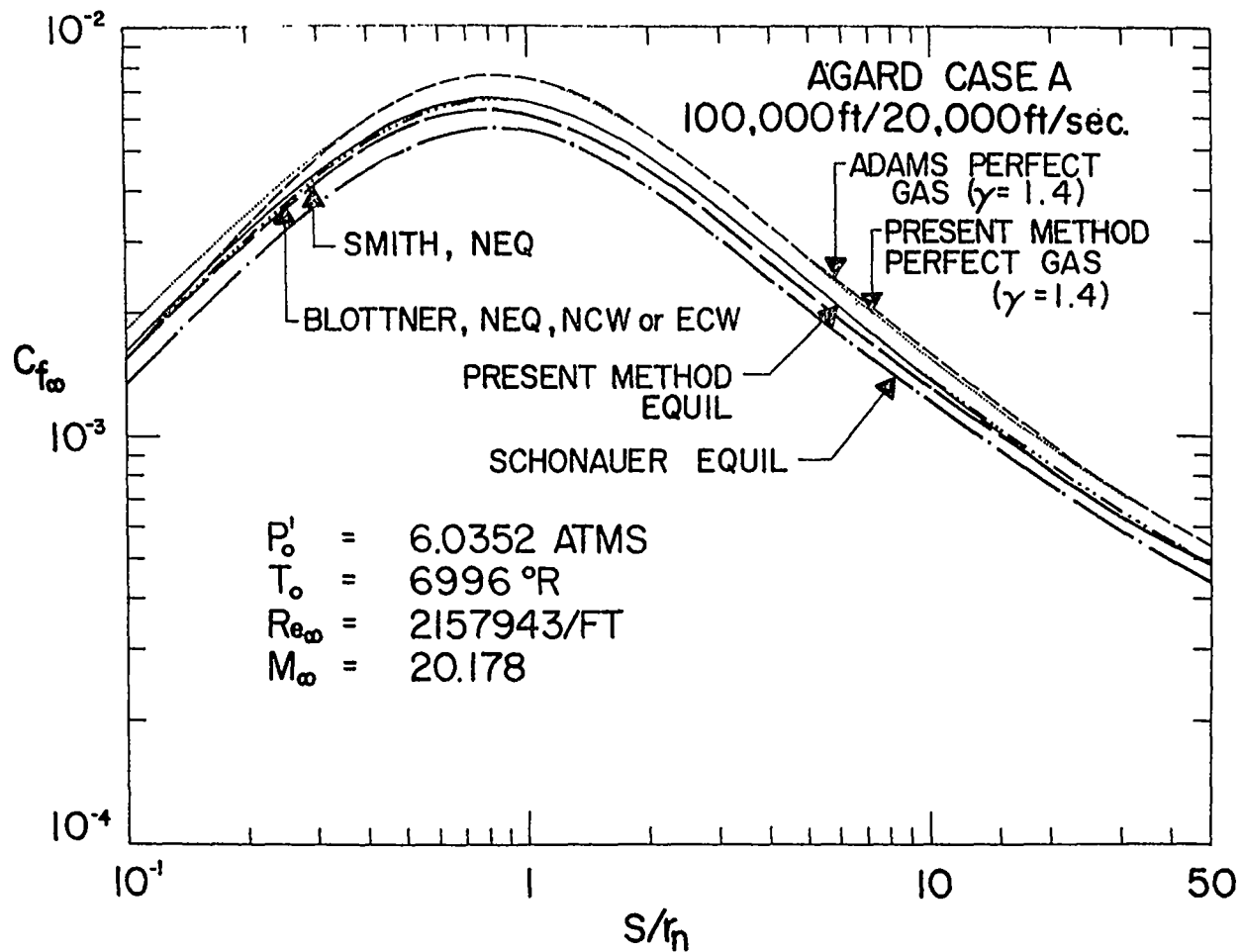
Figure 29: Skin Friction Distribution for a 10° Half-Angle Hyperboloid-AGARD Case A
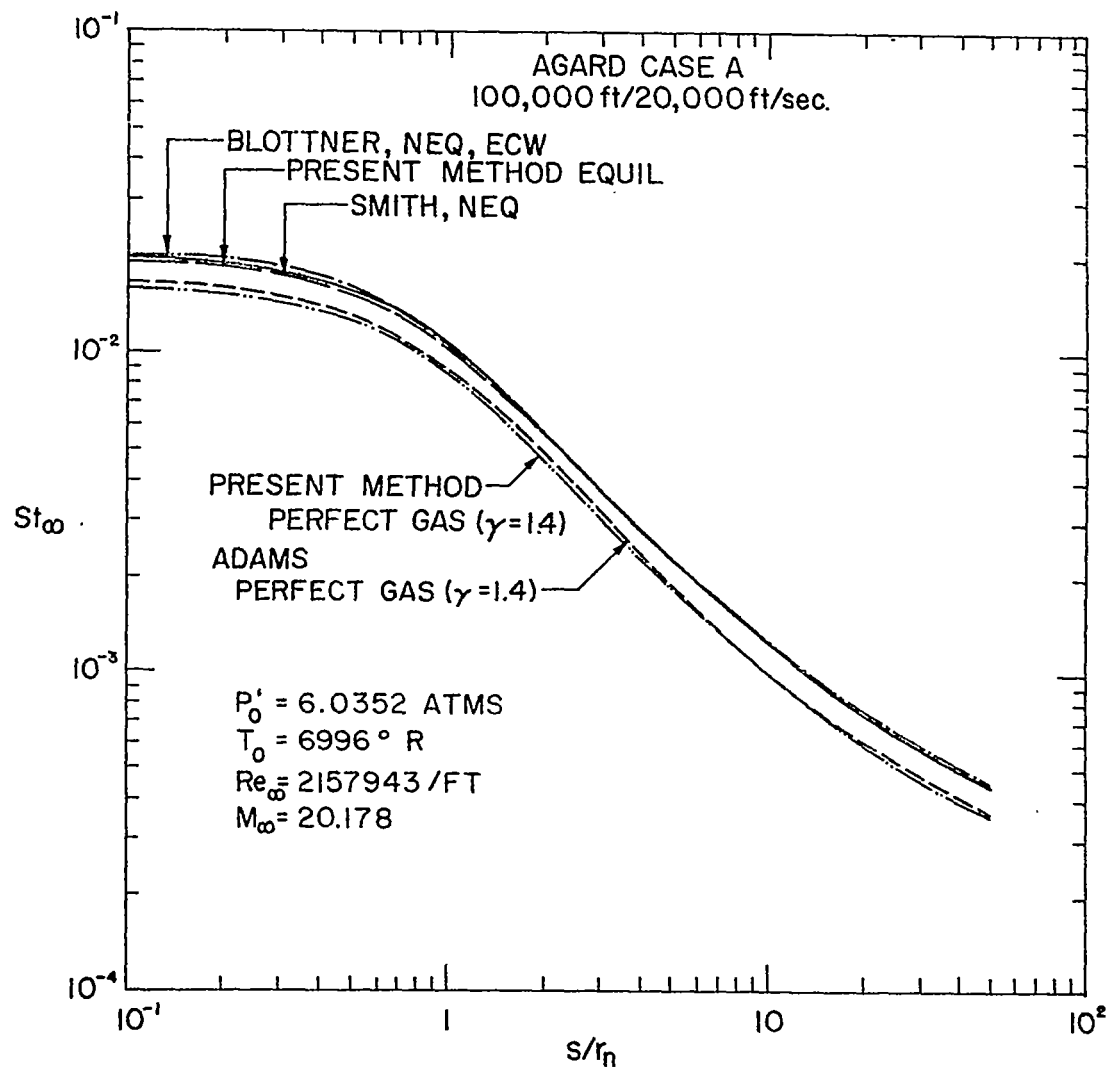
Figure 30: Stanton Number Distribution for a 10° Half-Angle
Hyperboloid-AGARD Case A
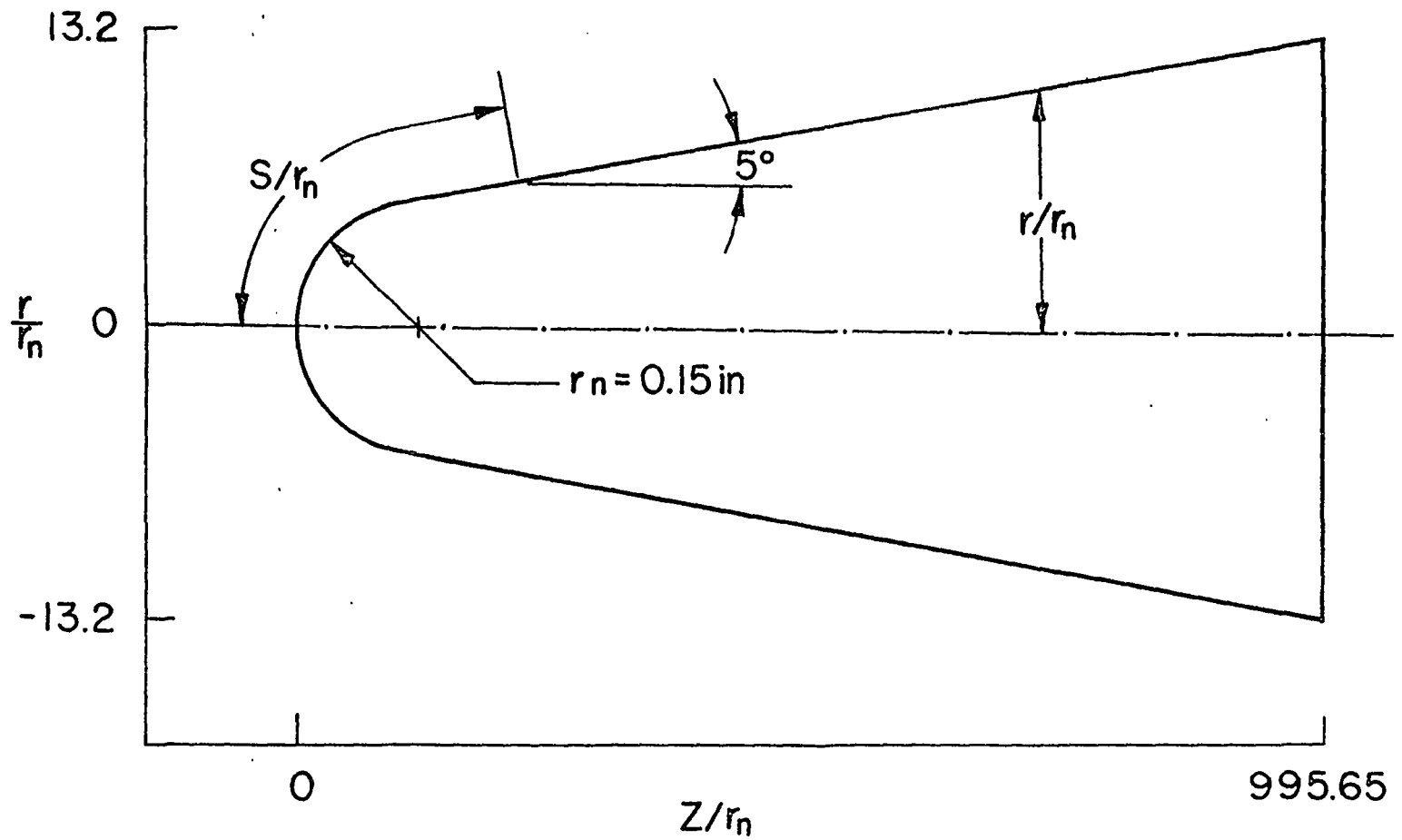
Figure 31: Geometry for a 5° Half-Angle Spherically-Blunted Cone
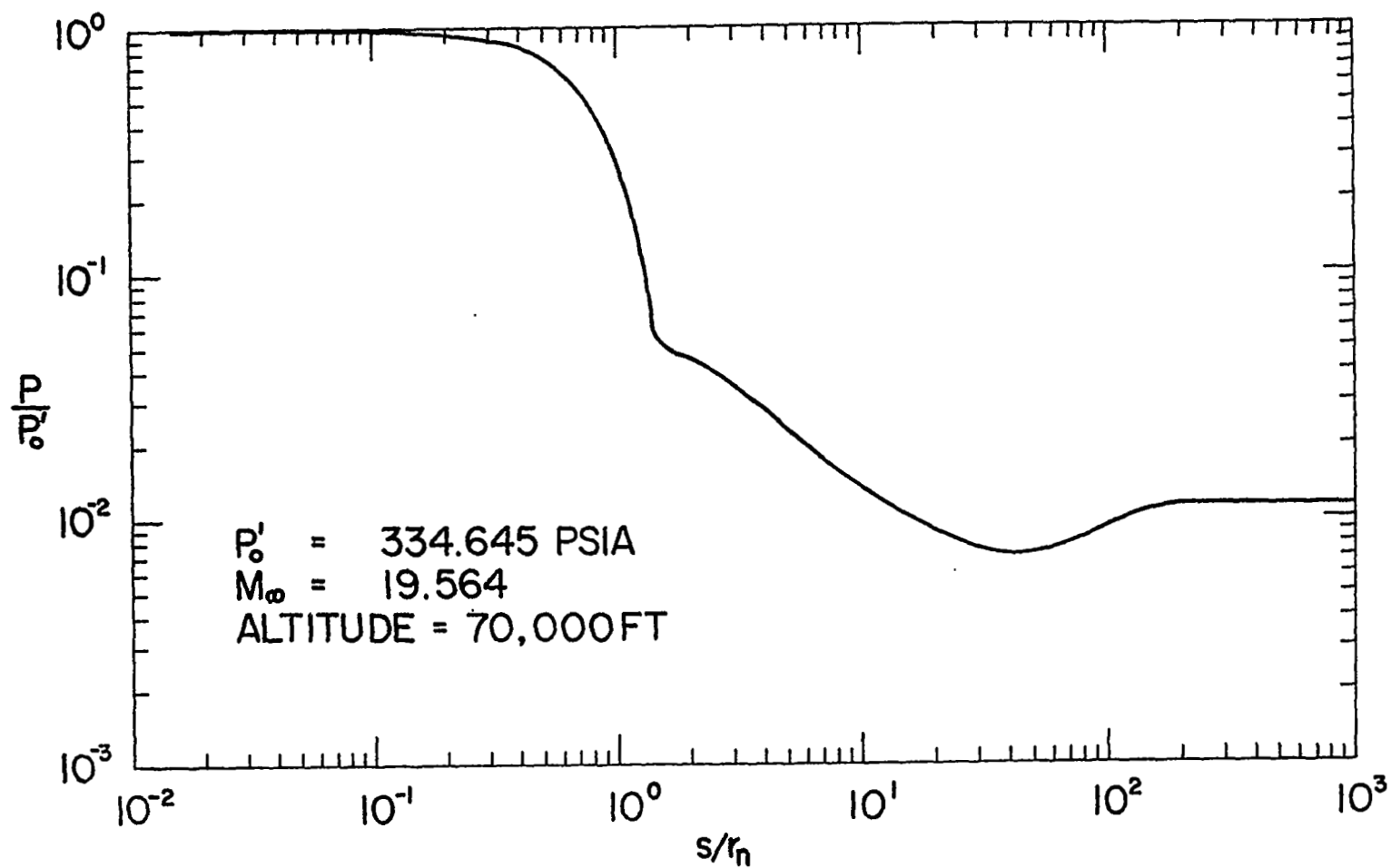
Figure 32: Pressure Distribution for a 5° Half-Angle Spherically-Blunted Cone
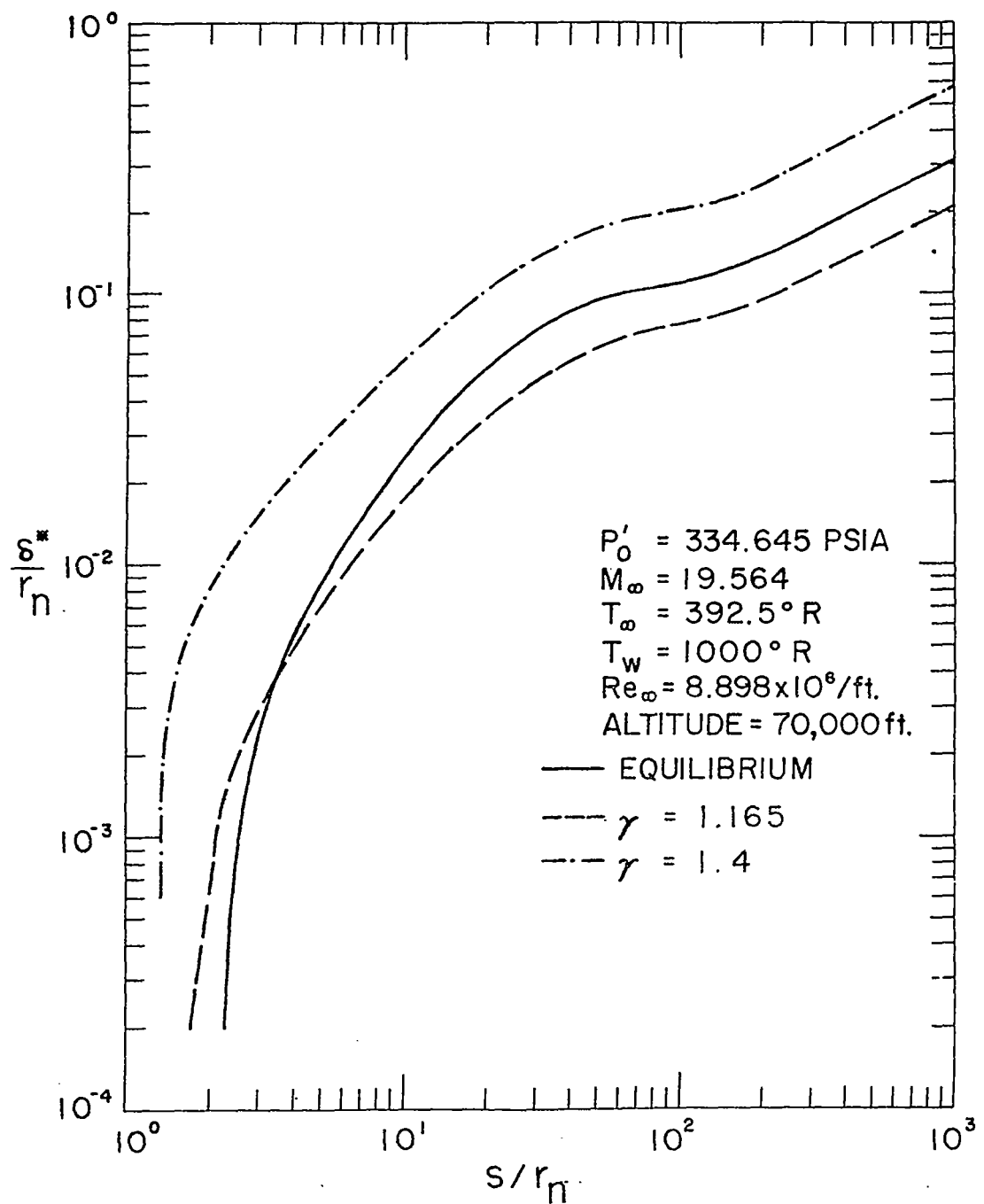
Figure 33: Displacement Thickness Distribution for Laminar Flow Over a 5° Half-Angle Spherically-Blunted Cone
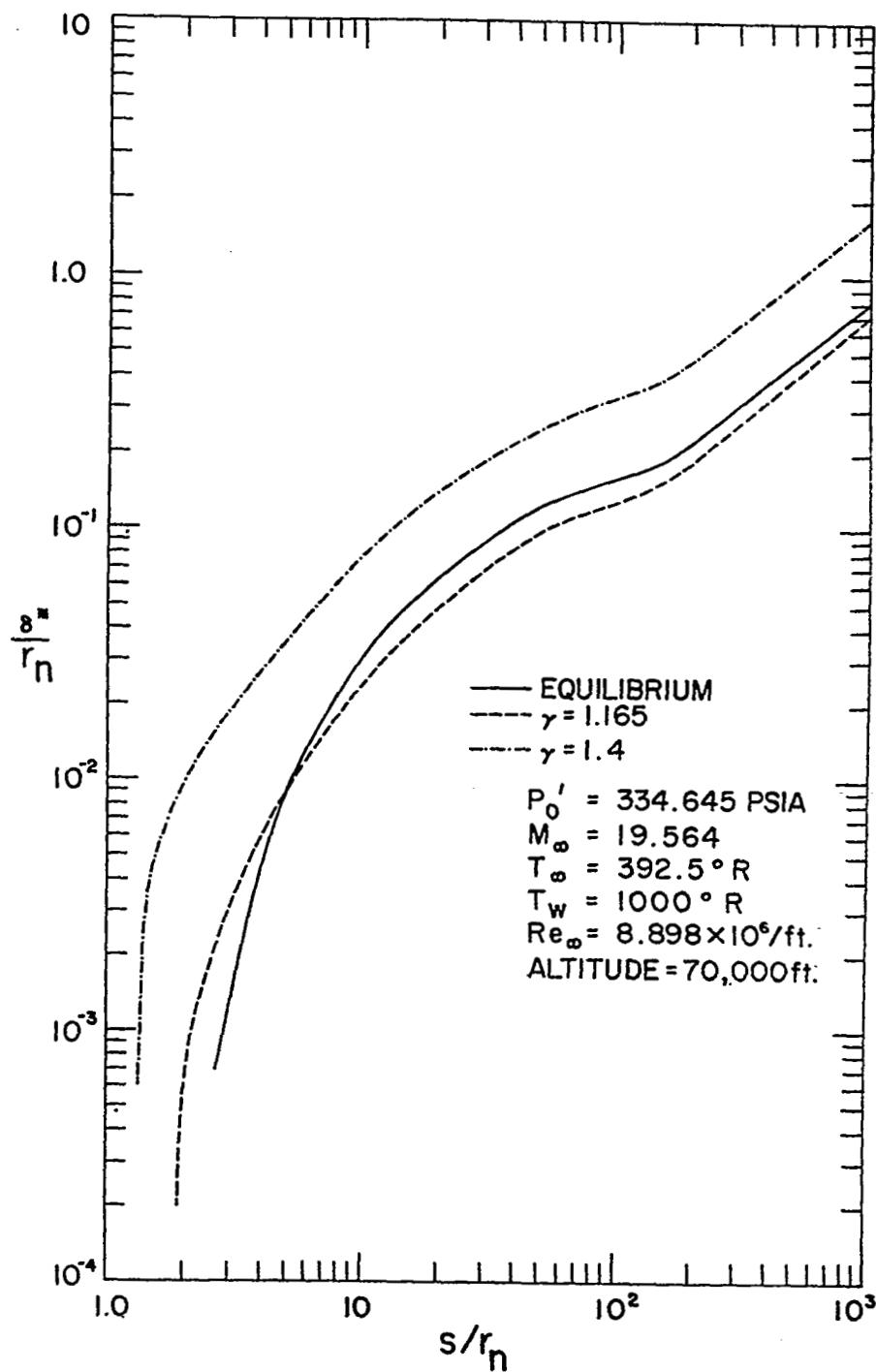
Figure 34: Displacement Thickness Distribution for Turbulent Flow Over a 5° Half-Angle Spherically-Blunted Cone

141
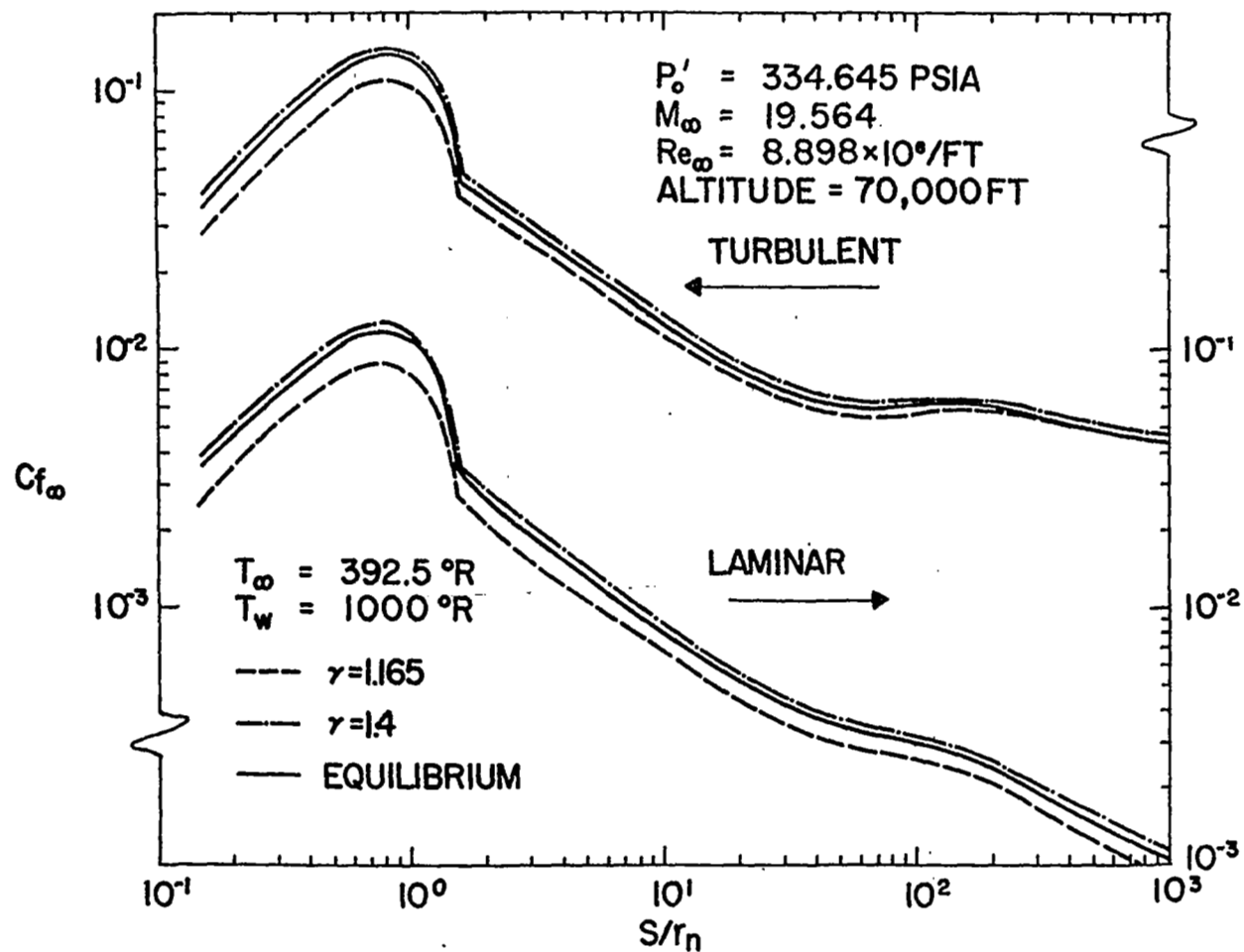
Figure 35: Skin Friction Distribution for a 5° Half-Angle Spherically-Blunted Cone
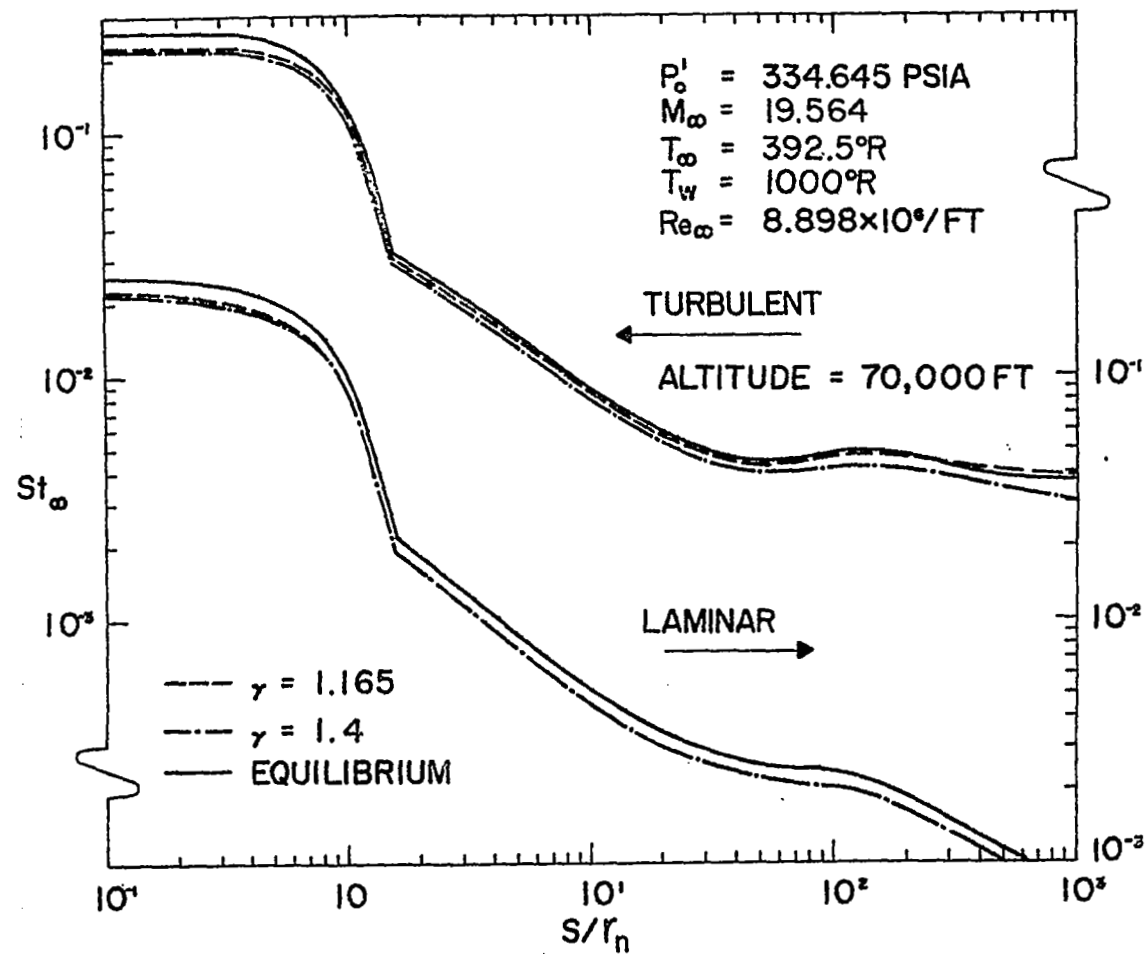
Figure 36: Stanton Number Distribution for a 5° Half-Angle Spherically-Blunted Cone
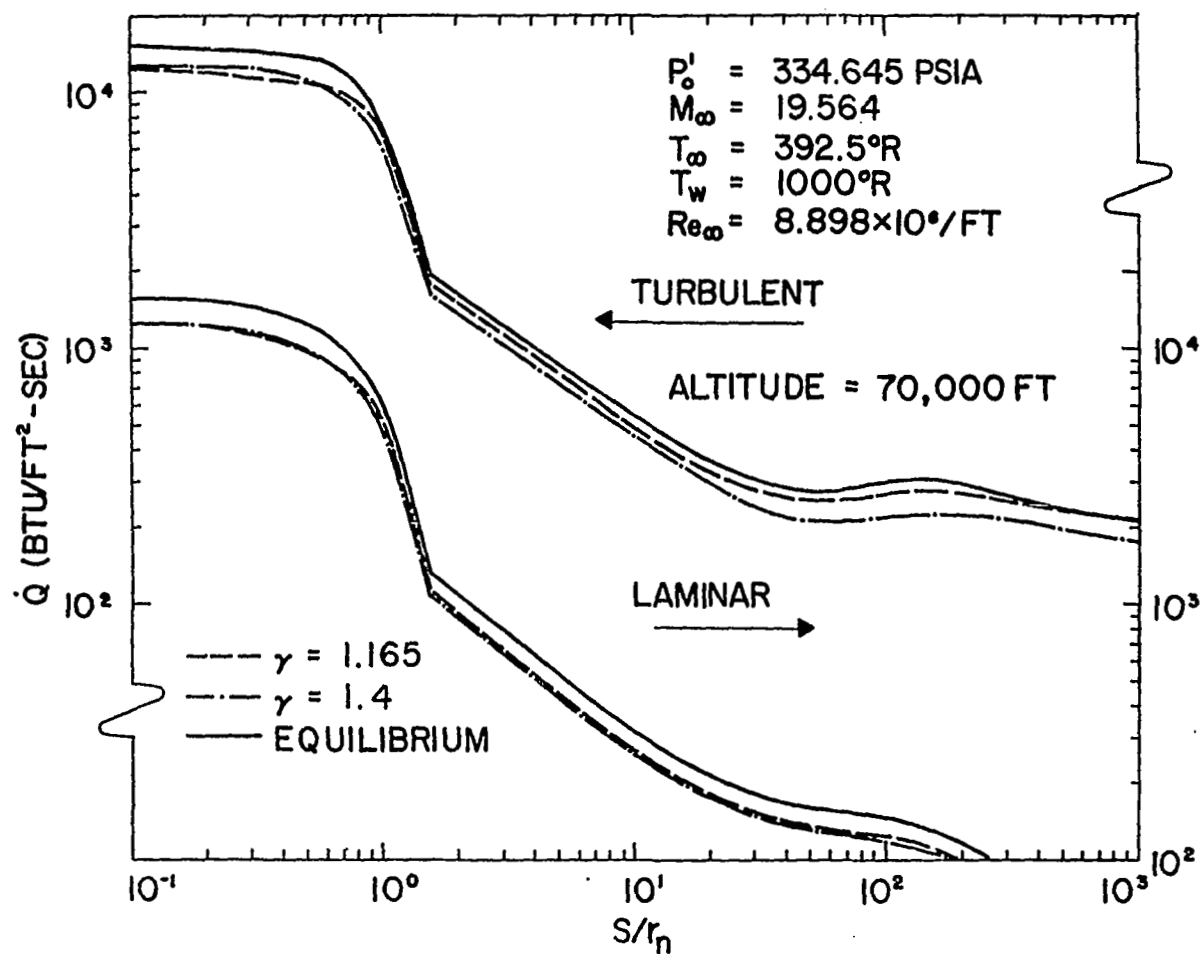
Figure 37: Heat Transfer Distribution for a 5° Half-Angle Spherically-Blunted Cone
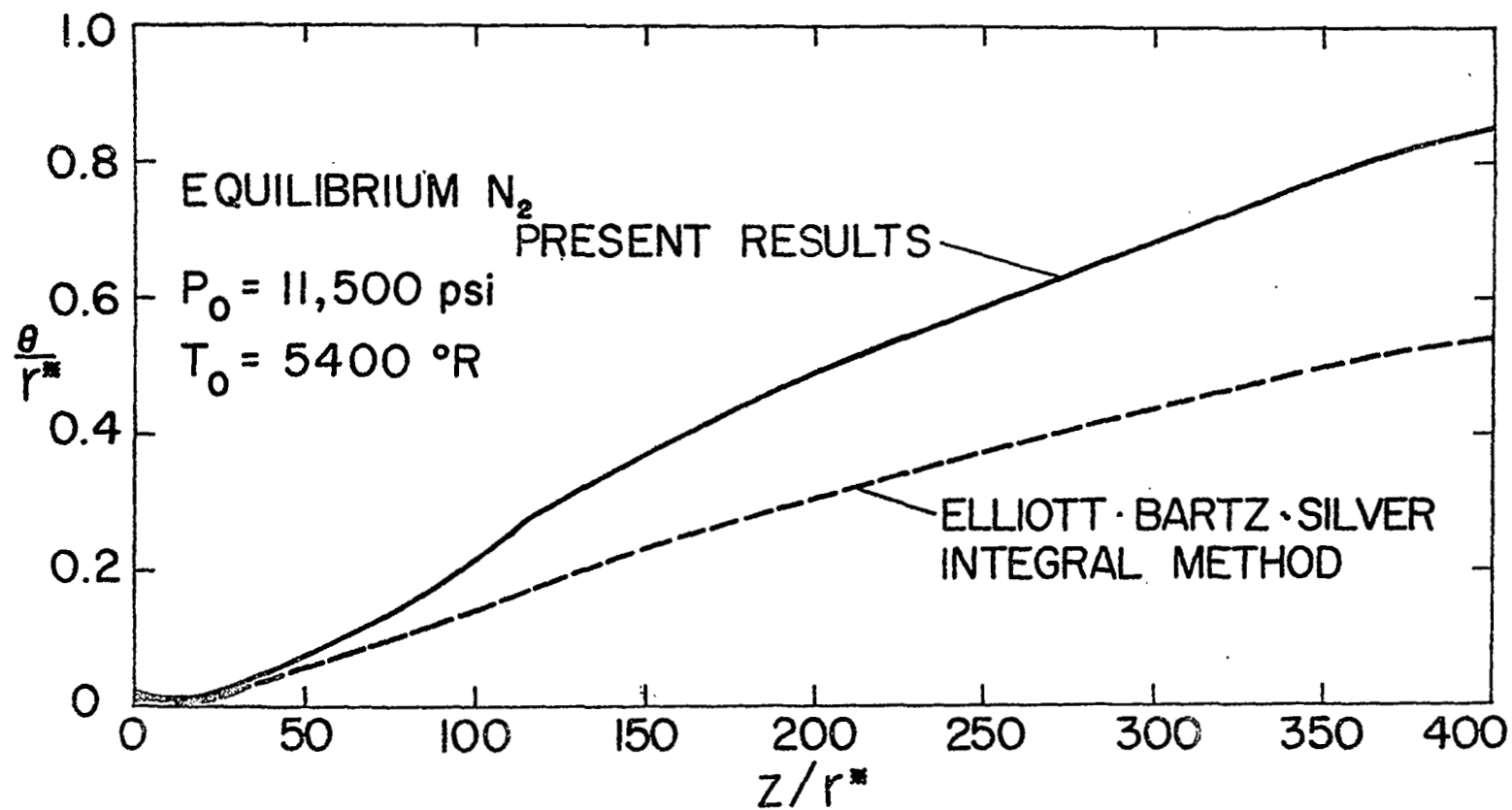
Figure 38: Momentum Thickness Distribution for the AEDC Hotshot-Nozzle
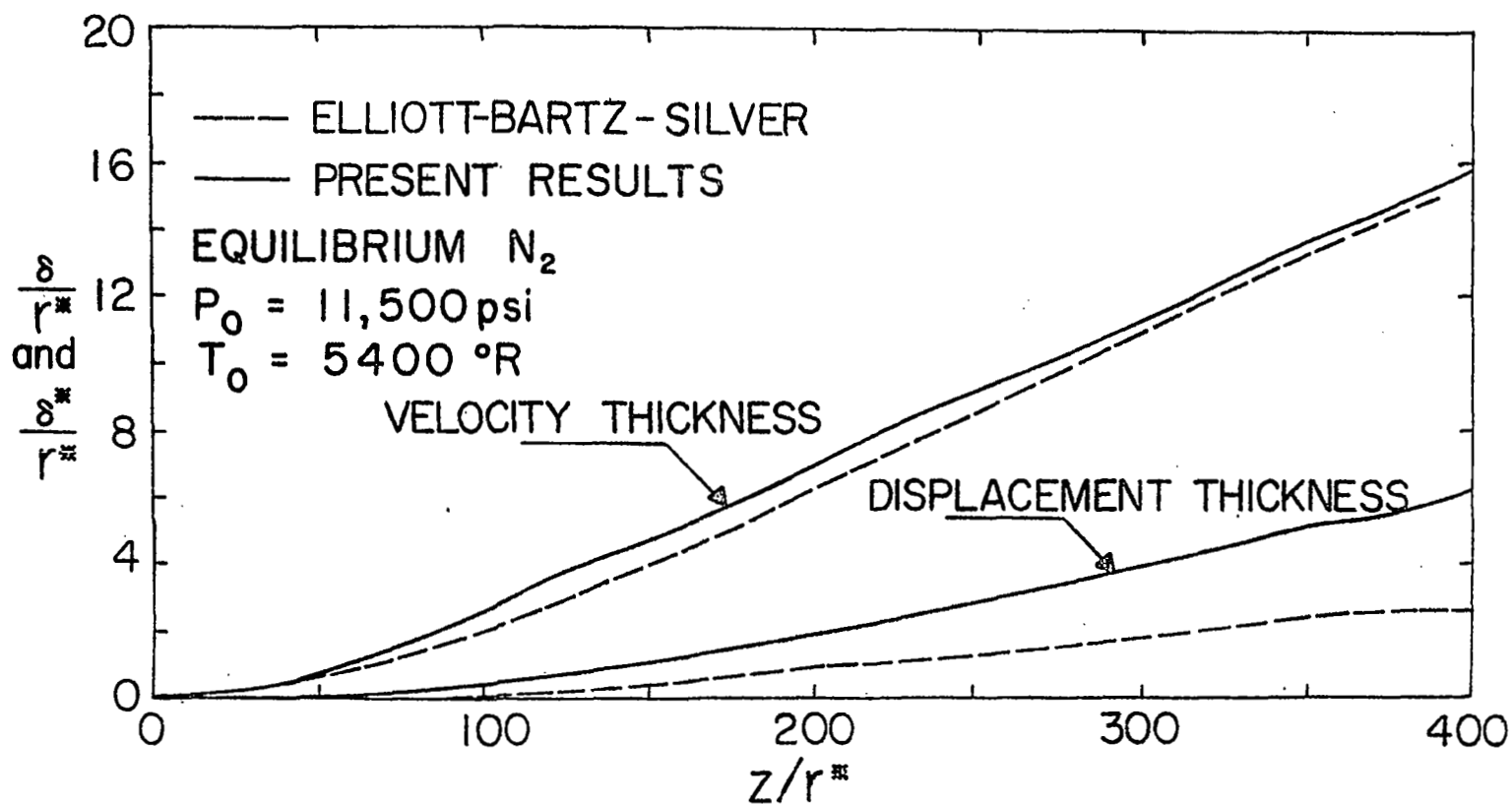
Figure 39: Boundary Layer and Displacement Thickness Distribution for the AEDC Hotshot-Nozzle
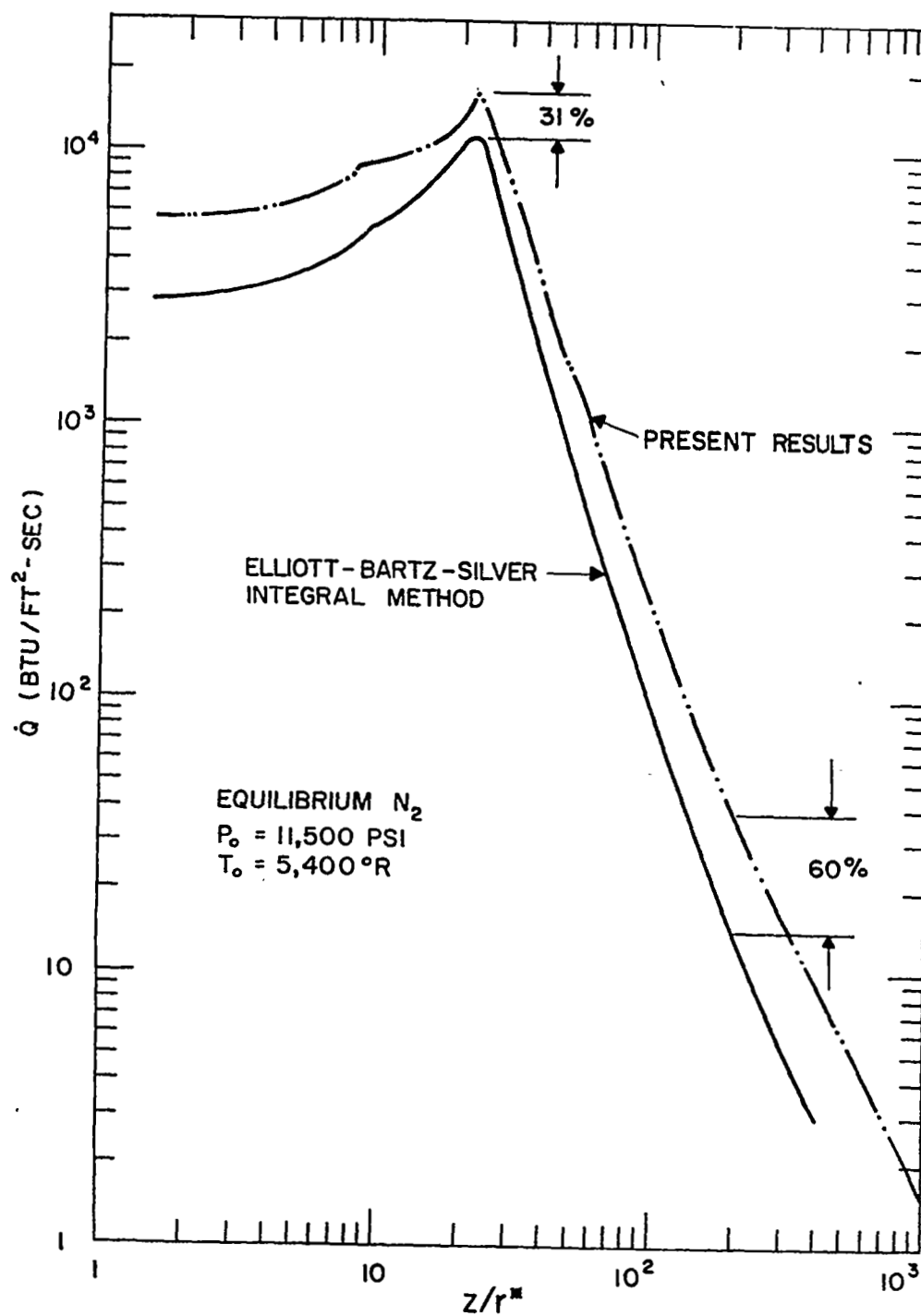
Figure 40: Heat Transfer Distribution for the AEDC Hotshot-Nozzle
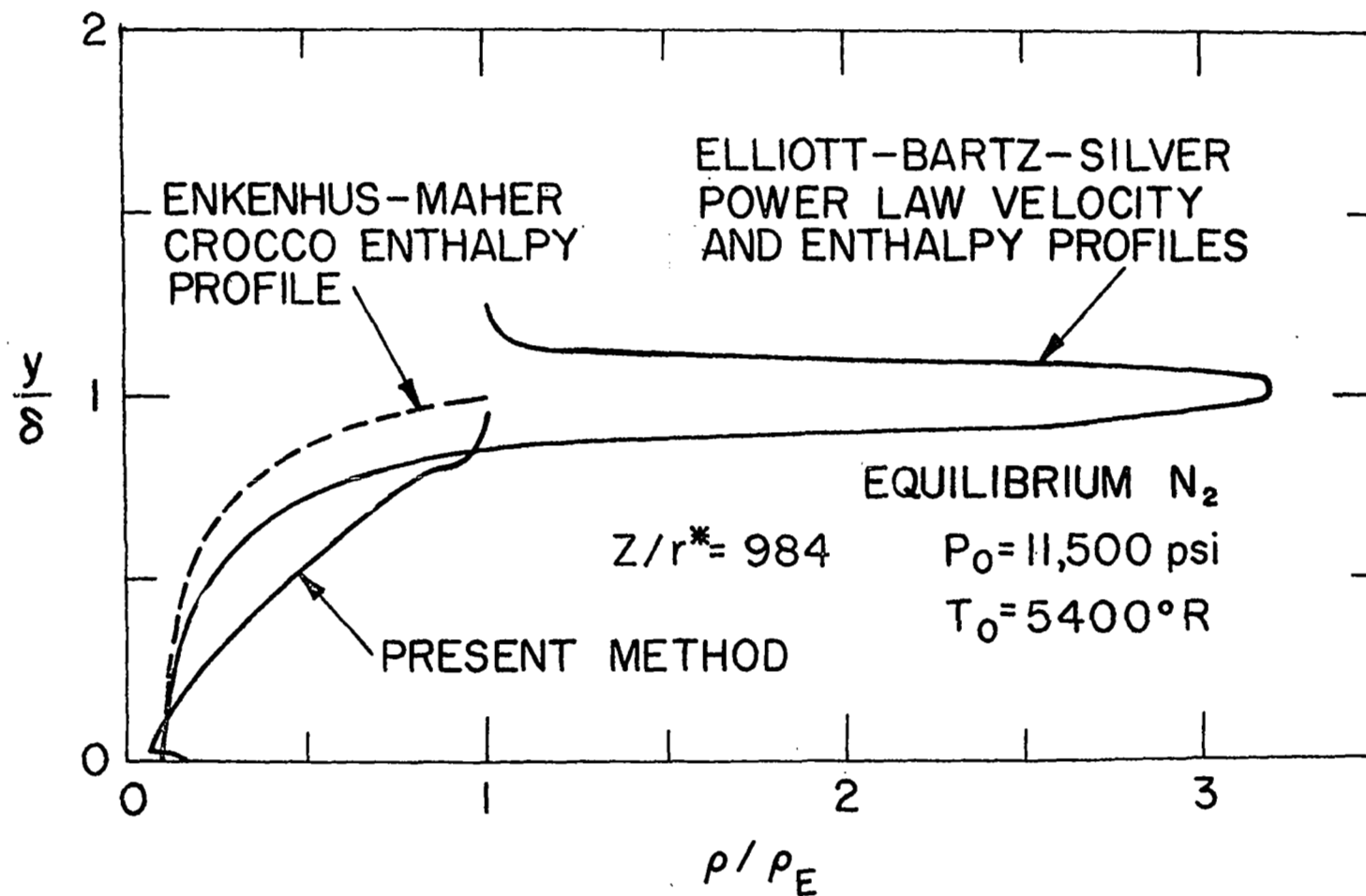
Figure 41: Density Profiles for the AEDC Hotshot-Nozzle
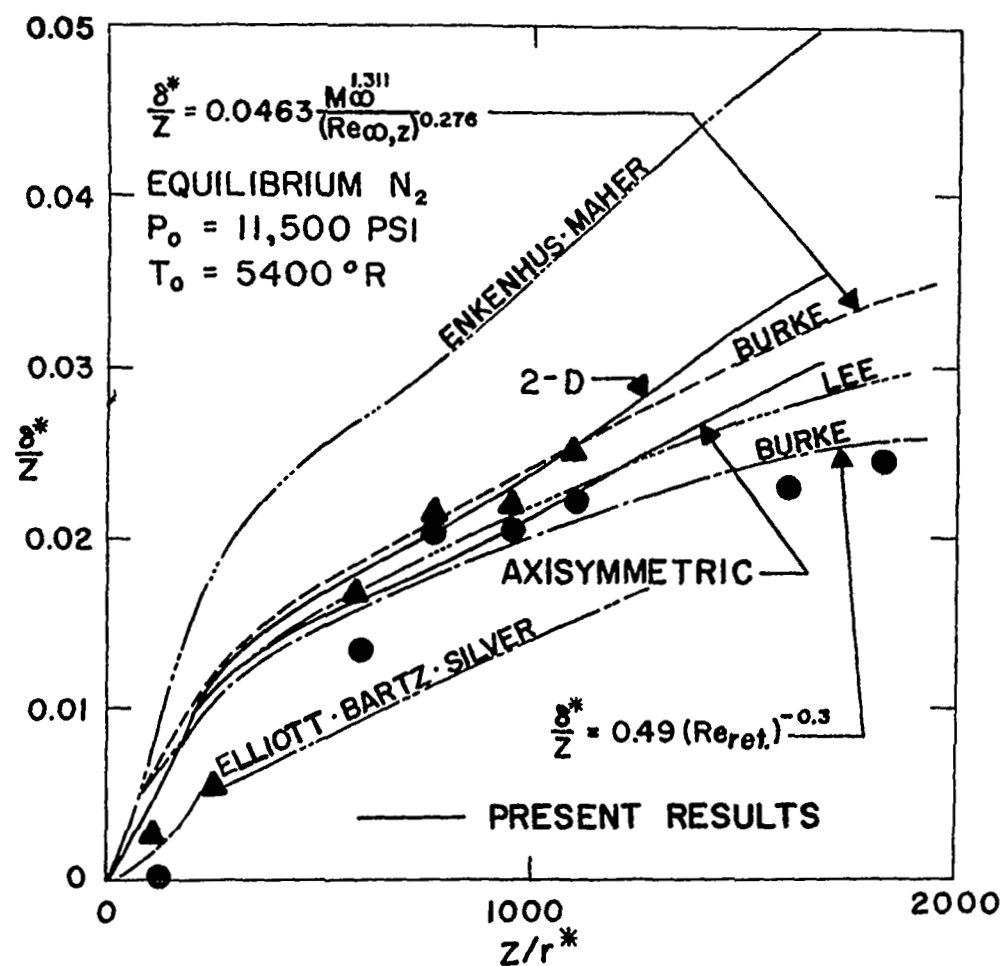
Figure 42: Comparison of the Predicted Displacement Thickness Distribution with Other Methods Using Both Momentum and Energy Equations—AEDC Hotshot-Nozzle
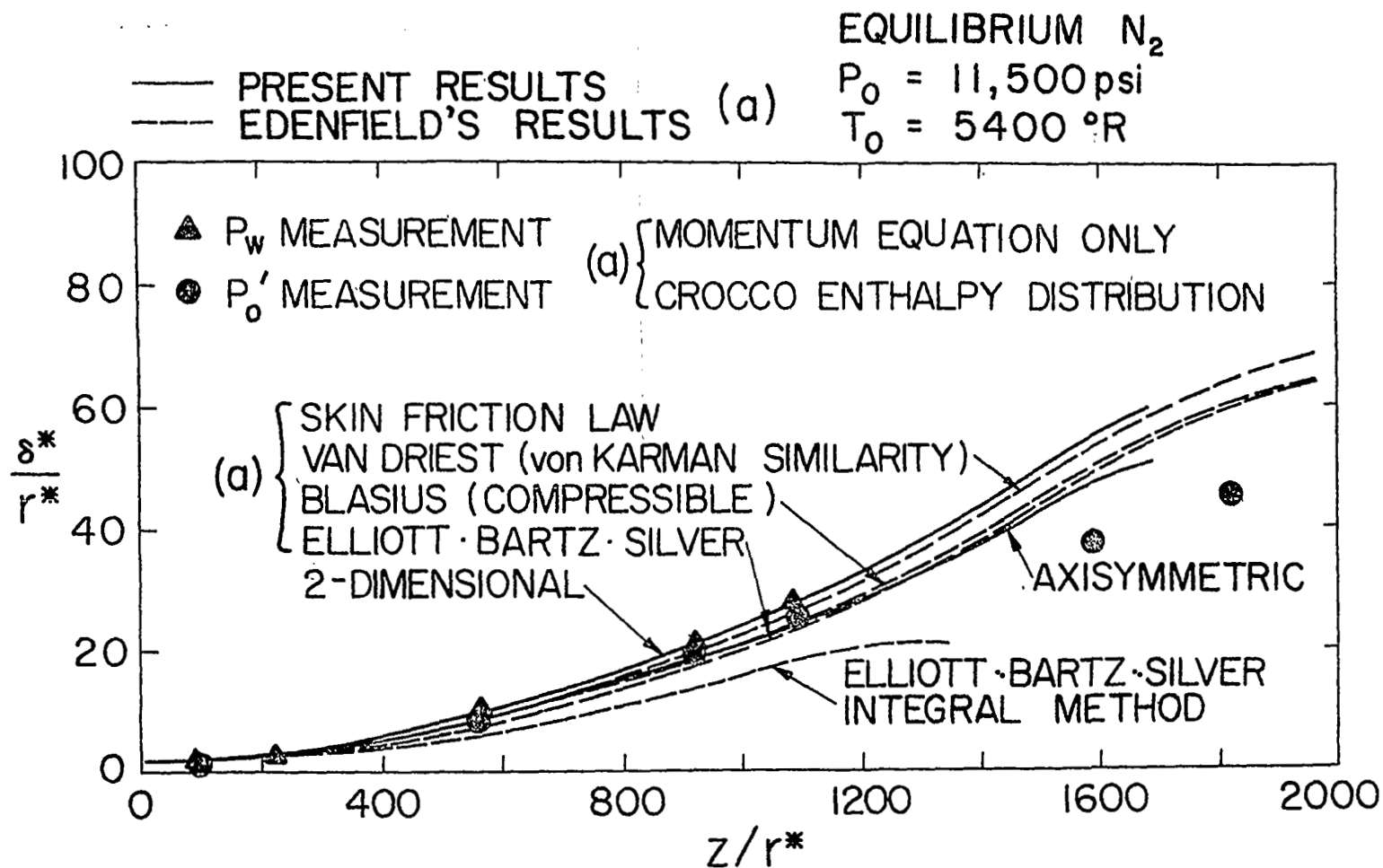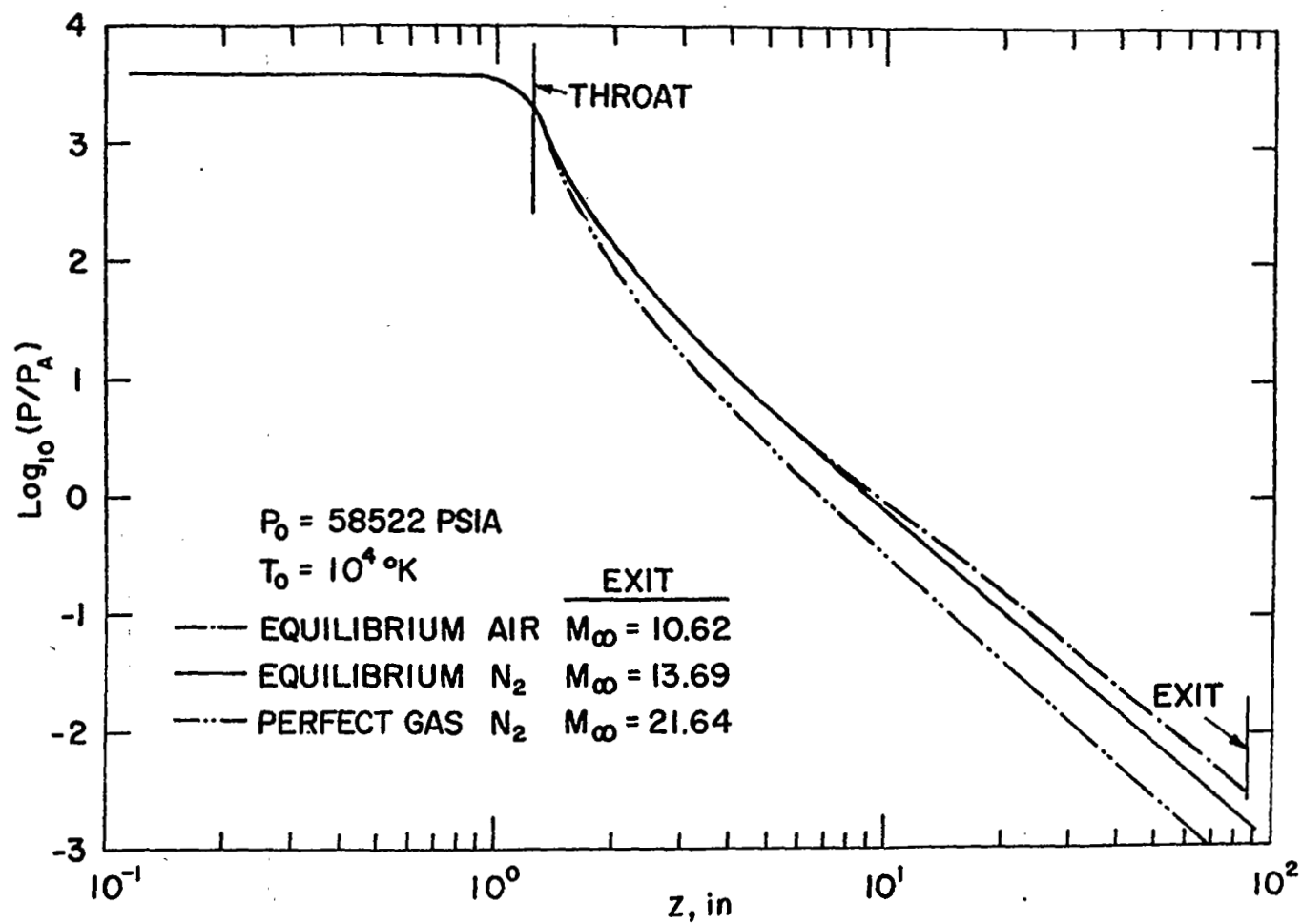
Figure 43: Comparison of the Predicted Displacement Thickness Distribution with Other Methods Which Use the Momentum Equation Only-AEDC Hotshot-Nozzle

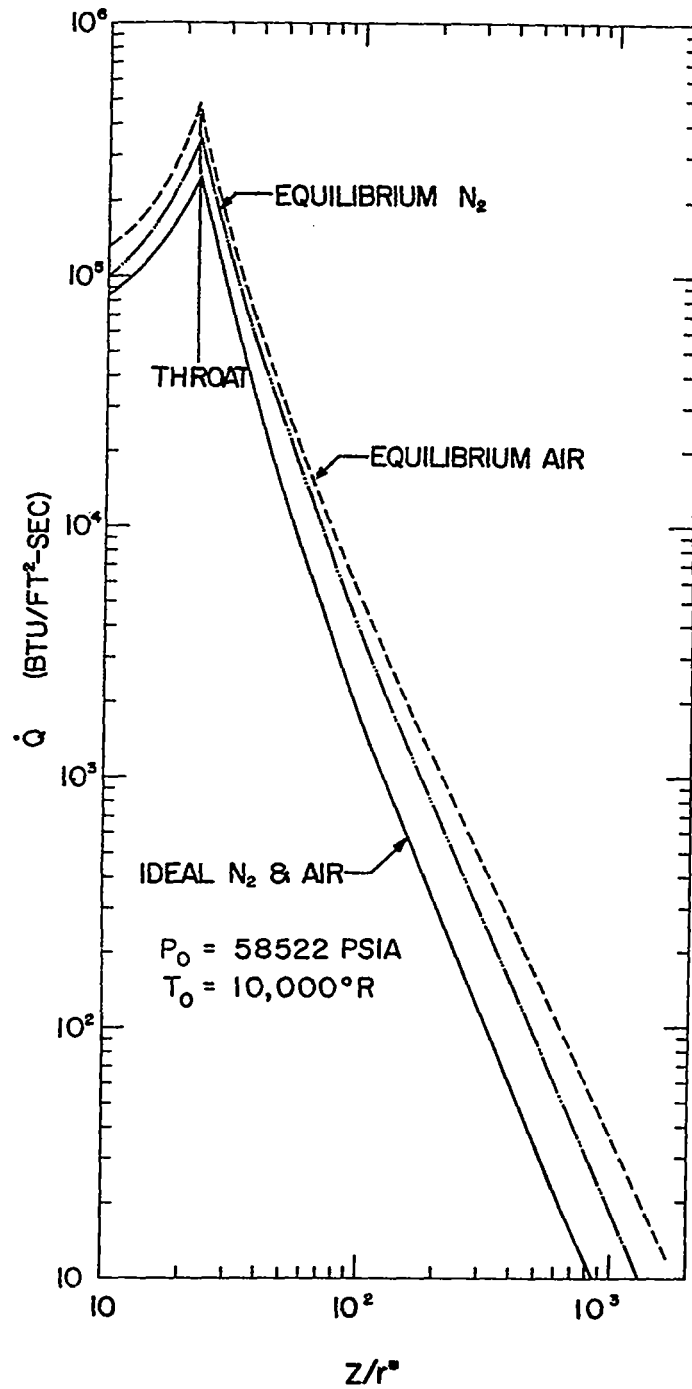Figure 44: Pressure Distribution for the AEDC Nozzle Configuration-P_o = 58,522 PSIA; T_o = 10,000°K

Figure 45: Heat Transfer Distribution for the AEDC Hotshot-Nozzle
Configuration-P_o = 58,522 PSIA; T_o = 10,000°K
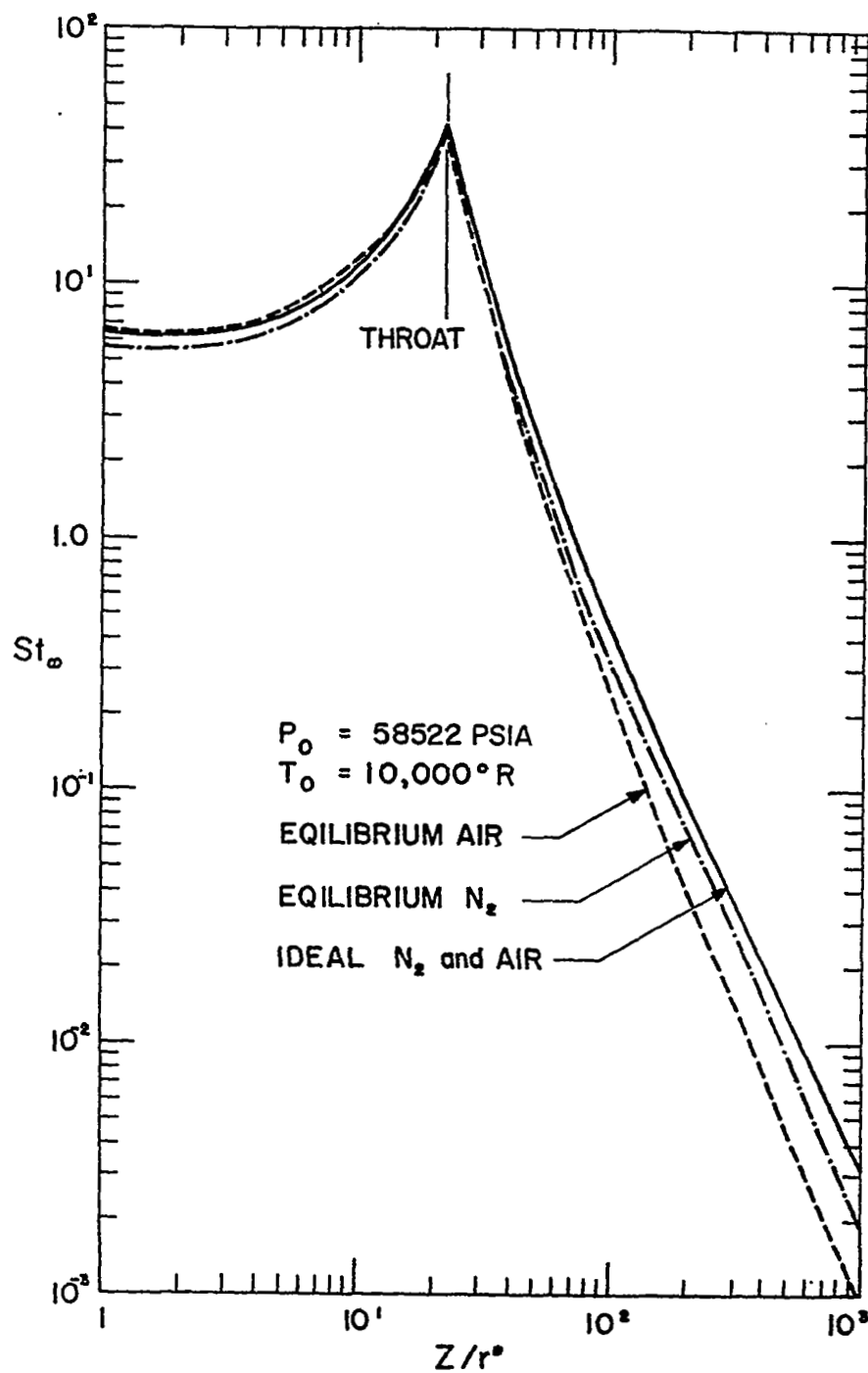
Figure 46: Stanton Number Distribution for the AEDC Hotshot-Nozzle Configuration-P_o = 58,522 PSIA; T_o = 10,000°K
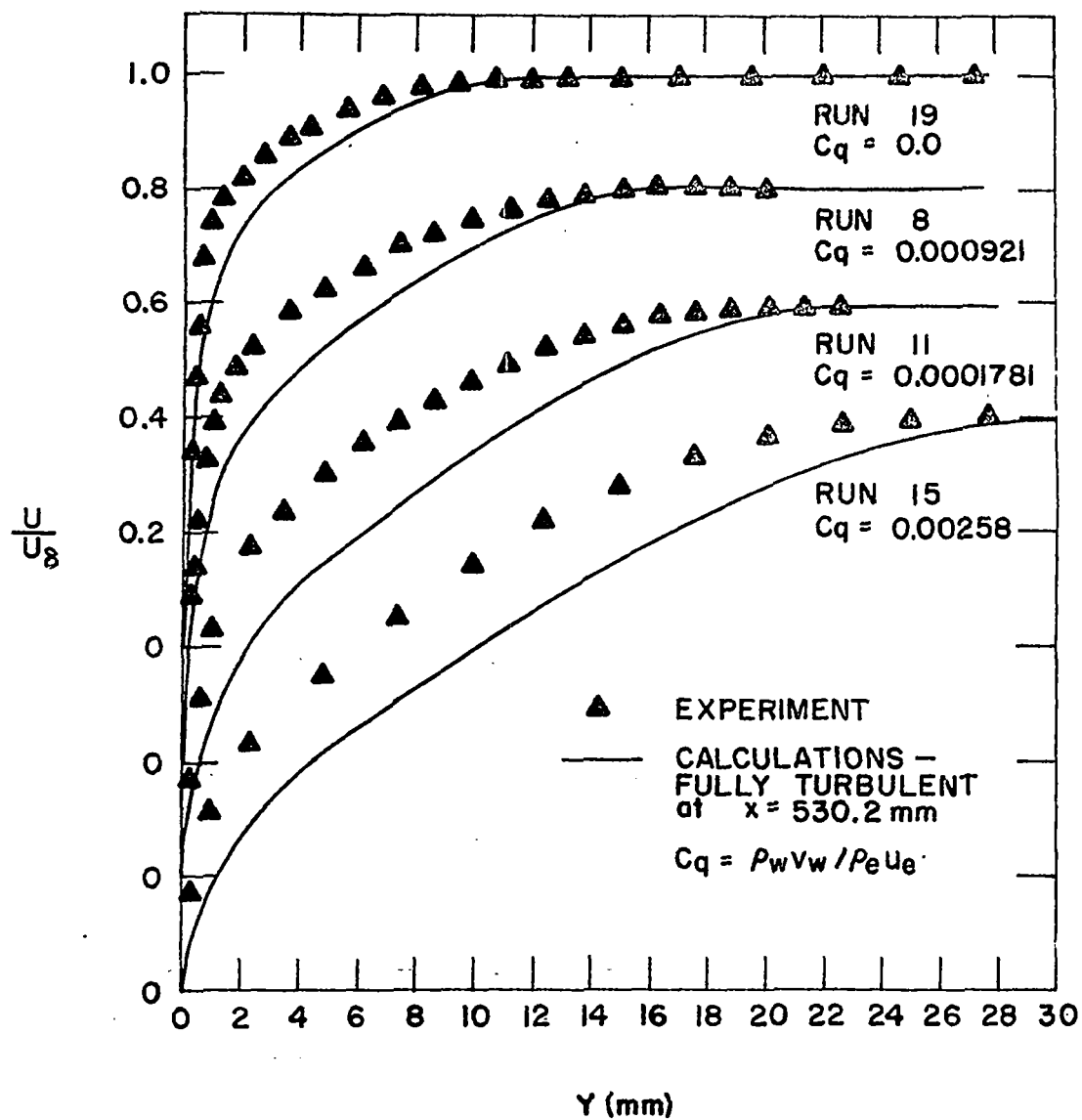
153

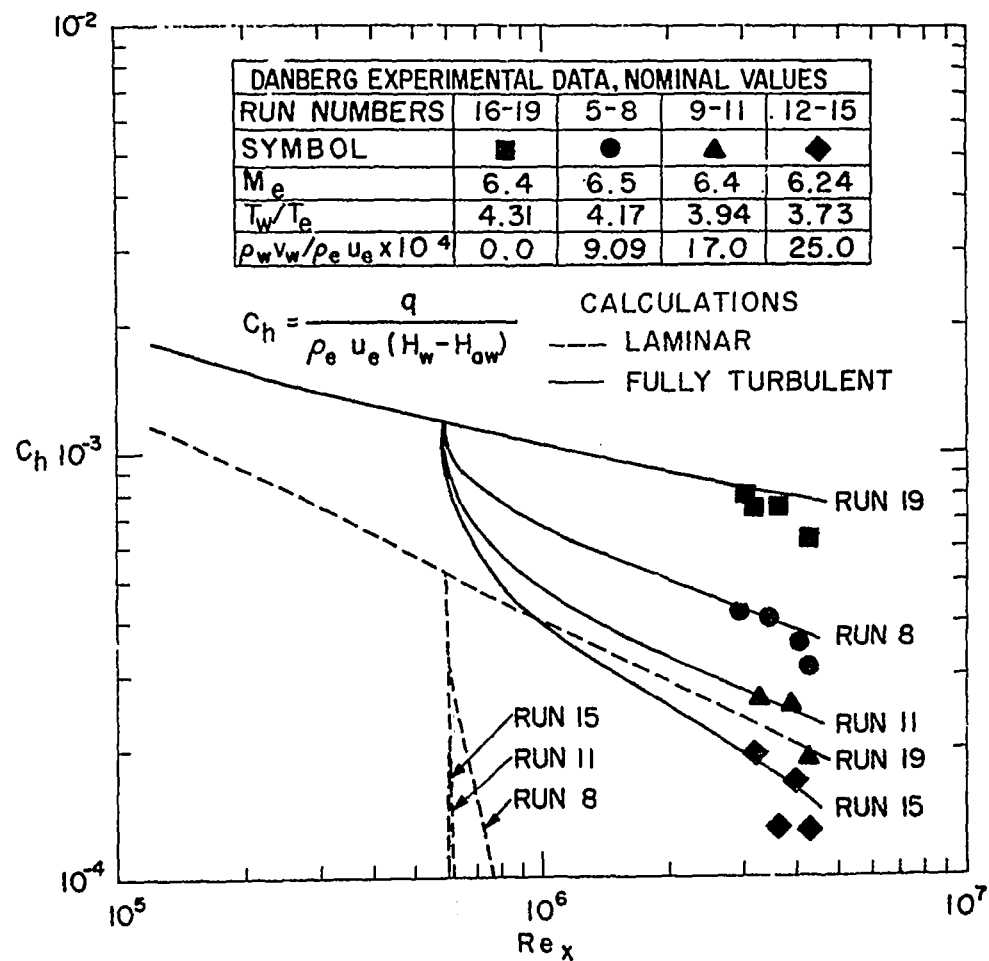Figure 47: Velocity Profiles for a Flat Plate With Mass Injection—
Danberg's Data

154

Figure 48: Stanton Number Distribution for a Flat Plate With Mass Injection-Danberg's Data

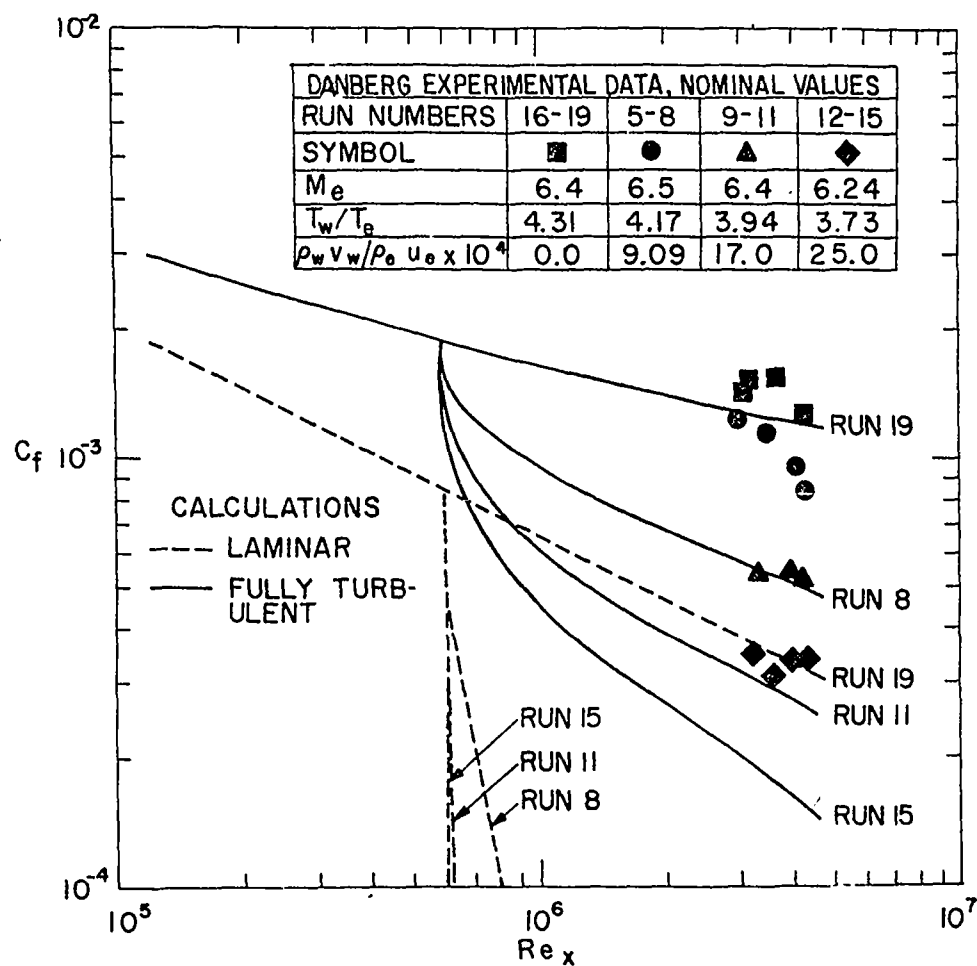| DANBERG EXPERIMENTAL DATA, NOMINAL VALUES				
RUN NUMBERS	16-19	5-8	9-11	12-15
SYMBOL	■	●	▲	◆
M_e	6.4	6.5	6.4	6.24
T_w/T_e	4.31	4.17	3.94	3.73
$\rho_w v_w/\rho_e u_e \times 10^4$	0.0	9.09	17.0	25.0

CALCULATIONS

--- LAMINAR

— FULLY TURB-ULENT

Figure 49: Skin Friction Distribution for a Flat Plate With Mass Injection-Danberg's Data